University of Strathclyde

The Smart Rotor Wind Turbine

Charles Plumley

A thesis presented in fulfilment of the requirements
for the degree of Doctor of Philosophy

Centre for Doctoral Training in Wind Energy Systems
Department of Electronic and Electrical Engineering
University of Strathclyde
Glasgow, G1 1XW
Scotland, UK

May 18, 2015

Acknowledgements

First of all I would like to thank my supervisors, Professor Bill Leithead, Dr Ervin Bossanyi, Professor Mike Graham and Peter Jamieson, for allowing me to conduct this PhD, all the advice they have given me along the way, and for the freedom I have been permitted to pursue the work in my own direction. They have made me feel like a true researcher, exploring and progressing independently in a methodical, yet sometimes haphazard, way.

This thesis is the culmination of four years study at the Wind Energy Systems Centre for Doctoral Training within the University of Strathclyde and this of course means a big thank you to Drew Smith, the guy that keeps everything running smoothly. A thank you is also due to all my fellow CDT colleagues that have kept me company throughout this endeavour and created an environment where it is actually fun to discuss work. A special thank you as well to those of you that have supported me over a pint or two on an almost weekly basis.

I would also like to thank my parents for supporting me through all my studies, all 22 years of them! Maybe it is now time to enter the 'real world,' but for the chance to be a student again I am eternally grateful, and must thank the Engineering and Physical Sciences Research Council (UK) for funding me these extra 4 years, grant number EP/G037728/1.

Finally, despite occasional protestations, I have thoroughly enjoyed being a student at Strathclyde University... from being able to party the nights away, to lying in during the mornings; from being Pub Captain of the postgraduate society and Commander of Unit Cohesion and Social Coordinator for the Intermingling of Years in the CDT, to joining all the sports clubs such as skydiving, snowsports, gymnastics, and of course, trampolining; from having the time to study Russian, Chinese and acting, to the ability to visit London every other weekend. These extra-curricular activities and the friends I have made doing them have been my lifeblood, motivation, source of consolement and inspiration, without which I may never have completed this PhD. Thank you!

Charlie

Abstract

The smart rotor is an upgrade to the wind turbine rotor that facilitates active modification of the blade aerodynamics, thus allowing enhanced control of the rotor loads. In this thesis a number of research areas relating to the smart rotor are explored and advanced.

The synthesised wind field spatial and temporal requirements are assessed, suggesting the current guidelines, of less than 5m spatial and 10Hz temporal resolutions, are more than adequate. Also regarding the wind field, it is shown that the smart rotor provides the greatest percentage benefits when there is high wind shear, but low turbulence intensity.

An analytical approach to selecting the chord-width of trailing edge flaps, based on thin aerofoil theory, is presented. Demonstrating a trade-off between flap size, flap actuator requirements and load reductions. The unsteady aerodynamics of trailing edge flaps and their modelling in Bladed is also considered, showing only a limited requirement to develop the aerodynamic code.

A comparison of individual pitch and smart rotor controllers shows that both methods can achieve similar load reductions. The main benefit of using a smart rotor system is the lower pitch motion. The smart rotor is also shown to reduce pitch motion by supplementing collective pitch control. The trade between pitch actuator requirements, load reductions and the cost of smart rotor control, is therefore considered the defining factor in valuing the smart rotor, rather than purely load reductions.

Finally, a fault scenario of a single jammed flap is detected and corrected for. With results suggesting that even unreliable systems can achieve a significant lifetime fatigue load reduction.

These studies are conducted using a methodical process detailed in this thesis, such that future researchers may build upon this work. Access to the models and code developed are provided in the appendix.

Contents

Chapter 1

Introduction

Smart rotor wind turbines possess additional control over wind turbines that operate using torque and pitch control. This additional control comes from devices placed along the wind turbine blades that can alter the local lift and drag characteristics in a responsive manner. With the correct controller and sensors, this has the potential to reduce loads on the turbine and so their construction costs. However, the smart rotor wind turbine has yet to gain acceptance within industry, because of concerns over modelling, the devices to be used, the cost benefits of such a system and the risks involved, including the risk of faults. This thesis therefore explores a number of themes associated with the smart rotor, some of which are an advancement on previous work and others that have not been covered before.

This chapter covers the contribution to knowledge made in this thesis in Section 1.1 and offers an overview of the thesis in Section 1.2. Publications that are the result of this PhD are detailed at the end of this chapter.

1.1 Contribution to knowledge

This thesis contributes the following to knowledge:

- The influence of wind field synthesis has been explored. Whilst guidelines exist for what resolution grid to use and for which wind field models should be used for certification, work here demonstrates what uncertainty the wind field synthesis has on wind turbine simulations and in particular smart rotor simulations. It is found a grid resolution of less than 5m spacing in the rotor plane and time resolution of 10Hz in the along wind direction will give accurate results. The Mann wind model is also shown to require a resolution high enough to avoid roll-off at high frequencies that result in lower turbulence and so reduced wind turbine loadings.
- The chord width of flaps on the wind turbine blades has been studied, including a brief consideration of leading edge flaps, this has been done while maintaining the span of the flaps. Reduced motion is required for flaps with larger surface area, however actuation then requires higher torques and power.
- The smart rotor has been shown capable of supplementary control. This is tested through assisting the collective pitch control with rotor speed control, which results in reduced pitch action. The smart rotor can also reduce loads at the same time though with increased actuator requirements.
- A new control system that was previously developed for individual pitch control has been deployed for smart rotor control. The independent pitch control is capable of similar load reductions as the dq-axis control method, but the control system is distributed rather than centralised.
- A system of evaluating the performance of a smart rotor control system based on actuator requirements in conjunction with load reductions has been conducted to more accurately demonstrate the advantages of using the smart rotor. The method involves achieving similar load reductions for a variety of control strategies and then comparing the actuator requirements. This avoids biasing results simply through choosing preferential gains.
- The influence of faults on the smart rotor has been evaluated for the first time. A fault tolerant system is described that can result in loads and energy capture similar to the collective pitch controlled case when a fault jams one of the smart rotor actuators. A detection system is also described that is capable of detecting a fault based on measurement of 1P cyclic loads in the event that a fault is left undetected directly by a sensor on the actuator. It is found that faults are not as prohibitive to the use of the smart rotor as might be expected. Load reductions can be maintained despite considerable operation in a fault condition.

1.2 Overview of thesis

The main body of the thesis contains four chapters looking at the baseline model, performance analysis and the background to the smart rotor, followed by another five chapters containing original research: the effect of the wind field on wind turbine performance, the effect of flap chord width on control, a comparison of smart rotor and individual pitch control, supplementary control and an analysis of fault conditions.

Chapter 2 contains background information that has led to smart rotor wind turbines being researched.

Chapter 3 consists of a technical review describing the current state of research into smart rotors and the areas that are deemed to require further research. Particular attention is also drawn to the unsteady aerodynamic modelling of trailing edge flaps.

Chapter 4 covers the model used to test the smart rotor wind turbine and the control strategies.

Chapter 5 contains the methodology used to assess the performance of the smart rotor. This includes the load cases and the metrics used.

Chapter 6 looks at wind field synthesis taking into consideration the wind field models, the resolution of the wind field, and the effect of turbulence and wind shear on the wind turbine loads. The effect of using two different wind field models, Kaimal and Mann, during assessment of smart rotor control is also noted.

Device selection has always been an interesting area of focus, with many different devices being considered: from trailing edge flaps to plasma actuators, active vortex generators, microtabs and inflatable structures. An analysis based on the control requirements has been less forthcoming, and therefore in Chapter 7 the lift, drag and moment coefficients are altered through a progressive change in the active chord length, to examine what influence these have on load reduction and actuator requirements.

In Chapter 8, a direct comparison is made between individual pitch control and smart rotor control. Individual pitch control may be seen as in direct competition to the smart rotor control, as both can achieve similar objectives. The cost of each system is evaluated based on actuator wear, rather than load reduction that is often done. This highlights the benefits of each system fairly as load reductions can be altered simply by making the actuators work harder. The results suggest that while pitch motion and power consumption is increased when using the individual pitch control, the torque requirements are not necessarily increased.

Following on from this in Chapter 9 a combined controller is considered that shows the trade-off between upgrading the pitch actuator and using smart rotor control. This is done not only for load reduction, but also for speed control. The smart rotor control is found capable in this respect too, but it is a question of whether implementing a smart rotor is cost effective in comparison to either upgrading the pitch actuator or indeed using a simpler control mechanism.

Another limitation is the fault tolerance of a smart rotor wind turbine. Traditionally the robustness of devices has been highlighted as a major disadvantage of the smart rotor, that could result in costly maintenance and downtime. Research presented in Chapter 10 however suggests this need not be the case, and that a fault tolerant system is possible that can result in load reductions and maintain power output despite faults. This helps alleviate this concern.

A summary of the work and an encouragement for future work is given in the conclusion to this thesis.

Publications

[1] C. Plumley, W. E. Leithead, P. Jamieson, E. A. Bossanyi, and M. Graham, "Comparison of individual pitch and smart rotor control strategies for load reduction," *Journal of Physics: Conference Series*, vol. 524, June 2014.

[2] C. Plumley, W. E. Leithead, P. Jamieson, M. Graham, and E. A. Bossanyi, "Supplementing wind turbine pitch control with a trailing edge flap smart rotor," in *IET Renewable Power Generation*, (Naples, Italy), 2014.

[3] C. Plumley, W. E. Leithead, P. Jamieson, M. Graham, and E. A. Bossanyi, "Fault Ride-Through for a Smart Rotor DQ-axis Controlled Wind Turbine with a Jammed Trailing Edge Flap," in *EWEA*, (Barcelona, Spain), 2014.

Chapter 2

Background

Wind energy is one of the cheapest forms of renewable energy, but it is still, in the vast majority of cases, not price competitive with traditional forms of electricity generation, this is largely because the environmental damage that fossil fuel generators cause is not accounted for. Research is therefore vital to the long term survival of the industry and its ability to compete without external dependencies. Whilst the majority of this research is through progressive improvements in cost and efficiency, other research paths are more radical and can be considered revolutionary. The smart rotor concept is one such solution. It involves distributing devices along the span of the wind turbine blades that are capable of altering the local aerodynamics and thus supplying an extra degree of freedom in the control and design of the wind turbine.

This chapter describes the development of wind power over the past couple of decades in Section 2.1, the technological advancements that have led to the smart rotor being considered in Section 2.2, and finally in Section 2.3 of this chapter there is a description of the smart rotor concept.

2.1 Development of wind as an energy source

Wind is an ancient source of energy. It has been used to transport goods and forge empires, help feed nations and reclaim land, and more recently to generate electricity. These electricity generating machines are termed wind turbines and they have proliferated since the turn of the new millennium. The reason for this recent rapid expansion in their construction, over continued use of fossil fuel generation, is fourfold.

Firstly, anthropogenic Climate Change is largely caused by greenhouse gas emissions, as described in the IPCC reports, and so burning fossil fuels to produce electricity will lead to further global warming [1], which will have serious consequences for the world's water supply, ecosystems, food production, coastal areas and health [2]. Renewable energy sources, such as wind power, are part of the solution to reduce emissions arising from electricity generation and the case for investment in such technologies is emphasised in [3], which makes clear that the benefits of action now far outweigh the costs associated with inaction.

Secondly, dependency on energy imports from another country can have serious consequences to national security. This has arguably led to interventions in Iraq and Libya, disputes over sea-beds in the South China Sea and the Falklands, and interrupted supplies through Ukraine and other former Soviet Union countries. Wind power is not an energy resource another country can cut-off or take control of, it is both indigenous and sustainable. This makes it an ideal option to reduce energy dependency, in a wider energy mix.

Thirdly, as stated above, wind is a renewable resource. This makes it a long term sustainable option. Fossil fuels on the other hand deplete over time and though new reserves are being found, once the fuel is used it takes millions of years to be naturally replaced. For oil in particular a peak in production is expected this century, which will lead to much more volatile energy prices. This concern leads back to the 1970's, when a sharp rise in oil prices led governments to consider alternatives to fossil fuel plants. Wind power can be used to hedge against price volatility and supports a long term renewable energy strategy.

Fourthly, by investing now there is the potential to save and make money, by developing an industry that will become ever more important given the previous three points. Denmark for example has already benefited substantially from its early investment in wind turbines, through export to other nations, and China for example is keen to develop its own expertise to cut costs.

These arguments have led to the adoption of legally binding targets in the European Union for renewable electricity generation and extensive investment around the globe [4]. Europe, China and the USA are leading the way, with global average annual growth of over 25% since 1993, leading to 2.7% of total world electricity generation from wind in 2013 [5]. This rapid growth has led to the technical development of large multi-megawatt wind turbines.

2.2 Wind turbine technology

Modern commercial wind turbines are typically horizontal axis 3-bladed upwind variable speed pitch-to-feather regulated machines, with rated power outputs from a couple to several megawatts. This has come about from a steady progression in research and development and it is perhaps worth quickly giving some background to this story, so that the context of the smart rotor is understood.

Professor James Blyth, a lecturer at the precursor to the University of Strathclyde, constructed the first wind turbine back in 1887. This first wind turbine was a horizontal axis sail-driven machine used to power his cottage in Marykirk, but it is perhaps his later vertical axis drag-style machine, used as backup power to Montrose Lunatic Asylum, that people remember better, shown in Figure 2.1a, which operated for 27 years. Drag-style machines though are less efficient than wind turbines that use lift to produce torque, and while small scale vertical axis Darrieus wind turbines can be seen around urban environments, horizontal axis wind turbines dominate the utility scale landscape. The reason for this is not as clear as one might expect. Vertical axis wind turbines have their advantages, such as the ability to have the heavy drive-train and generator at the bottom of the structure, and indeed there are continuous research efforts to explore vertical axis wind turbines. Perhaps though the biggest driver behind horizontal axis wind turbines is innovation resistance and the desire to use and build upon a proven product. An example of this can be seen during the initial 'wind rush' in California, where the simpler Danish wind turbines, holding certification from Risoe, came to dominate the market despite lacking the efficiency and some of the innovations of the American designs. Regardless of the reason for the proliferation of horizontal over vertical axis wind turbines, this thesis focusses on further advancement of this dominant technology, so having the greatest initial impact. This work also is aimed at reducing the resistance to the smart rotor innovation.

The design of the horizontal axis wind turbine has also evolved over the years. The machine Charles Brush built back in 1888 was much larger than that of James Blyth, and consisted of a high solidity horizontal axis rotor capable of producing a peak output of 12kW, Figure 2.1b. High solidity rotors have high torques at low rotor speeds, this means a higher gearbox ratio is required to step up the shaft speed for the generator, the large number of blades also clearly come at a cost. Poul Le Cour found fewer faster rotating blades worked more effectively at the turn of the 20th century, and three blades have been found to be a good balance between cost of the blades, rotor solidity and rotor speed. Three blades also look symmetrical upon rotation and the forces across the rotor are more balanced, such that a teetering hub is not required and shaft torque is not heavily cyclic in wind shear. Nevertheless, one and two-bladed machines are still being considered, particularly offshore where tip speeds may be higher due to reduced noise constraints. Again though, the dominance of the 3-bladed machine means that is the one considered in this work.

The early 3-bladed horizontal axis machines were fixed speed and stall regulated, and the work on this design is best seen from the example Johannes Juul constructed in 1957, the Gedser 200kW upwind machine, with induction generator and aerodynamic tip brakes used to protect against over speed, Figure 2.1c. The main disadvantages of fixed speed stall regulated machines is the reduced energy capture and uncertainty about the stall characteristics, but it is a highly reliable design. Wind turbines as large as 1.5MW using this technology have been operated. Larger machines though require a different control mechanism to reduce loads and have more control over the power

(a) Blythe's wind turbine

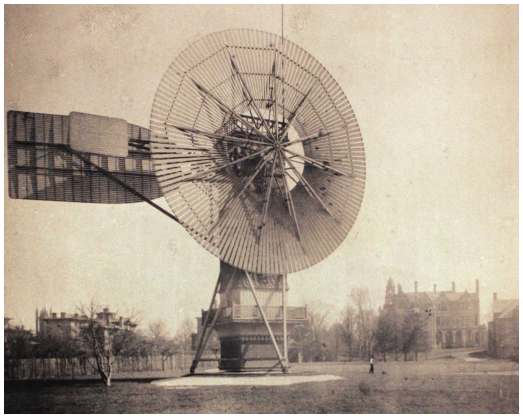

(b) Brush's wind turbine

(c) Gedser wind turbine

(d) Tvind wind turbine

Figure 2.1: History of wind turbines

output.

The world's first multi-megawatt wind turbine was constructed by teachers, students and volunteers in 1978. The Tvind Power wind turbine had a rated power of 2MW and was a downwind 3-bladed wind turbine with full span pitch control, remarkably similar to modern 3-bladed machines, see Figure 2.1d. Full-span pitch control allows greater energy capture as the wind turbine is able to operate at rated power for a larger set of wind speeds, as opposed to passive stall controlled wind turbines that must be designed to stall such that rated power is only reached at one wind speed. Pitch control also has the ability to reduce noise that would otherwise be induced by stall and reduces the torque requirements from the generator. There are two types of pitch control: pitching to feather and pitching to stall. While pitching to feather reduces the angle of attack of the blade and so reduces the lift, pitching to stall increases the angle of attack of the blade and induces stall, limiting lift. Generally pitching to feather is used due to uncertainty over the loads and the nature of stall. However, pitch to stall may be advantageous as regards to fatigue loads in high wind speeds, as while the mean thrust is higher, the torque and thrust are more stable, varying less [6].

The Tvind Power wind turbine also had a fully-rated converter so that it could supply power to the grid. A fully-rated converter, like a doubly fed induction generator, is capable of operating at a variety of generator speeds. This allows the rotor speed to be adjusted to the incoming wind field, achieving closer to optimum energy capture at low wind speeds. This has led to the modern variable speed pitch regulated wind turbine. In these turbines both the torque control and pitch control use as a single input the generator speed. The torque control operates to optimise energy capture below rated wind speed and can either be programmed to hold torque or power constant above rated. The pitch control acts to maintain a constant rotor speed above rated. A more detailed description of the operation of variable speed wind turbines can be found in Section 4.3 of this thesis.

To bring down the cost of energy the size of wind turbines has increased considerably in the past few decades and offshore, where unit costs such as foundations, construction and connections are high, the trend is to even larger wind turbines [7]. The increasing size of wind turbines comes with its problems though. The size of the turbines is naturally limited by scaling laws, as while energy capture scales with the square of the rotor diameter, mass scales approximately to the power of three [8], but the size is also limited by loads on the rotor. In particular, the non-uniformity of the wind field encountered by the rotor due to wind shear and turbulence, causes large cyclic loadings. These loads increase the material requirements and so need mitigating to allow a reduction in the cost of energy [9].

Control is an essential component of modern multi-MW wind turbine design, and has the ability to reduce loads through avoiding resonant frequencies and active damping, while also optimising energy capture [10]. A further development that is being trialled on commercial wind turbines is individual pitch control, whereby each blade pitches individually to reduce loads on the rotor of the wind turbine. By pitching the blades individually the effects of a non-uniform wind field can be mitigated to a certain extent [9]. There are a couple of methods to do so which, again, are described in detail in the control section. The two principal options are a differential pitch control where pitch angle for each blade is determined by a central controller and the demanded change in pitch is 120 degrees out for each blade, based on blade azimuth; and a control where each blade

pitch is independent of the individual pitch control of the other blades, which can be referred to as a form of distributed control.

Individual pitch control is relatively simple to adopt into modern wind turbines due to the fact that most wind turbines are already manufactured so that the actuators to pitch each blade are already independent. This is partly done as a safety measure for over-speed protection, which requires two different ways of stopping a wind turbine in an emergency. To adopt individual pitch control all that is physically required is an additional sensor input. This could be a strain gauge at the blade root, a LIDAR detection system to determine the incoming wind loadings, a Pitot tube protruding from the leading edge of the blades or some other sensor capable of allowing the controller to predict the pitch demand for each blade to achieve the control object, typically defined as reduction of fatigue loads on the rotor. The advantages of this control over the conventional, collective variable speed wind turbine controllers are the reduction in loadings. The concept of the smart rotor builds again on what has been done so far.

2.3 The smart rotor wind turbine

The ultimate goal of technical research into wind turbines is to bring down the cost of electricity from wind. There are numerous ways this can be done and it is not necessarily all about money: public acceptance, risk and politics are some other areas that also need to be considered. The smart rotor though is a technology that has potential to reduce the cost of energy.

Smart rotor wind turbines possess additional control over variable speed wind turbines that operate using torque and pitch control. A smart rotor could use the same sensors as an individual pitch control, but in addition to these sensors there are control devices attached to the wind turbine blades capable of altering the local aerodynamics. These can then be activated to change lift and drag characteristics of the blades in a responsive manner. A wide variety of control devices are being considered and while this thesis focusses on using trailing edge flaps, other devices are also suitable for the control systems used.

The control method can be complex, especially as the controller objective may not be as simple as load reduction and needs to be robust. Two control systems are adopted from individual pitch control techniques that are known to have achieved positive results, and implemented on the smart rotor to assess their performance and that of the smart rotor. The diagram in Figure 2.2 portrays the general control method, which can be considered the template for most systems where a control is present.

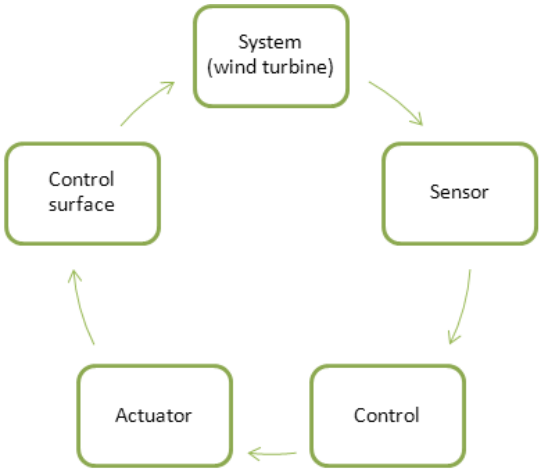

Figure 2.2: Schematic of the smart rotor concept

The potential of the smart rotor concept to reduce fatigue loadings has been shown in a number of papers. The load reduction and the impact that the smart rotor has on the pitch actuator is something that is examined in this thesis, to help quantify the benefit such a system might provide. As such the ability to use them for supplementing collective pitch control is also considered for reducing pitch demands.

No commercial wind turbine manufacturers are currently designing wind turbines with the smart rotor in mind. However, there are two demonstration plants in existence: one at Sandia National Laboratories, Texas [11], and the other at the Technical University of Denmark [12], see Figure 2.3. Both of the demonstration plants use trailing edge flaps as the control surface, with a multitude of sensors. This thesis includes a study to determine the effect of changing the flap chord length,

particularly on the smart rotor actuator requirements.

(a) Sandia National Laboratories (b) Technical University of Denmark

Figure 2.3: Smart rotor demonstration wind turbines

The results from the two demonstration plants are just starting to be published and leading on from successful demonstrations industry might become more involved. This therefore seems an opportune moment to be studying the smart rotor concept, particularly with the emphasis being on what benefits the smart rotor can offer.

References

[1] S. Solomon, D. Qin, M. Manning, R. B. Alley, T. Berntsen, N. Bindoff, Z. Chen, A. Chidthaisong, J. M. Gregory, G. C. Hegerl, M. Heimann, B. Hewitson, B. J. Hoskins, F. Joos, J. Jouzel, V. Kattsov, U. Lohmann, T. Matsuno, M. Molina, N. Nicholls, J. Overpeck, G. Raga, V. Ramaswamy, J. Ren, M. Rusticucci, R. Somerville, T. F. Stocker, P. Whetton, R. A. Wood, and D. Wratt, "Technical Summary. In: Climate Change 2007: The Physical Science Basis. Contribution of Working Group I to the Fourth Assessment Report of the Intergovernmental Panel on Climate Change," tech. rep., Cambridge, UK and New York, USA, 2007.

[2] B. Lenny, B. Peter, C. Osvaldo, C. Zhenlin, C. Renate, D. Ogunlade, H. William, H. Saleemul, K. David, K. Vladimir, K. Zbigniew, L. Jian, L. Ulrike, M. Martin, M. Taroh, M. Bettina, M. Bert, M. Monirul, N. Nicholls, N. Leonard, P. Rajendra, P. Jean, P. Martin, Q. Dahe, R. Nijavalli, R. Andy, R. Jiawen, R. Keywan, R. Cynthia, R. Matilde, S. Stephen, S. Youba, S. Susan, S. Peter, S. Ronald, S. Taishi, S. Rob, T. Dennis, V. Coleen, and Y. Gary, "Climate Change 2007 : Synthesis Report: An Assessment of the Intergovernmental Panel on Climate Change," tech. rep., IPCC, Valencia, Spain, 2007.

[3] N. Stern, "Stern Review on the Economics of Climate Change," tech. rep., HM Treasury, UK, 2006.

[4] C. Lins, "Renewables 2014 Global Status Report," tech. rep., REN21, Paris, 2014.

[5] BP, "BP Statistical Review of World Energy June 2014," tech. rep., 2014.

[6] E. A. Bossanyi, "The Design of closed loop controllers for wind turbines," *Wind Energy*, vol. 3, pp. 149–163, July 2000.

[7] R. Wiser, Z. Yang, M. Hand, O. Hohmeyer, D. Infield, P. H. Jensen, V. Nikolaev, M. OMalley, G. Sinden, and A. Zervos, "Wind Energy. In IPCC Special Report on Renewable Energy Sources and Climate Change Mitigation," tech. rep., IPCC, 2011.

[8] P. Jamieson, *Innovation in Wind Turbine Design*. Wiley, 2011.

[9] D. Berg, D. G. Wilson, M. F. Barone, B. R. Resor, J. Berg, S. Kota, G. Ervin, and D. Maric, "The impact of active aerodynamic load control on fatigue and energy capture at low wind speed sites," in *EWEC*, (Marseille, France), US Government: Sandia National Laboratories, FlexSys Inc., 2009.

[10] E. A. Bossanyi, "Wind Turbine Control for Load Reduction," *Wind Energy*, vol. 6, pp. 229–244, July 2003.

[11] J. Berg, B. R. Resor, J. Paquette, and J. White, "SMART Wind Turbine Rotor: Design and Field Test," tech. rep., Sandia National Laboratories, Albuquerque, New Mexico and Livermore, California, 2014.

[12] D. Castaignet, T. K. Barlas, T. Buhl, N. K. Poulsen, J. J. Wedel-Heinen, N. A. Olesen, C. Bak, and T. Kim, "Full-scale test of trailing edge flaps on a Vestas V27 wind turbine: active load reduction and system identification," *Wind Energy*, vol. 17, pp. 549–564, Apr. 2014.

Chapter 3

Technical review

The Smart Rotor has been studied for some time now and has been included in large projects like the pan-European project UpWind. As such there has already been considerable work in the smart rotor field. A lot of the research conducted has focussed on specific control devices and their development, while work has also been conducted on the control of smart rotor systems embedded in wind turbines. There has also been some research into the modelling of smart rotor wind turbines, with particular attention drawn to the unsteady aerodynamics that could be important during rapid deployment of control devices.

In Section 3.1 of this chapter the control strategies proposed for the smart rotor are reviewed, in Sections 3.2 and 3.3 the sensors and flow devices are looked at respectively, and finally in Section 3.4 the modelling of smart rotor wind turbines is considered, with particular reference to the unsteady aerodynamics.

3.1 Smart rotor control strategies

A number of control strategies have been proposed and used for testing smart rotor wind turbines. These include systems with centralised, decentralised and distributed architectures, and also both open-loop and closed-loop control.

A typical centralised closed-loop control for the smart rotor is the dq-axis system developed for individual pitch control, as in [1]. For example, in [2] this was used effectively with trailing edge flaps to reduce loads through monitoring the blade root bending moment. The blade root out-of-plane bending moment was measured for all three blades and these were converted into a fixed tilt-yaw axis plane using the Coleman transform based on the position of the blades. Two decoupled Proportional Integral (PI) controllers then worked to minimise these tilt and yaw imbalances, with the inverse transform setting the demands for each of the blades.

Using this method the 1P cyclic loads on the blades are substantially reduced and the rotor imbalances eliminated. This resulted in blade root out-of-plane load reductions of 12.6 to 14.6%. However, loads caused by the stochastic nature of the wind are largely unaffected, apart from those that impact on cyclic loads due to rotational sampling. This was observed when a localised gust was trialled in [3]. Depending on the azimuthal location of the gust, the pitch of all three blades varies, rather than just the blade experiencing the gust. For this reason the dq-axis system is sometimes referred to as a differential or cyclic pitch control.

In [2], individual pitch and smart rotor control were also combined into a hybrid controller, again using the dq-axis transform, with high frequency motions assigned to the flaps and low frequency motions to the pitch actuator. This resulted in load reductions of upto 16.9%. It is also significant that the individual pitch and smart rotor architectures used are the same. This suggests most of the control research into individual pitch control is interchangeable with that of the smart rotor, though with possible different operating regimes (frequencies and wind speeds) and with different gains.

In [4], alongside the dq-axis control, two decentralised close-loop controllers were trialled. The first of these controllers was a simple Proportional Integral Differential (PID) controller monitoring the blade root bending moment, the second splits the flap on each blade into three and PID controllers then act to reduce local deformations of the blade. Both decentralised controllers reduce the loads on the blades by more than the centralised controller, with the multiple flap feed-back control working best to reduce loads, see Table 3.1 for the reductions in blade root out-of-plane moments.

Table 3.1: Reduction in the standard deviation of the blade root out-of-plane bending moment [%] [4]

Controller	Wind speed [m/s]		
	8.0	11.4	18.0
Centralised dq-axis control	9.26	5.78	7.92
Decentralised PID control	15.41	10.23	17.32
Multiple flap PID control	19.3	16.35	22.41

These two decentralised controllers are fairly basic, with potentially better results to be seen for controllers that decouple the smart rotor systems from the rest of the wind turbine dynamics.

For example, in [5], this was done by taking into account fictitious forces on the blades and load reductions of up to 44% were achieved [6].

Alternative decentralised controllers were described in [7] with promising results. These included: proportional and integral controllers filtered to focus on 1P signals; a 'skyhook' control that acts as a damper reacting proportionally to either velocity, deflections or accelerations that works to hold these constant; and a multi-rotational modulated distributed blade control (mmDBC), which, similar to the dq-axis control, converts the rotational sensor signals into fixed plane signals for a number of harmonics [8]. These controllers all used either the local flap-wise bending moment or flap-wise velocities at the location of the actuators as the controller inputs, and flaps as the aerodynamic control surfaces. Combinations of individual pitch and smart rotor control were also tested, achieving higher load reductions. The load reduction results from this paper are displayed in Table 3.2.

Table 3.2: Reduction in damage equivalent loads for the blade root out-of-plane bending moment [%] [7]

Controller	Wind speed [m/s]		
	11	15	20
IPC	5.2	27.0	19.3
mmDBC	20.4	39.8	38.3
mmDBC + IPC	21.0	42.4	39.7
Skyhook 2P	19.3	33.9	38.0
Skyhook 2P + IPC	23.4	46.4	47.4

Multiple-input-multiple-output controllers (MIMO), such as the Linear Quadratic Regulator (LQR) and H-infinity type controllers, are also potential options. In [9] a MIMO LQR controller was used to control flap deflections using multiple flaps per blade. An Observer/Kalman filter IDentification (OKID) process was adopted to determine the dynamics of the wind turbine with chirp signals activating the flaps and a steady input wind field, with the prospect that in the future more realistic wind fields are used for system identification purposes. The blade deflection rate and maximum deflection angles of the flap are used in the controller cost function.

The LQR control showed a 15.5% reduction in fatigue damage equivalent loads compared to reductions of 26.0% for a simple PD flap control based on tip displacement and 30.1% reduction for a highpass and notch filter control tested in [10]. These simulations were run on the same model and demonstrate the effect changing the controller can have. It is interesting to note that the simpler PD control and filter control are both better at achieving load reductions than the multivariable approach, though it is presumed that a multivariable approach could achieve similar results.

Proportional Differential (PD) controllers for flaps based on tip deflection have also been combined with dq-axis individual pitch control in [11], with load reductions greater than either one acting alone, displayed in Table 3.3. These PD controllers have also been trialled using tip deflection rates and for microtabs in place of trailing edge flaps for similar results [12].

The use of both individual pitch control and smart rotor control together has therefore been raised a few times. The load reduction potential presented though does vary and in particular it is not clear what the costs of implementing either of the systems are.

Feed-forward open-loop controllers have also been considered for smart rotor control. In [13]

Table 3.3: Reduction in the standard deviation of the blade root out-of-plane bending moment [%] [11]

Controller	Wind speed [m/s]	
	16	20
IPC	14.00	19.98
PD	21.54	21.68
PD + IPC	27.81	32.19

an experimental deformable trailing edge flap was tested in a wind tunnel with two types of inflow sensor, a Pitot tube and protruding sensor aerofoil. Blade root load reductions of 50% were recorded. Similarly individual pitch control has shown that feed-forward operation can achieve a 25% reduction in lifetime out-of-plane blade root fatigue loads, suggesting smart rotor control could be equally beneficial in this scenario [14].

Finally, there are controllers that combine both feed-back and feed-forward control. This is demonstrated in [15] with Model Predictive Control (MPC), which attempts to optimise performance based on the known current state, predictions of the future state and the constraints of the system. In this case the MPC utilises inflow measurements in addition to high-pass filtered local blade deflections, with marginal, of the order of a couple of percent, improvement in load reductions.

An important observation in this paper is the effect that the simulation conditions have on the load reductions. Namely that increased turbulence intensity results in lower load reductions. It is not made clear what causes this. Additionally something to note from the tabulated results in this section are the large variations in load reductions presented for what are often similar controllers. This is sometimes due to the conditions under which the simulations are run, but also due to different metrics being used. A fair open description of the methods and metrics used to test controllers is therefore essential for future comparisons.

Finally regarding control, in [16] robustness is raised as a serious issue. Whilst this is primarily about operational robustness should a particular sensor or actuator fail and the motivation therefore towards a distributed system, this does raise the interesting prospect of faults on the smart rotor system.

3.2 Sensors

A full review of the sensors being considered for the smart rotor is contained within [17] and [18].

While Pitot tubes [19], [15], leading edge protruding aerofoils [13], the hinge moment on the trailing edge flaps [20], pressure sensors, aerodynamic probes [21], LIDAR [22], [23], [24], and deflection sensors [13] all have potential for use in smart rotor control, accelerometers and strain gauges are the most likely candidates based on the control strategies considered above.

3.2.1 Accelerometers

Accelerometers are cheap, robust, light weight, easily installed, have low power requirements, are insensitive to temperature changes in the environmental conditions they will experience and are relatively immune to electromagnetic waves. This make them close to ideal sensors. They also have a high bandwidth which, depending on the accelerometer used, may range from 0Hz to 10's of kHz. They are being considered for blade condition monitoring purposes with several sensors along the blade length to monitor mode shape [25] [26] [27] and have been proposed as a sensor for the smart rotor by a number of authors, and, indeed, both smart rotor demonstration plants, at DTU and Sandia National Laboratories, have embedded accelerometers that could be used for control. An example of some accelerometers that have been used to trial structural health monitoring of a wind turbine blade are shown in Figure 3.1.

Figure 3.1: An example of accelerometers used for blade condition monitoring [28]

Their use can also extend beyond measurement of the acceleration, integrating to get the velocity or deflection of a blade, which is typical of the PD controllers considered in the previous section. In such cases it is important that drift is avoided and this can be done, assuming that the absolute position is less important for the controller, by high-pass filtering.

3.2.2 Strain gauges

The blade root bending moment, and indeed other moments, are measured using strain gauges. This is typically done on wind turbines at the blade root, but may also be applied along the blades as needed for some distributed controllers. Types of strain gauges include electrical and optical, with electrical strain sensors currently more common but difficult to install and unlikely to have the lifetime required over the number of stress cycles of a wind turbine blade. Optical type strain sensors have the ability to overcome these constraints. The bandwidth of both types of strain gauges is likely to be acceptable for smart rotor control. As an example, strain measurements have been used for smart rotor control in [29], and while highlighting the drawback that strains will take time to develop due to the inertia of the blade, they are shown as a suitable sensor for control purposes.

In [17] the different types of strain gauges are compared, with fibre optic strain gauges considered the most suitable due to the complexity of the other techniques. The benefits of an optical system are described as follows:

- Very light
- Small in diameter
- Resistant to corrosion and fatigue
- Capable of wide bandwidth operation
- Dielectric in nature
- Immune to electrical interference
- Mechanically flexible, diverse geometry possible
- Do not represent electrical pathways within the host structure
- No protection required against lightning
- Extreme sensitivity
- Do not generate heat or electromagnetic interference
- Low attenuation of signals
- Low maintenance, high reliability
- Possibility for detecting health status of the structure
- High versatility of the measures

They can also be used much more effectively than conventional strain gauges due to their ability to multiplex, effectively allowing measurements along the whole span of the blade using a single optical fibre and different wavelengths of light. They are however a relatively new technology, so at the very least there are likely to be teething problems.

Bragg grating sensors are the most common type of optical fibre strain gauge. The fibre contains a distributed Bragg reflector that reflects only a certain wavelength of light, the Bragg wavelength (λ_B) given by $\lambda_B = 2n_e\Lambda$, where n_e is the effective refractive index of the grating in the fibre core and Λ is the grating period. The wavelength however is sensitive to both strain and temperature, as shown in the equation:

$$[\Delta\lambda_B/\lambda_B] = C_S\epsilon + C_T\Delta T \tag{3.1}$$

where ϵ is the strain, ΔT the change in temperature, and C_S and C_T are the coefficients of strain and temperature respectively.

Fibre Bragg grating sensors are already used in blade monitoring and there are various commercial systems based on these sensors, e.g. Smart Fibres' SmartScan, FiberSensing's windMETER and Moog's Blade Sensing System. They therefore seem the likely technology to be implemented in the future.

3.3 Flow control devices

There are a large number of flow control devices being considered for use on the smart rotor and there are already a number of reviews considering the options available. The two most uptodate reviews are [30] and [18]. In [30] the devices are classified by their flow control technique, placement, method of altering the lift curve and whether the activation is steady or unsteady for a fixed state (e.g. flaps are steady while a pulsed vortex jet generator is unsteady), see Figure 3.2. This helps inform the control methods that may be appropriate for the given devices and modelling that may be appropriate. A control strategy for instance that uses the change in lift coefficient to affect loads will likely be applicable regardless of the device, as long as the end result of activation is the same.

In [18], a slightly different approach is used to estimate the performance of various devices. The minimum, maximum and mean change in lift coefficient from various papers are reported for a number of devices, shown in Figure 3.3, which gives an estimate of the effectiveness of the various devices.

Techniques/Devices	Geometric (G) Fluidic (F) Plasma (P)	Leading Edge (LE) Trailing Edge (TE) Mid-Chord (MC)	Inc. Lift (I) Dec. Lift (D) Delay Stall (DS)	Steady (S) Unsteady (U)
Non-traditional Trailing-Edge Flaps	G	TE	I/D	S/U
Plasma Actuators	P	LE	DS	S
Vortex Generator Jets	F	LE	DS	S/U
Microtabs	G	TE	I/D	S/U
Traditional Trailing-Edge Flaps	G	TE	I/D	S/U
Miniature Trailing-Edge Effectors	G	TE	I/D	S/U
Microflaps	G	TE	I/D	S/U
Active Stall Strips	G	LE	D	S
Vortex Generators	G	LE	DS	S
Blowing and Suction	F	LE/MC/TE	I/D, DS	S/U
Circulation Control	F	TE	I/D	S
High-Frequency Micro Vortex Generators	G	LE	DS	U
Synthetic Jets	G/F	LE	DS	U
Active Flexible Wall	G	LE	DS	U
Shape Change Airfoil	G	MC	I/D	S/U

Figure 3.2: Classification chart for aerodynamic flow control techniques/devices [30]

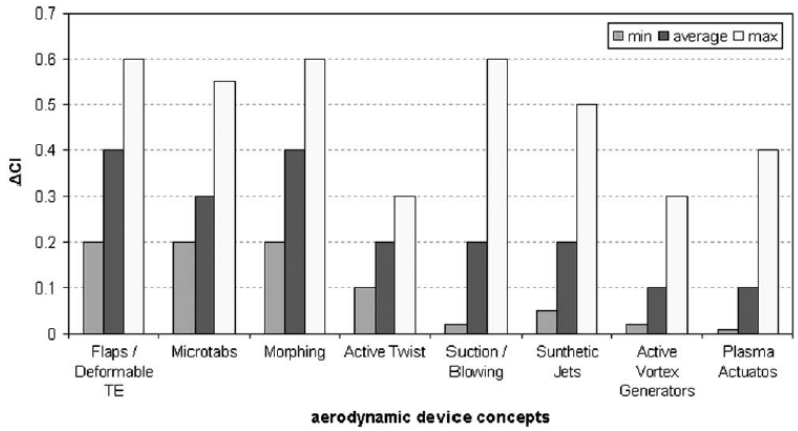

Figure 3.3: Comparison of aerodynamic device concepts in terms of reported capability to alter the lift coefficient [18]

Rather than reviewing all the options, from the current reviews microtabs and trailing edge flaps are seen as front runners, and with the application of trailing edge flaps on the two demonstration plants this further supports the modelling of trailing edge flaps [31] [32]. Trailing edge flap are also used extensively across the smart rotor field, not only as regards to its design, but also in papers examining smart rotor control [2] [4] [29] [10] [9] [33] [15] [13] [7]. They therefore seem an appropriate device to model for control purposes, and bearing in mind that the control works only to alter the aerodynamic coefficients of the blades, devices that alter the coefficients in a similar manner to flaps will likely also work with the proposed control strategies.

3.3.1 Trailing edge flaps

Trailing edge flaps are analogous to ailerons on an aircraft wing: deployment alters the camber of the aerofoil increasing (deployment on the pressure side) or decreasing (deployment on the suction side) the lift coefficient of the aerofoil. Small deflections of trailing edge flaps can significantly alter the local lift coefficient of the aerofoil and this, and their size, means power requirements are much less than for full or part-span pitch control. Their size also means they can deploy much faster than rotation of entire blade sections and on wind turbines with large rotor diameters multiple flaps may be deployed along the length of the blades allowing local variations in wind speed to be controlled and the negative effects mitigated. Trailing edge flaps can be rigid or deformable, as compared in Figure 3.4.

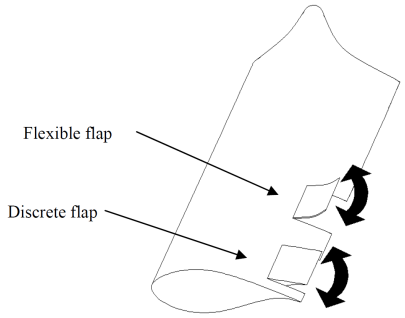

Figure 3.4: Trailing edge flap concepts [17]

Rigid trailing edge flaps operate in much the same way as ailerons and elevators on aircraft, and as such have been in use for just over a century. They are mounted at the rear of the blade (on the trailing edge) and are actuated by providing a moment about the hinge. They can be deployed at a range of angles and, using the correct actuator, at high bandwidths.

Deformable trailing edge flaps are similar, but form part of the continuous surface of the blade. This has two main advantages. Firstly the aerodynamic efficiency is improved, and secondly the actuation can be integrated into the design of the trailing edge flaps so that no separate mechanical parts are required. Although this should result in fewer reliability problems, they could be harder to fix and the control has to work against the structural rigidity of the trailing edge (depending on the material). Its skin will also probably be subject to severe fatigue. This concept is actually a combination of the idea of an aileron-flap and camber control based on skin deformation, see Figure 3.5.

Figure 3.5: Conceptual design layout of a profile with a deformable trailing edge flap [34]

Two examples of research into deformable trailing flaps follow. At Risoe a controllable rubber trailing edge flap has been developed. The flap is controlled by modifying the pressure in reinforced voids within the elastic flap, see Figure 3.6. A maximum ΔC_l of 0.2 was measured in wind tunnel tests and from simulations using HAWC2 maximum equivalent load reductions of 50% for blade root bending moment [13]. An adaptive compliant wing has been developed by FlexSys Inc. and the US Air Force Research Laboratories that can deflect a flap $\pm 10^\circ$ and at a rate of $20^\circ s^{-1}$, and can twist differentially up to $3^\circ m^{-1}$ over the span of the model [30].

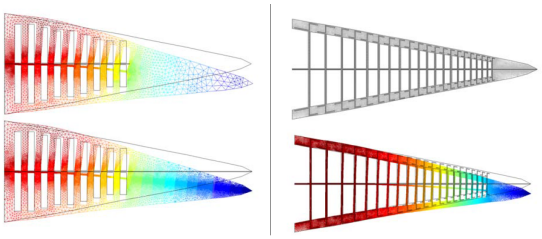

Figure 3.6: A finite element analysis of a controllable rubber trailing edge flap design, showing the deflection of a flap due to pressure in the upper row of voids. Red = high stress, blue = low stress [13]

While deformable trailing edge flaps have better aerodynamic properties and can potentially be integrated into the blades to reduce wear and maintenance issues, the design and extensive testing of such devices is not complete. Hence why the two demonstration plants, and in particular the Vestas V-27 at Risoe [32] where there is a group specifically working on deformable trailing edge flaps [29], still use rigid trailing edge flaps.

The placement of flaps and whether multiple flaps per blade should be used has been considered in [29]. This also raises the question of flap size, with a number of papers opting for flaps with 10% chord, see Table 3.4, while the Sandia demonstration plant has flaps of 20% chord, and the Risoe turbine has flaps of chord 13-18%. The span of the flaps also varies, with the Sandia turbine [35] opting for again 20% of the blade span, and the Risoe turbine three flaps per blade of 5% span each. The dimensions of the flaps, and constraints that they operate to, will have an effect on the load reductions and actuator requirements, it is therefore worth exploring what impact different set-ups will have.

Table 3.4: Flap dimensions and constraints [15]

Paper	Chord [%]	Blade span [%]	Max deflection [±deg]
Riziotis and Voutsinas [36]	10	15-47	6
Andersen et al. [37]	10	63	8
Lackner and van Kuik [2]	10	20	10
Barlas and van Kuik [38]	10	20	10
Andersen et al. [29]	10	15-30	8
Resor et al. [10]	10	24	10
Wilson et al. [9]	10	24	10
Berg et al. [33]	10	25	10
Barlas et al.[15]	10	18	8

3.4 Bladed: wind turbine modelling software

This project is run in partnership with DNV GL, who have developed a world leading, well validated, industry used wind turbine simulation package, Bladed. Other software packages are actually more prevalent in the smart rotor field, such as HAWC and HAWC 2 [29] [14] [39]; and NRELs FAST (AeroDyn) [40] [12] [41], which are also capable of simulating additional flaps.

There are some concerns about the limitations of FAST: inaccurate wake models and problems with the unsteady aerodynamics upon activation of control surfaces; limited modelling resolution of the blades; and limited controller opportunities [33]. In response, as part of the UpWind project DU_SWAMP was created [42]. This aeroservoelastic tool, like FAST, is primarily for academic use. Although this means they tend to be less well validated, they are open source and allow the user to modify the code. DU_SWAMP is in the process of being updated, but has already been used in some published papers regarding the Smart Rotor [35] [10].

Due to the availability of Bladed and concerns regarding FAST, Bladed is used to simulate the smart rotor wind turbine. Bladed has previously been used to compare smart rotor control with individual pitch control [2], and the performance of smart rotor control under extreme gusts [3], however a point raised in these papers is the uncertainty over how activation of the flaps may cause unsteady aerodynamic effects that are not modelled in Bladed. This is discussed in the following section.

3.4.1 Aerodynamic modelling

Bladed uses a combined blade element and momentum theory to model the rotor aerodynamics, with extensions to treat the dynamics of the wake and dynamic stall [43]: 'dynamic inflow' based on [44] and a modified 'Beddoes-Leishman' model [45] respectively. It is a well validated code and is used in the certification of wind turbines. Bladed's general performance is not in doubt then, but its specific application of using it to model flaps on the blades has been cast into doubt [2] [3].

In these two papers Bladed was used to model a full wind turbine model with trailing edge flaps and concern was raised that Bladed does not effectively take account of the unsteady aerodynamics that are a response to changing flap angles, as has been done for instance in [46]. Instead an argument was made that these unsteady aerodynamics were not required as the majority of the control was acting on changes in angle of attack of the blade that are quasi-steady.

This has been recreated using a MATLAB script and turbulent wind field, and can be seen in Figure 3.7 for a 14m/s mean wind speed. The peak in the spectrum is due to the rotational sampling of the wind field, which corresponds to the rotational frequency of the wind turbine, and is caused in the most part by wind shear. This is created by taking the Power Spectral Density (PSD) of the angle of attack for a section of a blade, at radius, r = 52.75m, over a simulation run. The result is a PSD as a function of frequency in Hz, this is then converted to radians per second and the reduced frequency found using the standard formula, $k = \frac{\omega c}{2U}$, with the chord at that blade station, c = 2.518m, and the average perceived velocity of the blade over the simulation, U.

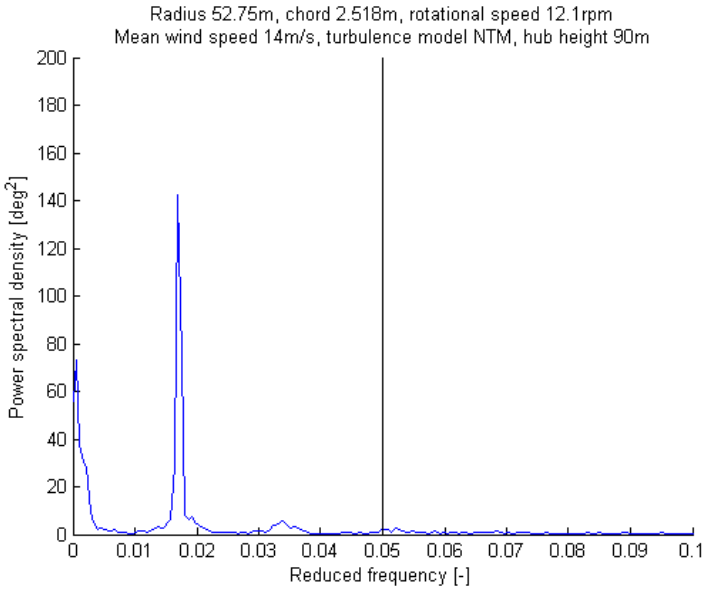

Figure 3.7: Power spectral density plot of the change in angle of attack of the blade

A boundary is then chosen whereby $k < 0.05$ can be considered quasi-steady and $k > 0.05$ unsteady. From the cumulative PSD plot it is clear most energy is in the quasi-steady regime, 80% or more, see Figure 3.8. This is shown as greater than 90% in [2] and [3] possibly due to limiting the reduced frequency between 0 and 1.5. However, although this suggests that the effects are small, they still exist, and indeed closer to the hub the unsteady effects will be greater due to the increased chord and lower perceived wind speed.

Bladed actually takes account of unsteady effects by utilising the Beddoes-Leishman model. An indicial response function is used for modelling attached flow, with the ability to adjust the time lag in the development of trailing edge separation. The concern though is that this is designed to take account of changes in angle of attack (pitching motion), rather than flap actuation. It therefore is worth comparing the two as regards to unsteady aerodynamics.

In [47] the unsteady effects of these two scenarios were looked at. This was done firstly through looking at motion with the flap at a fixed angle and harmonic pitching about the quarter chord point, and secondly with the aerofoil at steady incidence with the flap in oscillatory motion. The parameters: mean angle of attack, flap chord section ratio, flap amplitude, pitch amplitude, and reduced frequency of oscillations; are all varied to determine their effect. The change in lift with a change in angle of attack of the aerofoil was reduced at higher frequency oscillations compared to the static case. At k=0.36, this was between 60-75% of the static case. Equivalently, the effectiveness

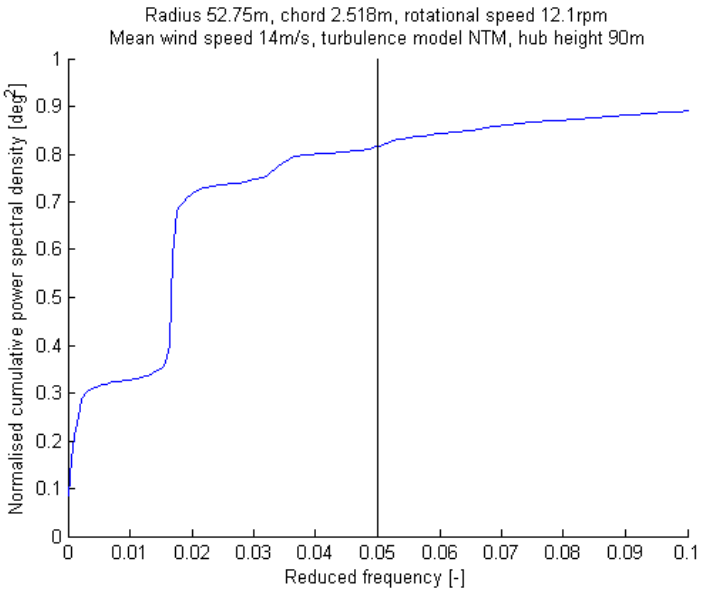

Figure 3.8: Cumulative power spectral density plot of the change in angle of attack of the blade

of the flap was reduced to 60-65% of the static case. Therefore the effectiveness of the flap decreases with increased frequency oscillations. Significantly though, the result of activating both pitch and flap in oscillatory motion results in a near constant lift coefficient when activated with the correct phase difference, Figure 3.9. This suggests that pitch and flap motions result in similar unsteady effects.

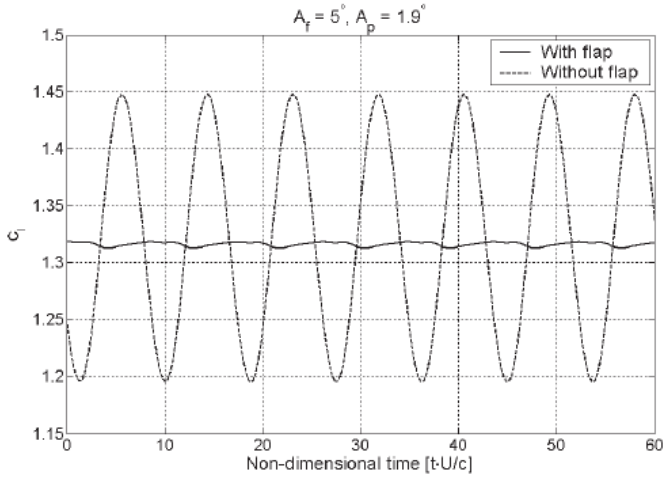

Figure 3.9: Lift signal for the airfoil undergoing harmonic pitch oscillations with and without a trailing edge flap in oscillatory motion. The length of the flap is 10% of the section chord, the mean angle of attack is $\alpha_m = 8^\circ$ and the reduced frequencies of airfoil and flap motion is k = 0.36 [47]

Exploration of the underlying theory helps understand this result. The lift per unit span, L, for

an aerofoil given by Theodorsen's Theory [48], is

$$\begin{aligned} L = &- \rho b^2 \left(v\pi\dot{\alpha} + \pi\ddot{h} - \pi ba\ddot{\alpha} - vT_4\dot{\beta} - T_1 b\ddot{\beta} \right) \\ &- 2\pi\rho vbC \left\{ v\alpha + \dot{h} + b\left(\frac{1}{2} - a\right)\dot{\alpha} \frac{1}{\pi} T_{10} v\beta + b\frac{1}{2\pi} T_{11}\dot{\beta} \right\} \end{aligned} \tag{3.2}$$

where ρ is the density of air, b the half chord width of the aerofoil, v the velocity of the flow, h vertical motion, α the pitch angle, β the flap angle, a the coordinate of rotation and $C = C(k) = F(k) + iG(k)$, Theodorsen's function, with the values of T defined below:

$$T_1 = -\frac{1}{3}\sqrt{1-c^2}\left(2 + c^2\right) + c\cos^{-1} c \tag{3.3}$$

$$T_4 = -\cos^{-1} c + c\sqrt{1-c^2} \tag{3.4}$$

$$T_{10} = \sqrt{1-c^2} + \cos^{-1} c \tag{3.5}$$

$$T_{11} = \cos^{-1} c\,(1-2c) + \sqrt{1-c^2}\,(2-c) \tag{3.6}$$

where c is the position of the flap hinge.

When looking at pure sinusoidal pitching oscillations with the coordinate of rotation positioned at the quarter-chord, this expression can be rewritten in terms of the lift coefficient [49], with $\alpha = \bar{\alpha}e^{i\omega t}$, as

$$C_{L\alpha} = \bar{\alpha}e^{i\omega t}\left[\left(\frac{\pi k}{2} - i\pi\right)k - 2C\left(\pi + i\pi k\right)\right] \tag{3.7}$$

and a similar result can be found for pure sinusoidal flap motion of the form $\beta = \bar{\beta}e^{i\omega t}$,

$$C_{L\beta} = \bar{\beta}e^{i\omega t}\left[\left(iT_4 - T_1 k\right)k - 2C\left(T_{10} + i\frac{T_{11}k}{2}\right)\right] \tag{3.8}$$

The difference between pitch and flap oscillations on the lift are displayed in Figure 3.10 for different reduced frequencies. At low reduced frequencies, of less than 0.1 as suggested by the PSD plots, the reduction in lift is almost identical for both pitch and flap oscillations. The phase is also similar with variations less than 10 degrees. This suggests for the lift coefficient that the same indicial function may be used for both pitch motions and flap motions. The plot also explains the reduction to 60-75% of the static lift experienced at k=0.36 stated above.

To determine how significant these effects are in normal operation an indicial response approach is used to compare the unsteady and quasi-steady lift resulting from the turbulent wind field. A MATLAB script that rotationally samples a turbulent wind field is used for this purpose. The Wagner indicial response function Equation 3.9 as approximated by RT Jones 1938/40 [50], and the Kussner function, Equation 3.10 as approximated by Sears and Sparks 1941 [51], are used:

$$\phi = 1 - 0.165e^{-0.045s} - 0.355e^{-0.3s} \tag{3.9}$$

$$\psi = 1 - 0.5e^{-0.13s} - 0.5e^{-1.0s} \tag{3.10}$$

These are used without using the Duhamel integral, to avoid further approximations being made, and instead are determined every time step on the change in angle of attack at each time

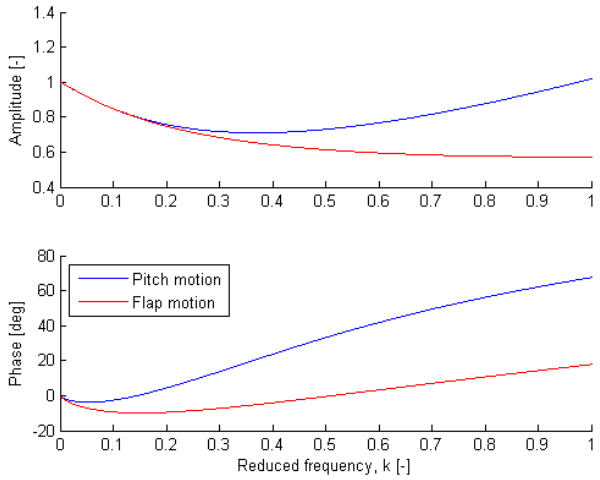

Figure 3.10: Unsteady lift amplitude and phase due to sinusoidal oscillations of pitch and flap angle

step. It should be noted that the distance in semi-chords, s, is considered constant: rather than using the perceived wind speed, the blades speed due to rotation is used.

As can be seen in Figure 3.11 the lift is attenuated and the phase is shifted. The cross-correlation between the quasi-steady and unsteady responses is conducted to assess the time delay involved. It appears to be about 0.01s when the Wagner function is used, and close to 0.05s when the Kussner function is used, see Figure 3.12. This is close to the sampling frequency, so a higher sampling rate may need to be used to verify the results. The effect of this time delay and attenuation of the lift needs to be considered to confirm whether such effects are significant, also variations of the model parameters need to be considered too.

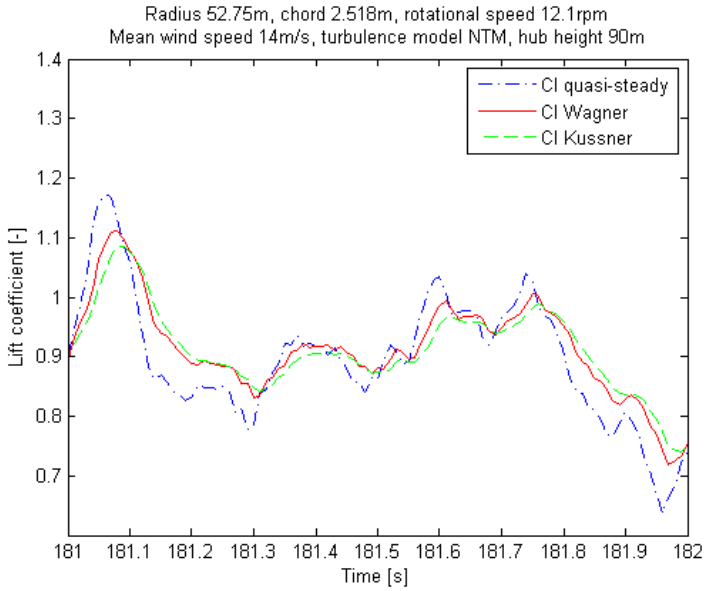

Figure 3.11: Comparison of quasi-steady and unsteady lift coefficients

In [29] the effect of a time lag and also a delay in the control signal were looked at. The lag was

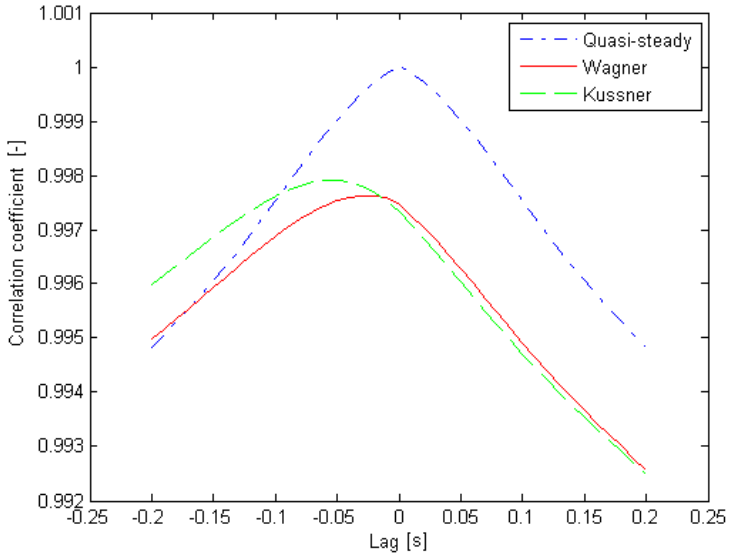

Figure 3.12: Cross-correlations of simulations with quasi-steady lift coefficient

modelled as a first order filter and with the delay the control signals are queued. A 50ms time lag results in a 10% performance drop in the fatigue load reduction potential, shown in Figure 3.13. If the lag due to unsteady aerodynamics is between 10 and 50ms as seen from the above analysis, then this will be detrimental to the load reduction potential when using trailing edge flaps. Therefore, any smart rotor controller that is to be implemented on a real wind turbine should to be created on a model that includes unsteady aerodynamics, or accounts for these uncertainties. As the difference between the unsteady lift coefficient due to pitch and flap oscillations are so similar, Bladed adequately accounts for this.

While the indicial function used in Bladed to determine the unsteady lift coefficient is suitable, it is less clear if the drag or turning moment are. The equivalent equation for the unsteady pitching moment given by Theordorsen's Theory is

$$\begin{aligned} M_\alpha = &-\rho b^2 \left[\pi \left(\frac{1}{2} - a \right) v b \dot{\alpha} + \pi b^2 \left(\frac{1}{8} + a^2 \right) \ddot{\alpha} \right. \\ &+ \left(T_4 + T_{10} \right) v^2 \beta + \left(T_1 - T_8 - \left(c - a \right) T_4 + \frac{1}{2} T_{11} \right) v b h \dot{\beta} \\ &\left. - \left(T_7 + \left(c - a \right) T_1 \right) b^2 \ddot{\beta} - a \pi b \ddot{h} \right] \\ &+ 2 \rho v b^2 \pi \left(a + \frac{1}{2} \right) C \left\{ v \alpha + \dot{h} + b \left(\frac{1}{2} - a \right) \dot{\alpha} + \frac{1}{\pi} T_{10} v \beta + b \frac{1}{2\pi} T_{11} \dot{\beta} \right\} \end{aligned} \tag{3.11}$$

When the position of rotation is about the quarter-chord point the circulatory terms reduce to zero. This leaves the non-circulatory terms, which for a pitching aerofoil result in

$$C_{M\alpha} = -\frac{\bar{\alpha}}{2} e^{i\omega t} \left(i\pi - \frac{3}{8} \pi k \right) k \tag{3.12}$$

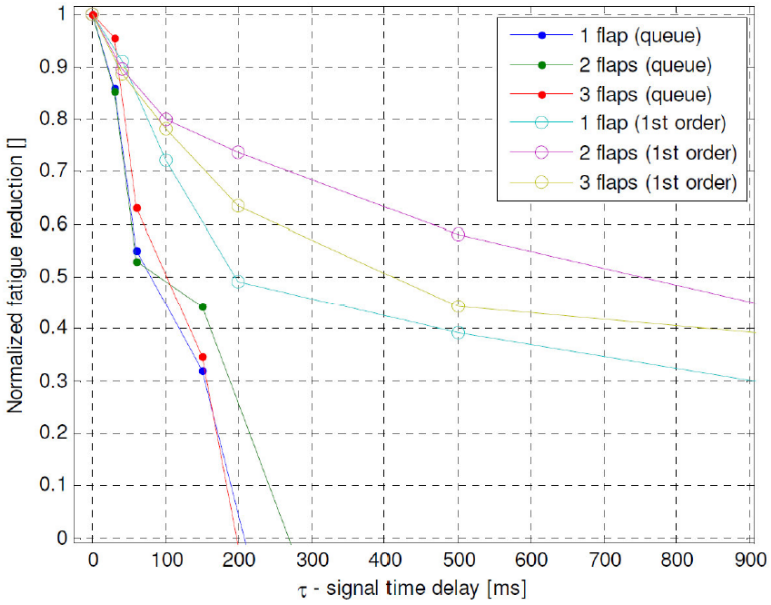

Figure 3.13: Effect of delayed signal (queue) and first order delay (1st order) on load reduction [29]

and for a flap in oscillation

$$C_{M\beta} = -\frac{\bar{\beta}}{2}e^{i\omega t}\left[(T_4+T_{10})+\left(T_1-T_8-\left(c+\frac{1}{2}\right)T_4+\frac{T_{11}}{2}\right)ik+\left(T_7+\left(c+\frac{1}{2}\right)T_1\right)k^2\right] \tag{3.13}$$

where T_7 and T_8 are defined as follows

$$T_7 = -\left(\frac{1}{8}+c^2\right)\cos^{-1}c+\frac{1}{8}c\sqrt{1-c^2}\,(7+2c) \tag{3.14}$$

$$T_8 = -\frac{1}{3}\sqrt{1-c^2}\,(2c^2+1)+c\cos^{-1}c \tag{3.15}$$

A similar plot as before for the lift is shown for the pitching moment in Figure 3.14. The differences between pitch oscillations and flap oscillations are more pronounced and if the same method for taking account of unsteady aerodynamics is used for flaps as for changes in pitch, the phase and amplitude of the turning moment will be incorrectly determined. Indeed the turning moment due to the flap is relatively constant regardless of the reduced frequency and the phase delay is also small, making quasi-steady probably more appropriate than use of unsteady calculations based on pitch motion. Future studies will need to be done to confirm what effect this has, but looking at the twisting of the blade when either collective pitch control, individual pitch control or smart rotor control are active, see Figure 3.15, suggests it is not vital to determine accurately during attached flow operation.

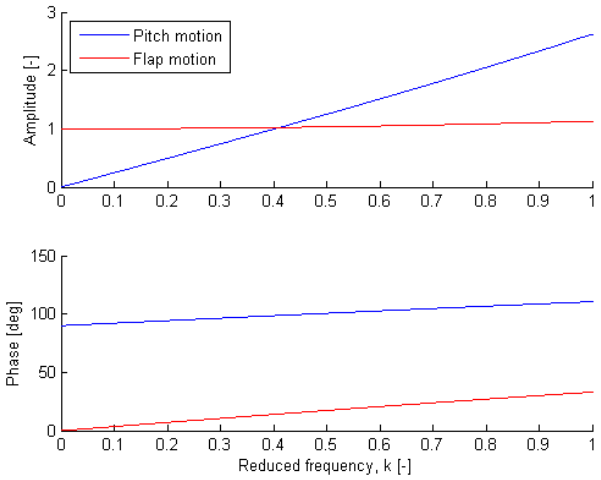

Figure 3.14: Unsteady pitch moment amplitude and phase due to sinusoidal oscillations of pitch and flap angle

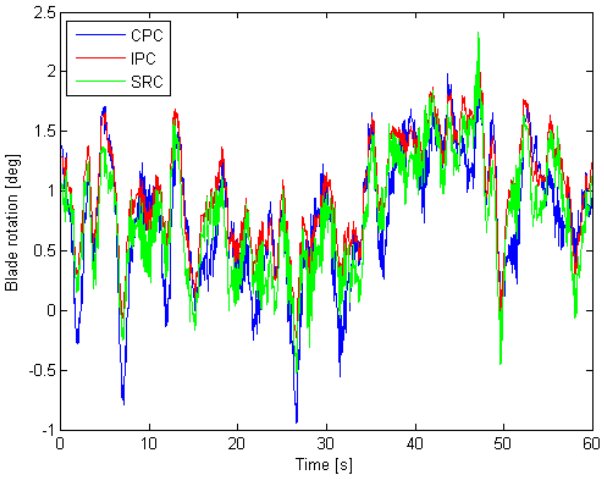

Figure 3.15: Blade rotation near the tip about the blade principal axis for collective pitch control (CPC), individual pitch control (IPC) and smart rotor control (SRC)

3.5 Discussion

As regards to smart rotor control of wind turbines a number of paths have been explored in the literature. In particular the use of individual pitch control strategies for the smart rotor is interesting and indeed the use of both individual pitch and smart rotor control at the same time. The advantages in load reduction are clear, but it is less clear why one would adopt one over the other or indeed combine the two. Indeed the costs and drawbacks of both systems, for example of faults occurring, have not been quantitatively taken into account.

The majority of the control papers and indeed the research into devices have focussed on trailing edge flaps, with control papers devoting time to the placement of flaps and the corresponding sensors, but with less detail on their design, activation and dimensions. This has led to a wide variety of systems, which make direct comparisons difficult.

Alongside this concern about comparisons are the environmental conditions under which the various controllers have been tested and the differing metrics used to assess load reduction. Use of specific conditions or metrics can lead to biased results. It is therefore seen as imperative to both quantify some of the sensitivities to external conditions, but also lay out clearly the method of assessing the wind turbine's performance.

It is also worth considering the sensors to be used, both accelerometers and strain gauges are often the proposed sensing device for advanced control, with dq-axis control dominated by blade root bending moment measurements and PD control focussed on blade deflections. These two options are both easily implemented in Bladed software.

Whilst Bladed is used for certification of wind turbines it has not been validated for smart rotor control, despite this the use of the outboard blade section for the flaps reduce the probability of unsteady aerodynamics coming into play. Additionally, the effect on the lift coefficient is similar for both pitching and flap motion. This means corrections to the lift are valid for low values of the reduced frequency. On the other hand, whilst the turning moment is significantly different for the two types of motion, the effect that this moment has on the wind turbine appears marginal.

References

[1] E. A. Bossanyi, "Individual Blade Pitch Control for Load Reduction," *Wind Energy*, vol. 6, pp. 119–128, Apr. 2003.

[2] M. A. Lackner and G. A. M. van Kuik, "A comparison of smart rotor control approaches using trailing edge flaps and individual pitch control," *Wind Energy*, vol. 13, pp. 117–134, Mar. 2010.

[3] M. A. Lackner and G. A. M. van Kuik, "The Performance of Wind Turbine Smart Rotor Control Approaches During Extreme Loads," *Journal of Solar Energy Engineering*, vol. 132, 2010.

[4] T. K. Barlas and G. A. M. van Kuik, "Aeroelastic modelling and comparison of advanced active flap control concepts for load reduction on the Upwind 5MW wind turbine," in *EWEC*, (Marseille, France), 2009.

[5] W. E. Leithead and V. Neilson, "Alleviation of Unbalanced Rotor Loads by Single Blade Controllers," in *EWEC*, (Marseille, France), 2009.

[6] D. Robb, C. Gonzalez, P. Clive, W. E. Leithead, and A. Giles, "Offshore Low Level Jets - Mitigating the Damage with Lidar and Individual Blade Control," in *EWEA Offshore*, (Messe Frankfurt, Germany), 2013.

[7] W. P. Engels, S. K. Kanev, and T. G. V. Engelen, "Distributed blade control," in *TORQUE: The Science of Making Torque from Wind*, (Heraklion, Crete, Greece), EWEA, 2010.

[8] T. G. V. Engelen, "Design model and load reduction assessment for multi-rotational mode individual pitch control (higher harmonics control)," in *EWEC*, (Athens, Greece), 2006.

[9] D. G. Wilson, B. R. Resor, D. Berg, T. K. Barlas, and G. A. M. van Kuik, "Active Aerodynamic Blade Distributed Flap Control Design Procedure for Load Reduction on the UpWind 5MW Wind Turbine," in *48th AIAA Aerospace Sciences Meeting Including the New Horizons Forum and Aerospace Exposition*, (Orlando, Florida), American Institute of Aeronautics and Astronautics, 2010.

[10] B. R. Resor, D. G. Wilson, D. Berg, J. Berg, T. K. Barlas, J.-W. van Wingerden, and G. A. M. van Kuik, "Impact of higher fidelity models on simulation of active aerodynamic load control for fatigue damage reduction," in *48th AIAA Aerospace Sciences Meeting Including the New Horizons Forum and Aerospace Exposition*, (Orlando, Florida), 2010.

[11] D. G. Wilson, D. Berg, B. R. Resor, M. F. Barone, and J. Berg, "Combined individual pitch control and active aerodynamic load controller investigation for the 5MW upwind turbine," in *AWEA Wind Power Conference*, (Chicago, Illinois), 2009.

[12] D. G. Wilson and D. Berg, "Active aerodynamic blade control design for load reduction on large wind turbines," in *EWEA*, (Marseille, France), 2009.

[13] H. A. Madsen, P. B. Andersen, T. L. Andersen, C. Bak, and T. Buhl, "The potentials of the controllable rubber trailing edge flap (CRTEF)," in *EWEC*, (Warsaw, Poland), 2010.

[14] T. J. Larsen, H. A. Madsen, and K. Thomsen, "Active load reduction using individual pitch, based on local blade flow measurements," *Wind Energy*, vol. 8, pp. 67–80, Jan. 2005.

[15] T. K. Barlas, G. van der Veen, and G. A. M. van Kuik, "Model predictive control for wind turbines with distributed active flaps: incorporating inflow signals and actuator constraints," *Wind Energy*, vol. 15, pp. 757–771, July 2012.

[16] J. K. Rice and M. Verhaegen, "Robust and distributed control of a smart blade," *Wind Energy*, vol. 13, pp. 103–116, Mar. 2010.

[17] T. K. Barlas, "Smart rotor blades and rotor control for wind: State of the Art: Knowledge Base Report for UpWind WP 1B3," tech. rep., Delft Technical University, 2006.

[18] T. K. Barlas and G. A. M. van Kuik, "Review of state of the art in smart rotor control research for wind turbines," *Progress in Aerospace Sciences*, vol. 46, pp. 1–27, Jan. 2010.

[19] P. B. Andersen, *Advanced Load Alleviation for Wind Turbines using Adaptive Trailing Edge Flaps: Sensoring and Control*. PhD thesis, Technical University of Denmark, 2010.

[20] T. Behrens and W. J. Zhu, "Feasibility of Aerodynamic Flap Hinge Moment Measurements as Input for Load Alleviation Control," in *EWEA*, (Brussels, Belgium), 2011.

[21] R. P. Benedict, *Fundamentals of Temperature, Pressure, and Flow Measurements*. John Wiley & Sons Ltd., third ed., 1984.

[22] D. Schlipf, L. Y. Pao, and P.-W. Cheng, "Comparison of feedforward and model predictive control of wind turbines using LIDAR," in *2012 IEEE 51st IEEE Conference on Decision and Control (CDC)*, (Maui, Hawaii, USA), pp. 3050–3055, IEEE, Dec. 2012.

[23] M. Harris, M. Hand, and A. D. Wright, "Lidar for turbine control," tech. rep., NREL, Colorado, USA, 2006.

[24] M. Mirzaei, L. C. Henriksen, N. K. Poulsen, H. H. Niemann, and M. H. Hansen, "Individual pitch control using LIDAR measurements," in *2012 IEEE International Conference on Control Applications*, no. October, (Dubrovnik, Croatia), pp. 1646–1651, IEEE, Oct. 2012.

[25] R. Rolfes, S. Zerbst, G. Haake, J. Reetz, and J. P. Lynch, "Integral SHM-System for Offshore Wind Turbines Using Smart Wireless Sensors," in *Proceedings of the 6th International Workshop on Structural Health Monitoring*, (Stanford, CA), 2007.

[26] B. F. Sorensen, L. Lading, P. Sendrup, M. McGugan, C. P. Debel, O. J. D. Kristensen, G. Larsen, A. M. Hansen, J. Rheinlander, J. Rusborg, and V. D. Jorgen, "Fundamentals for Remote Structural Health Monitoring of Wind Turbine Blades - a Preproject," tech. rep., Risoe National Laboratory, Roskilde, Denmark, 2002.

[27] C. C. Ciang, J.-R. Lee, and H.-J. Bang, "Structural health monitoring for a wind turbine system: a review of damage detection methods," *Measurement Science and Technology*, vol. 19, Dec. 2008.

[28] M. Rumsey and J. A. Paquette, "Structural health monitoring of wind turbine blades," in *The 15th International Symposium on: Smart Structures and Materials & Nondestructive Evaluation and Health Monitoring* (W. Ecke, K. J. Peters, and N. G. Meyendorf, eds.), Mar. 2008.

[29] P. B. Andersen, L. C. Henriksen, M. Gaunaa, C. Bak, and T. Buhl, "Deformable trailing edge flaps for modern megawatt wind turbine controllers using strain gauge sensors," *Wind Energy*, vol. 13, pp. 193–206, Mar. 2010.

[30] S. J. Johnson, J. P. Baker, C. P. van Dam, and D. Berg, "An overview of active load control techniques for wind turbines with an emphasis on microtabs," *Wind Energy*, vol. 13, pp. 239–253, Mar. 2010.

[31] J. Berg, B. R. Resor, J. Paquette, and J. White, "SMART Wind Turbine Rotor: Design and Field Test," tech. rep., Sandia National Laboratories, Albuquerque, New Mexico and Livermore, California, 2014.

[32] D. Castaignet, T. K. Barlas, T. Buhl, N. K. Poulsen, J. J. Wedel-Heinen, N. A. Olesen, C. Bak, and T. Kim, "Full-scale test of trailing edge flaps on a Vestas V27 wind turbine: active load reduction and system identification," *Wind Energy*, vol. 17, pp. 549–564, Apr. 2014.

[33] D. Berg, D. G. Wilson, B. R. Resor, J. Berg, T. K. Barlas, A. Crowther, and C. Halse, "System ID Modern Control Algorithms for Active Aerodynamic Load Control and Impact on Gearbox," in *TORQUE: The Science of Making Torque from Wind*, (Heraklion, Crete, Greece), 2010.

[34] T. Buhl, C. Bak, M. Gaunaa, and P. B. Andersen, "Load alleviation through adaptive trailing edge control surfaces: ADAPWING overview," in *EWEC*, (Athens, Greece), 2006.

[35] D. Berg, J. Berg, J. White, B. R. Resor, and M. Rumsey, "Design, Fabrication, Assembly and Initial Testing of a SMART Rotor," in *49th AIAA Aerospace Sciences Meeting including the New Horizons Forum and Aerospace Exposition*, vol. 4-7, (Reston, Virigina), American Institute of Aeronautics and Astronautics, Jan. 2011.

[36] V. Riziotis and S. Voutsinas, "Aero-elastic modelling of the active flap concept for load control," in *EWEC*, (Brussels, Belgium), 2008.

[37] P. B. Andersen, L. C. Henriksen, M. Gaunaa, C. Bak, and T. Buhl, "Integrating deformable trailing edge geometry in modern mega-watt wind turbine controllers," in *EWEC*, (Brussels, Belgium), 2008.

[38] T. K. Barlas and G. A. M. van Kuik, "Aeroelastic modelling and comparison of advanced active flap control concepts for load reduction on the upwind 5MW wind turbine," in *European Wind Energy Conference*, (Marseille, France), 2009.

[39] L. Bergami, "Adaptive Trailing Edge Flaps for Active Load Reduction," in *7th PhD Seminar on Wind Energy in Europe*, (Delft University of Technology, Netherlands), 2011.

[40] D. Berg, D. G. Wilson, B. R. Resor, M. F. Barone, J. Berg, S. Kota, and G. Ervin, "Active aerodynamic blade load control impacts on utility-scale wind turbines," in *AWEA Windpower*, (Chicago, Illinois, USA), 2009.

[41] D. Berg, D. G. Wilson, M. F. Barone, B. R. Resor, J. Berg, S. Kota, G. Ervin, and D. Maric, "The impact of active aerodynamic load control on fatigue and energy capture at low wind speed sites," in *EWEC*, (Marseille, France), US Government: Sandia National Laboratories, FlexSys Inc., 2009.

[42] G. A. M. van Kuik, "Final Report, showing the potential of smart rotor blades and rotor control," tech. rep., Delft University of Technology, Delft, Netherlands, 2011.

[43] E. A. Bossanyi, "Bladed Theory Manual," tech. rep., DNV GL, Bristol, 2013.

[44] D. M. Pitt and D. A. Peters, "Theoretical prediction of dynamic-inflow derivatives," *Vertica*, vol. 5, pp. 21–34, 1981.

[45] J. G. Leishman and T. S. Beddoes, "A Semi-Empirical Model for Dynamic Stall," *Journal of the American Helicopter Society*, vol. 34, no. 3, pp. 3–17, 1989.

[46] P. B. Andersen, M. Gaunaa, C. Bak, and M. H. Hansen, "A Dynamic Stall Model for Airfoils with Deformable Trailing Edges," *Journal of Physics: Conference Series*, vol. 75, July 2007.

[47] N. Troldborg, "Computational study of the Risø-B1-18 airfoil with a hinged flap providing variable trailing edge geometry," *Wind Engineering*, vol. 29, no. 2, pp. 89–114, 2005.

[48] T. Theodorsen, "General theory of aerodynamic instability and the mechanism of flutter," *NACA Technical Report,*, vol. 496, pp. 413–433, 1935.

[49] J. G. Leishman, "Challenges in modelling the unsteady aerodynamics of wind turbines," *Wind Energy*, vol. 5, pp. 85–132, Apr. 2002.

[50] R. T. Jones, "The unsteady lift of a wing of finite aspect ratio," tech. rep., NACA, Langley, VA, 1939.

[51] W. R. Sears and B. Sparks, "On the Reaction of an Elastic Wing to Vertical Gusts," *Journal of the Aeronautical Sciences (Institute of the Aeronautical Sciences)*, vol. 8, pp. 64–67, Dec. 1941.

Chapter 4

Baseline and controllers

To assess the performance of the smart rotor concept and the control strategies applied to it a baseline needs to be specified. This requires a well validated model, as described in Section 3.4 of the previous chapter, a reference wind turbine, and a baseline controller from which to draw comparisons. The advanced load reduction control strategies for the comparisons are also needed.

Additionally, load cases, similar to that which the wind turbine would experience in real life, and a series of metrics, that satisfactorily show the influence of the smart rotor, are also required and are considered in Chapter 5 and Chapter 6.

In this chapter the baseline wind turbine, central controller and advanced load reduction controls are described. To this end in Section 4.1 the UpWind/NREL 5MW conceptual three-bladed upwind variable-speed pitch-to-feather regulated wind turbine is detailed as the baseline wind turbine, upon which trailing edge flaps are added to test smart rotor control, Section 4.2. The baseline controller is then explained in Section 4.3, with two advanced load control strategies considered in Section 4.4. A validation of the controllers is given in Section 4.5.

4.1 Baseline wind turbine

The NREL 5-MW reference wind turbine is a conceptual three-bladed upwind variable-speed pitch-to-feather regulated wind turbine. Its size makes it suitable for trialling advanced concepts such as smart rotor control and the open source definition given in [1] has meant that it has been extensively used for simulation and modelling work. For example, as stated in the definition, large projects such as the US Department of Energy's Wind and Hydropower Technologies Program, the International Energy Agency Wind Annex XXIII Subtask 2 Offshore Code Comparison Collaboration and the pan-European UpWind research project have used it. Consequently, many authors studying smart rotor wind turbines have also adopted the modified NREL 5-MW wind turbine as used in the UpWind project, often referred to as the UpWind 5-MW machine [2] [3] [4] [5] [6] [7].

There are though other wind turbines that have also been used for control research purposes. For example the WindPACT 1.5MW turbine [8] [7], the DOWEC project wind turbine [9] [10], and the Supergen project exemplar wind turbines [11] [12]. Others have also used unspecified turbines. A major drawback though of not specifying what turbine is used, or the details of the wind turbine, is that comparisons with other works are made difficult. However, the current reference turbines, although some extensively used, may not be of best design when considering the smart rotor concept. For instance the smart rotor concept is of growing importance with the increase in rotor diameter, so larger than 5MW turbines may be more suitable for the inclusion of the smart rotor, perhaps on turbines of 10 or 20 megawatts, as considered in the UpWind project [13]. On these very large rotors the smart rotor control will have the ability to reduce turbulent wind field loads across the blade span, not controllable by current methods, and so the benefit of using the concept may be greater. Nevertheless, the 5-MW wind turbine is a good place to start and, due to the prevalence of the NREL 5MW wind turbine, it is used in this work. Additionally, thanks to both the NREL 5MW wind turbine and the UpWind project being publicly funded they are open source. The 9th version UpWind/NREL 5-MW wind turbine has been acquired for use from Jan-Willem van Wingerden at Delft University, an UpWind project member.

4.1.1 UpWind/NREL 5-MW description

The UpWind 5-MW wind turbine model acquired is based on the NREL 5MW wind turbine as described in detail in [1], which is based on published information from wind turbine manufacturers, in particular the Multibrid M5000 [14] and the REpower 5M machine [15], and also previous conceptual models used in the WindPACT [16], RECOFF [17] and DOWEC [18] projects. The full details for the blade structure and aerodynamics, hub and nacelle properties, drivetrain, tower and controllers are all given in the appendices: Appendix A includes the structural characteristics and general model parameters along with the aerodynamic performance coefficients for the standard blade profiles, Appendix B includes the method of acquiring the aerodynamic characteristics for the blade profiles with the flap present, and Appendix C contains the C++ code for the external controllers, along with a compiled controller. The general properties of the baseline wind turbine acquired are given in Table 4.1, and some key parameters are highlighted in this section.

The major change that has been made to the NREL model is the tower. The tower in the definition is a land-based design, but because wind turbines of this size are likely to be placed offshore, a monopile foundation has been used instead [18], and the turbine situated offshore. This

Table 4.1: Characteristics of NREL 5MW reference wind turbine

Rating	5 MW
Rotor orientation, configuration	Upwind, 3 blades
Control	Variable speed, collective pitch
Drivetrain, transmission ratio	High speed multiple-stage gearbox, 97
Rotor, hub diameter	126m, 3m
Hub height	90m
Cut-in, rated, cut-out wind speed	3 m/s, 11.4 m/s, 25 m/s
Cut-in, rated rotor speed	6.9 rpm, 12.1 rpm
Rated tip speed	80 m/s
Overhang, shaft tilt, precone	5 m, 5 degrees, 2.5 degrees
Rotor mass	110,000 kg
Nacelle mass	240,000 kg
Tower mass	347,460 kg
Coordinate location of overall c.o.m.	(-0.2 m, 0.0 m, 64.0 m)

Table 4.2: Natural frequencies of the blades and tower calculated in Bladed

Frequency (Hz)	Damping ratio	Mode type
0.681	0.004775	Blade flapwise normal mode
1.083	0.004775	Blade edgewise normal mode
1.971	0.004775	Blade flapwise normal mode
4.021	0.004775	Blade edgewise normal mode
4.523	0.004775	Blade flapwise normal mode
0.278	0.01	Tower side-side translational attachment mode
0.28	0.01	Tower fore-aft translational attachment mode
1.706	0.01	Tower side-side rotational attachment mode
2.023	0.01	Tower fore-aft rotational attachment mode
3.017	0.01	Tower side-side normal mode
3.017	0.01	Tower fore-aft normal mode
7.578	0.01	Tower side-side normal mode

adjustment has the effect of reducing the tower's natural frequency, from 0.32 to 0.28Hz. A tower structural-damping ratio of 1% critical is assumed in all modes of the isolated tower, as per the NREL definition.

The drivetrain properties are from the REpower 5M machine, with a multiple-stage gearbox assumed, but with no frictional losses, instead the generator is assumed to have an electrical efficiency of 94.4%, roughly the same as the total rotor-mechanical to electrical losses of the DOWEC machine at rated power. The blade extensional stiffness for the NREL 5MW reference wind turbine came from a rule of thumb derived from the WindPACT project, but was not considered important due to the low rotational speed of the turbine. A structural damping ratio of 0.477465% is used for all modes of the isolated blade, corresponding to the 3% logarithmic decrement as used in the DOWEC study. The natural frequencies of the blades and tower are shown in Table 4.2 for reference.

The blade pitch actuator is modelled as a second order passive filter with a natural frequency of 1Hz and damping ratio of 0.7 as in the UpWind project. This is a lower bandwidth than that defined in the NREL report, which was set unrealistically high due to the limitation of FAST not

including actuator dynamics [1]. A pitch rate limit of 8 degrees/s is also applied.

The blades themselves consist of two cylinder and six aerofoil profiles. The aerofoil profiles are the Delft DU40, DU35, DU30, DU25, DU21 and the NACA64-6. While the aerodynamic characteristics for the Delft aerofoils used are those given in the definition, for the NACA64-6 aerofoil the 2D aerodynamic characteristics for angles of attack between -20 and +20 degrees are obtained using XFOIL, which can rapidly determine the aerodynamic coefficients of a 2D aerofoil [19]. These angles of attack cover the normal power production operating region of the wind turbine.

The reason XFOIL is used is that the blade sections where the NACA aerofoil profile is present are also those where the trailing edge flap smart rotor devices are located. XFOIL is used in the determination of the aerodynamic characteristics for these flaps, and therefore so as to avoid discontinuities that might occur due to a different modelling processes the zero flap angle NACA64-6 aerodynamic characteristics are also determined using this method. The polars for this are displayed in Figure 4.1 and the method of including flaps described in the following section.

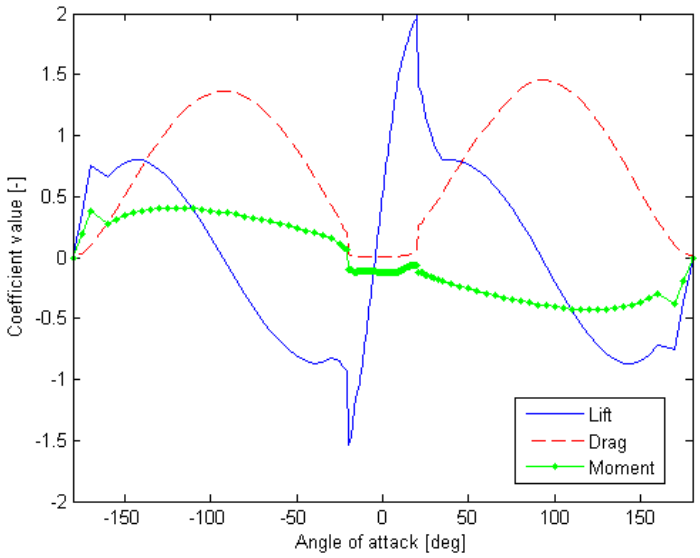

Figure 4.1: Aerodynamic characteristics of the NACA64-6 aerofoil

4.2 Smart rotor trailing edge flaps

As seen in the technical review, Section 3.3, there are a number of actuators that may be used to create a smart rotor wind turbine and despite desires to keep the devices as general as possible for control purposes, realistic device characteristics help in validating this work. Therefore trailing edge flaps are modelled here. This choice is based on the fact that these devices are aerodynamically well understood, due to their similarity to the ailerons found on aircraft wings, and have been implemented on the two smart rotor demonstration plants which is encouraging [20] [21].

The properties chosen for these devices are deliberately similar to the Sandia smart rotor demonstration plant [21]. They are modelled as consisting of 20% of the blade chord width, 20% of the rotor radius and centred at 87% of the rotor radius, such that there is a gap between the end of the flap and tip of the blade to minimise the impact of the blade tip vortex. The use of percentage values is beneficial when it comes to scaling the wind turbine, though only the 5MW model is used here. The flaps are limited to a maximum deflection angle of 20 degrees, with the aerodynamic characteristics of these flaps determined using XFOIL.

The span of the blade on which the flaps are located is from 48.51m to 61.11m. Along the entirety of this section the NACA64-6 aerofoil profile is used, with 18% thickness. This profile is loaded into XFOIL as a set of polar coordinates, before adjusting the flap angle in XFOIL. This is done at the 0.8 chord value, using the camber line as the hinge point. Flap angles up to deflections of 22 degrees are recorded to fulfil the operating regime of the flaps from +20 degrees to -20 degrees.

XFOIL is then used to determine the lift, drag and moment coefficients for the aerofoil profile for angles of attack between -20 and +20 degrees, which encompass the standard operating region for the wind turbine blades. The change in lift due to the flap is shown for the 0 degree angle of attack case in Figure 4.2. As can be seen the lift coefficient can be altered by 1.89, from -0.61 to 1.28 at minimum and maximum deployments respectively, with a zero deployment lift coefficient of 0.53. The reduction in the lift slope at high angles of deployment is due to boundary layer separation and the onset of stall.

These results can be compared to the change in lift coefficient when pitching the blade, equivalent to a change in the angle of attack, displayed in Figure 4.3. The angle of attack of the blade can be seen to achieve a greater change in lift coefficient and has a steeper gradient. This means that to achieve the same change in lift, the flap would need to move by 1.89 degrees for every 1 degree change in pitch.

Due to the shorter span of the blade covered by the flap, one fifth of the rotor diameter, the effectiveness of the flap is reduced further compared to pitching of the entire blade. Figure 4.4 shows the effectiveness of the flap compared to the pitch at a steady 16 m/s wind speed. As can be seen a 1 degree change in pitch angle actually requires a 4.6 degree change in the flap angle to maintain rotor speed. This is actually 2.4 times rather than 5 times the pitch angle required than might be expected due to only 20% of the span being with the flap. The lower value is a result of the outboard section providing a higher proportion of the torque, not least because it is approximately 36% of the swept rotor area. By increasing the size of the flap the ratio of pitch angle to flap angle can also be reduced, as demonstrated by increasing the chord width in Chapter 7, which has certain benefits for the pitch actuator.

The flap rates of the Sandia demonstration plant are high, averaging 200 degree/s and peaking at 330 degrees/second [22]. Rather than accept these values, which might be hard to achieve on a

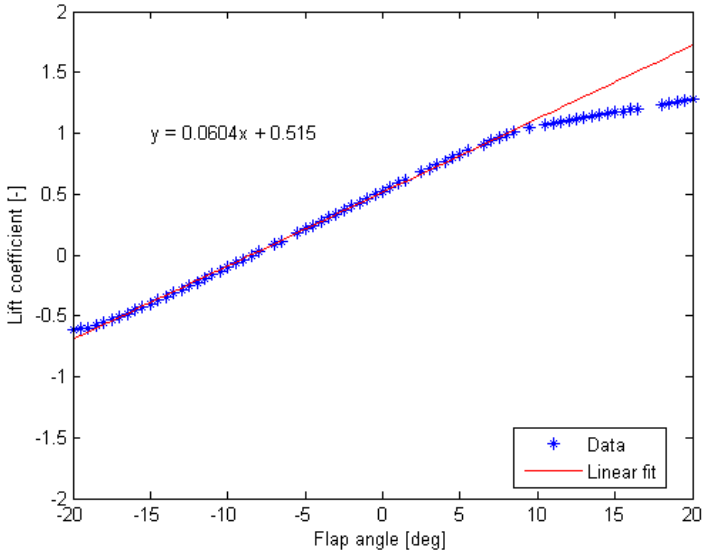

Figure 4.2: Lift coefficient at 0 degrees angle of attack for various flap angles

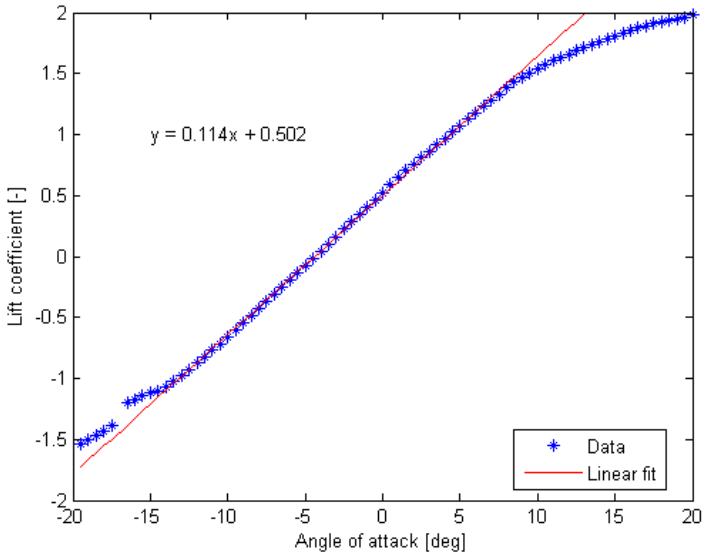

Figure 4.3: Lift coefficient for various angles of attack with 0 degree flap angle

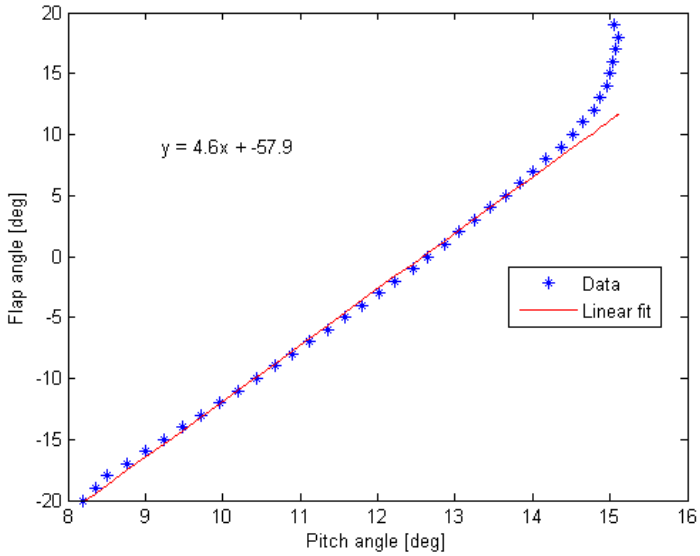

Figure 4.4: Required pitch angle at 16m/s wind speed for various flap angles

large wind turbine, the flaps simulated are not rate or acceleration limited in the model. Instead the maximums reached during the simulations are shown for reference.

The flap actuators are set as having an identical response as the pitch actuators and so modelled by a 2nd order passive filter with a natural frequency of 1Hz and damping coefficient of 0.7. This is seen as a conservative approach, as flap actuators will likely be able to respond much faster compared to pitch actuators designed for rotating the entire blade. Future work should adjust this accordingly.

4.3 Collective pitch control

Two baseline variable speed pitch controllers are described in this section. The NREL 5MW controller as supplied in the description of the reference wind turbine [1] and the UpWind project controller described in [6]. Both are variable speed pitch regulated controllers as portrayed in the torque-speed diagram in Figure 4.5.

The NREL 5MW controller is much simpler than the UpWind controller, however it lacks some of the performance of the UpWind controller and some of the more advanced controller options. A difficulty with this is that it might not accurately represent the controllers that are currently used in commercial wind turbines. However, an advantage is that the simplicity means it may be easier to determine the effects that a smart rotor control strategy is having on the wind turbine. Neither of these controllers are original and both are well documented so both act as a good baseline from which to start.

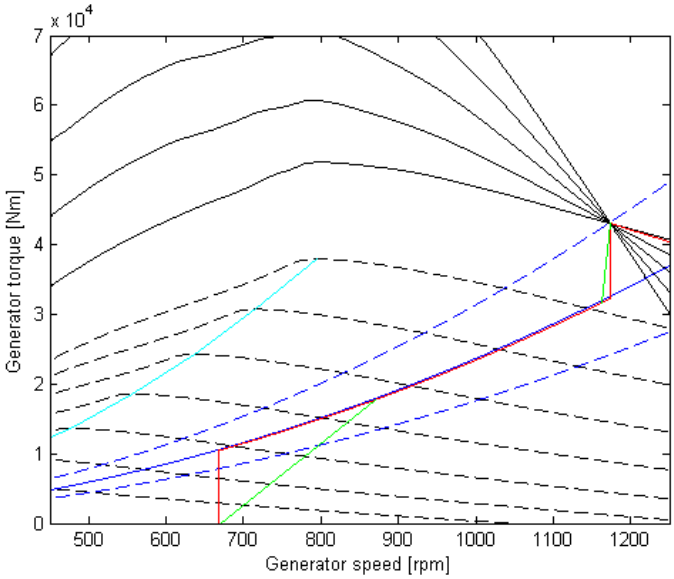

Figure 4.5: Torque-generator speed diagram for the two controllers: green = NREL 5MW, red = UpWind control strategy

The NREL 5MW and UpWind controllers are programmed in C++ using the FORTRAN controller description in the NREL 5MW definition report as a template [1], with the full code attached in Appendix C along with a compiled UpWind controller for Bladed. What follows is a detailed description of these two controllers.

4.3.1 NREL 5MW controller

The NREL 5MW wind turbine is a variable speed pitch to feather machine, as such the controller has two main control systems: one to manage the generator torque for optimum energy capture below rated, and the other to regulate the generator speed above rated by collectively pitching the blades. Both control systems use the generator speed measurement as the sole input.

The torque control system operates differently depending on the region of operation. Four distinct regions are described by the generator speed in each region, see Figure 4.8.

Torque control

In region 1, before cut-in, the generator torque is set to zero to encourage acceleration of the rotor. In region 1.5 the generator torque demand, $Q_{GenD:R1.5}$, is a linear function of the filtered high speed shaft generator speed, ω_{HSSF}, given by the equation

$$Q_{GenD:R1.5} = m_{R1.5}(\omega_{HSSF} - \omega_{cut\_in}) \tag{4.1}$$

The slope, $m_{R1.5}$, is set so that it goes from zero at the generator cut-in speed, ω_{cut_in}, to reach the optimum power curve at 30% above the rotor cut-in speed. The cut-in speed at the high speed shaft where the signal is measured is 670rpm; this corresponds to 6.9rpm at the rotor which is the REpower 5MW cut-in speed, as the NREL 5MW machine has a 97:1 gearbox ratio. 30% on top of this is 871rpm.

The optimum power curve is given by

$$Q_{GenD:R2} = K_{R2}\omega_{HSSF}^2 \tag{4.2}$$

The peak power coefficient of 0.482 was found to occur at a tip speed ratio of 7.55 and resulted in an optimal constant of proportionality of, $K_{R2} = 0.0255764 Nm/rpm^2$. This peak power tracking is done in region 2, and is also used to calculate the value of the torque at the end of region 1.5 as well as the start of region 2.5. Region 2.5 ramps from 99% of the generator speed up to the rated power of the generator based on a generator-slip percentage of 10%.

Above rated, in region 3, the generator torque is inversely proportional to the generator speed to hold the power output constant at rated power, P_{rated}.

$$Q_{GenD:R3} = P_{rated}/\omega_{HSSF} \tag{4.3}$$

An alternative control method in region 3 is to hold the torque constant, though this leads to larger power fluctuations. The switching logic between the regions is based on the high-speed-shaft generator speed measurement. This measurement is low pass filtered to avoid high-frequency excitation of the controller. The controller signal is also saturated based on maximum torque and maximum torque rate of the generator.

The filter on the high speed shaft generator speed measurement is a simple recursive, single-pole low-pass filter with exponential smoothing. Defined by

$$y[n] = (1 - \alpha)u[n] + \alpha y[n - 1] \tag{4.4}$$

with

$$\alpha = e^{2\pi T_s f_c} \tag{4.5}$$

where y is the filtered generator speed, u is the unfiltered generator speed, α is the low-pass filter coefficient, n is the discrete-time-step counter, T_s the discrete time step and f_c the corner frequency. The corner frequency was set at 0.25Hz, roughly one-quarter of the blades first edgewise natural frequency. The filtered generator speed measurement is also used in the pitch controller described below.

Pitch control

The pitch controller is a gain-scheduled PI controller based on the difference between the filtered generator speed and the rated generator speed of 1173.7rpm. The gains were computed with the response characteristics recommended in [23] using a single-degree-of-freedom model of the wind turbine, with angular rotation of the shaft the degree of freedom. From this the proportional gain was calculated as

$$K_P(\theta) = \frac{2I_{Drivetrain}\Omega_0\zeta_\phi\omega_\phi}{N_{Gear}(\frac{\partial P}{\partial\theta}(\theta=0))}GK(\theta) \tag{4.6}$$

and the integral gain as

$$K_I(\theta) = \frac{I_{Drivetrain}\Omega_0\zeta_\phi\omega_\phi^2}{N_{Gear}(\frac{\partial P}{\partial\theta}(\theta=0))}GK(\theta) \tag{4.7}$$

where $I_{Drivetrain}$ is the inertia of the drivetrain cast to the low-speed shaft, Ω_0 is the rated rotor speed of 12.1rpm, $\omega_{\phi n}$ is the natural frequency of the system, ζ_ϕ the damping ratio and $\frac{\partial P}{\partial\theta}(\theta=0)$ the sensitivity of the aerodynamic power to collective blade pitch angle at zero degrees. $GK(\theta)$ is the gain scheduling parameter defined by the function

$$GK(\theta) = \frac{1}{1+\frac{\theta}{\theta_K}} \tag{4.8}$$

where θ_K is the value of θ by which the sensitivity of the aerodynamic power to collective blade pitch doubles from the zero pitch angle. This is needed as at low wind speeds the power output is less sensitive to changes in pitch than at higher wind speeds, as portrayed in Figure 4.6. Numerically, the gains were as follows, $K_P(\theta=0) = 0.01882681s$, $K_I(\theta=0) = 0.008068634$ and with $\theta_K = 6.302336°$. The gain correction factor, proportional and integral gains are shown in Figure 4.7.

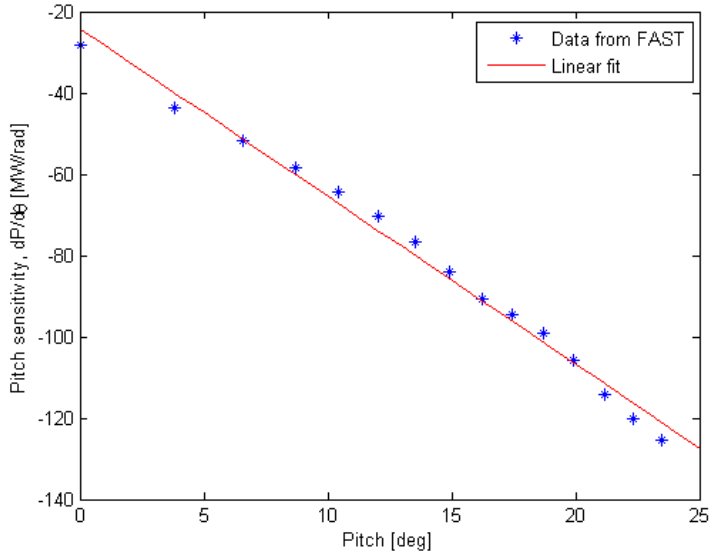

Figure 4.6: Sensitivity of the power output to pitch variations as a function of pitch angle, which is proportional to the wind speed due to separability

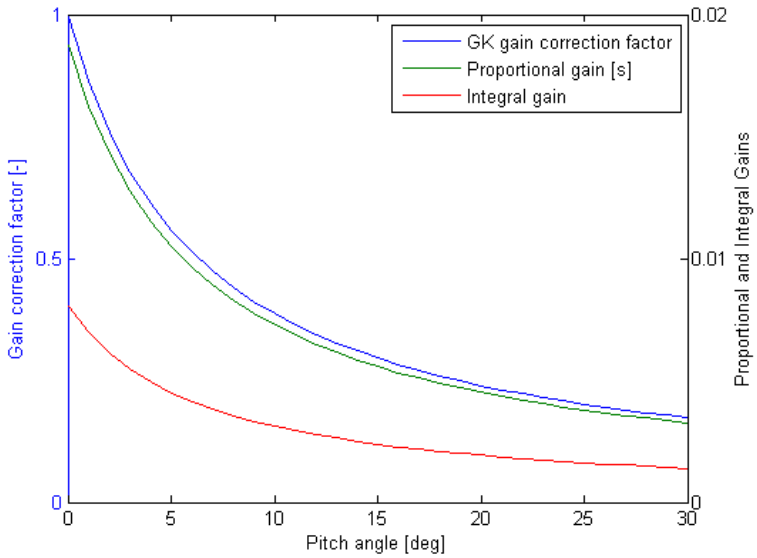

Figure 4.7: NREL 5MW pitch gain correction factor

Quasi-steady results

The steady power curve results for the torque controller are shown in Figures 4.8 and 4.9 for reference. All operating regions are clearly visible. Note that the transitions between regions are not particularly smooth, a slight loss in efficiency in region 1.5 and 2.5, and the maintenance of constant power above rated by reducing the torque inversely proportional to the generator speed.

Quasi-steady results of a Bladed simulation are also plotted on the graphs. These were created using a point wind speed ramping up from 1 to $25m/s$ at $0.02m/s^2$, it is assumed this is slow enough to give effectively quasi-steady results.

The correct behaviour can be seen for the combined torque and pitch controller when run on Bladed, as compared to the ideal results from the NREL 5MWs torque control strategy in thick black. Losses are accounted for between the mechanical and electrical power, such that the rated power of the generator is reached. These losses account for 5.6%, as in the NREL definition of the turbine [1]. The pitch control can be seen to effectively limit the generator speed above rated. The pitch angle as a function of wind speed is shown in Figure 4.10 for quasi-steady operation.

4.3.2 UpWind controller

The UpWind controller, although similar to the NREL 5MW controller [1], is more advanced. In addition to better power tracking and smoother transitions between the various operating regions, the controller also has a tower feedback loop, using an accelerometer in the nacelle and pitch control, a filter to damp torsional vibrations in the drivetrain, and a non-linear pitch control term which activates in response to sudden gusts. The pitch controller was also better designed to interact with the torque controller, allowing the pitch controller to become active near rated power when the wind speed was increasing rapidly. Each of these aspects of the controller is designed in a modular fashion such that various controller components may be activated/deactivated independently as required. The commented code is given in Appendix C.

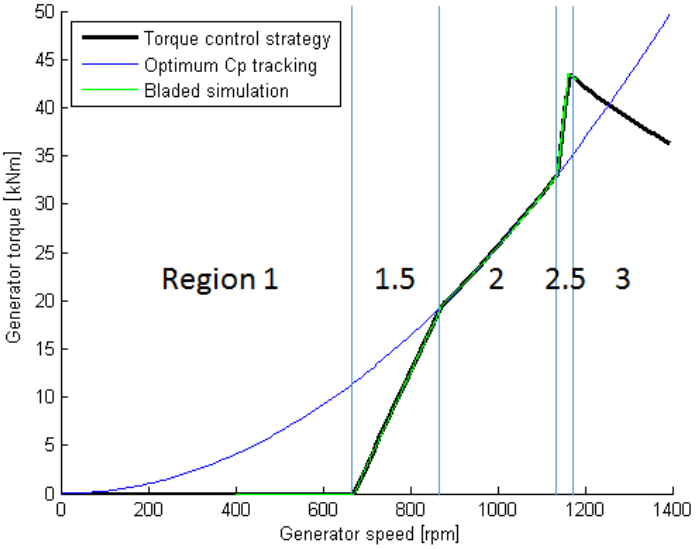

Figure 4.8: NREL 5MW baseline torque control strategy

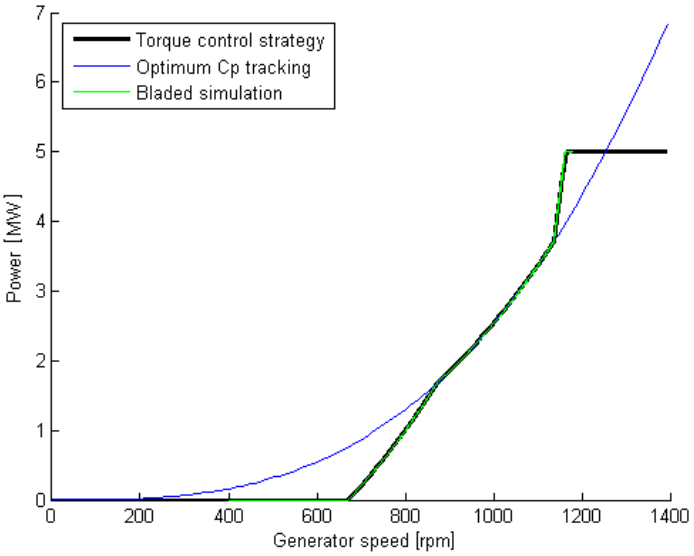

Figure 4.9: NREL 5MW baseline torque control power curve

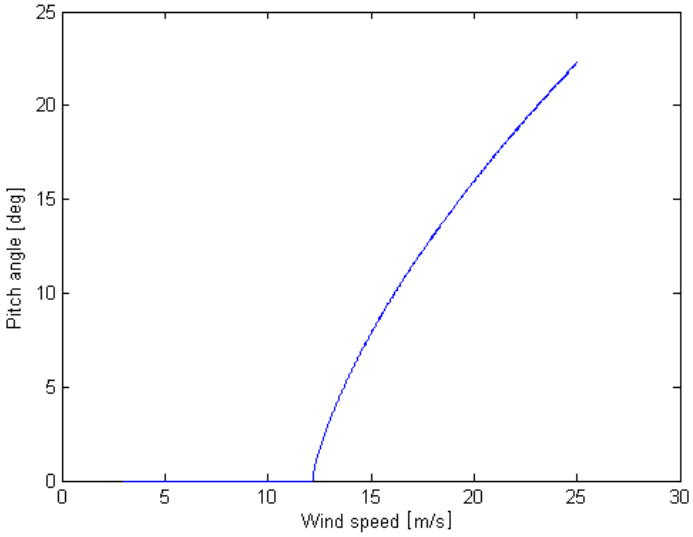

Figure 4.10: Blade pitch as a function of wind speed

Torque control

The basic torque control is made up of a PI controller with changing set point, saturated using the optimum torque curve below rated, and a strategy to maintain constant power above rated. The above rated region is defined as when the blades are not at fine pitch (0°). The torque to track the optimum power curve, which was also used in the NREL 5MW control, was defined by

$$Q_{opt} = \frac{\pi \rho R^5 C_p(\beta = 0, \lambda)}{2\lambda^3 G^3} \omega_{gen}^2 \tag{4.9}$$

where ρ was air density, R the rotor radius, C_p the power coefficient at given pitch, β, and tip speed λ, G was the gearbox ratio and ω_{gen} the generator speed.

A switching speed half way between cut-in generator speed and rated generator speed defines which set point is used and the saturation limits of the PI torque controller. Below the switching speed the set point of the controller is set as the cut-in generator speed and the controller is saturated so as not to allow the torque to exceed the optimum torque, Q_{opt}. When the generator speed is greater than the switching speed the set point is changed to that of the rated generator speed and the torque is limited so as not to drop below the optimum torque. The gains of the PI controller are set with $K_P = 4200$ and $K_I = 2100$, as in the UpWind controller description. After this process, the torque demand is saturated based on the maximum torque limits and rate limits as with the NREL 5MW control.

To reduce vibrations of the drivetrain a filter creates a ripple on the torque demand at the drivetrain frequency. This has the effect of damping the vibrations. The open loop linearised model of system highlights why the drivetrain filter was required, see Figure 4.11. The high peak at the drivetrain frequency needs damping to increase stability.

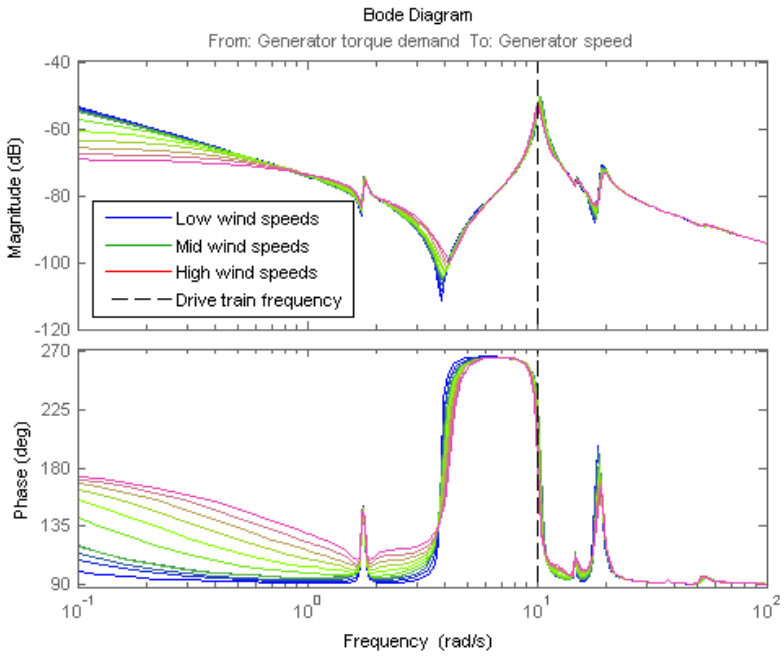

Figure 4.11: Bode plot of the open loop generator torque to generator speed transfer function

The fourth-order filter used was given as two second-order transfer functions

$$K_1 \frac{2\zeta_1 s/\omega_1}{1 + \frac{2\zeta_1 s}{\omega_1} + s^2/\omega_1^2} + K_2 \frac{2\zeta_2 s/\omega_2(1+\tau_2)}{1 + \frac{2\zeta_2 s}{\omega_2} + s^2/\omega_2^2} \tag{4.10}$$

with the parameters values: $K_1 = 1560 Nms/rad$, $\omega_1 = 24.20 rad/s$, $\zeta = 0.132$, $K_2 = 1625 Nms/rad$, $\omega_2 = 8.998 rad/s$, $\zeta_2 = 0.5041$, and $\tau_2 = 0.0138 s$.

The transfer function is discretised for use by the controller using the Tustin approximation,

$$z \approx \frac{1 + sT/2}{1 - sT/2} \tag{4.11}$$

where T is the time step. A MATLAB script is used to facilitate the conversion of this function for the controller operating with a timestep of 0.01s, the torque controller time step. The bode-plots for the continuous filter and the discretised filter are shown in Figure 4.12.

Unlike the original UpWind control, an exclusion zone is not required between 450 and 650rpm, because the tower is no longer excited by the 3P blade passing frequency. This is due to the monopile tower used. A look at the Campbell diagram in Figure 4.13 shows that the tower fore-aft translational frequency is between 1P rotational and 3P blade passing frequencies and so will not be significantly excited by these because resonance is avoided.

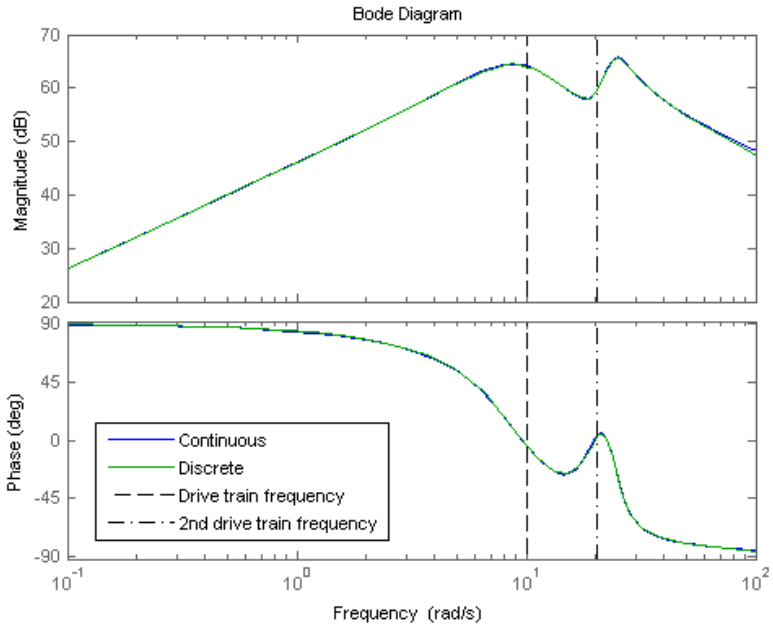

Figure 4.12: Bode plot of the Upwind drivetrain filter

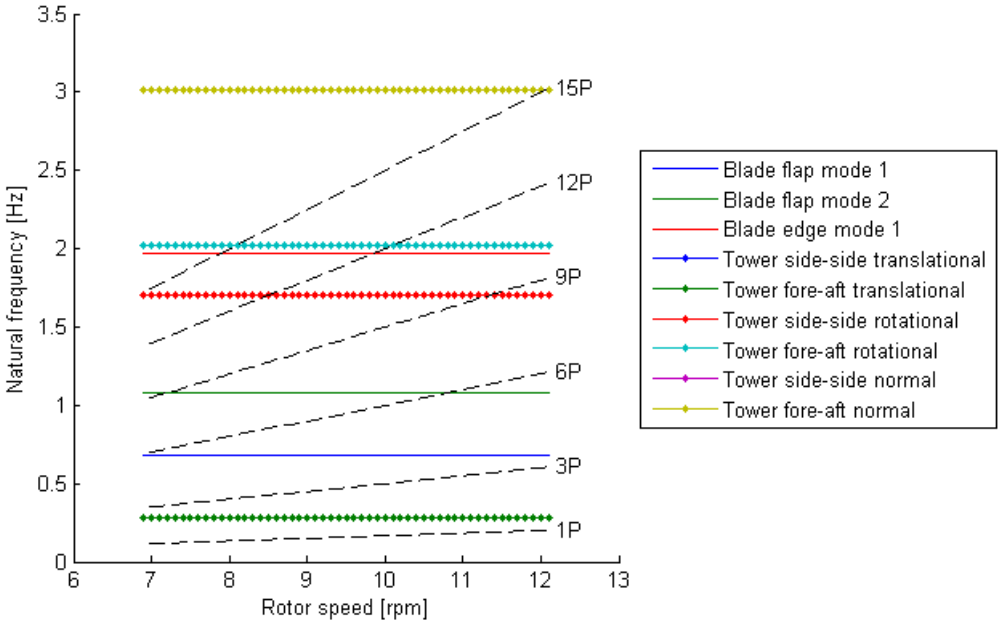

Figure 4.13: Campbell diagram for the baseline wind turbine. The tower fore-aft translational and tower side-side translational and normal natural frequencies are very similar. The tower translation mode lies between the 1P and 3P lines so will not be excessively excited

Pitch control

The basis of the pitch controller is similar to that of the NREL 5MW pitch control, although with slightly different gains and with the integral term being scaled first prior to integration that allows for a more intuitive understanding of the anti-wind-up limits. It may also result in smoother pitch action [24].

The generator speed was also put through a low pass filter to stop excessive pitch action with cut-off frequency of $10rad/s$ and damping coefficient of 1. Two more notch filters were also included to reduce pitch action at the blade passing frequency, $\omega = 3.8rad/s$ and at $\omega = 8.2rad/s$. The damping coefficient applied to each was $\zeta = 0.15$ and $\zeta = 0.2$ respectively, and they have the form

$$\frac{1 + \frac{s^2}{\omega^2}}{1 + \frac{2\zeta}{\omega}s + \frac{s^2}{\omega^2}} \tag{4.12}$$

with the discretised combination of these filters is shown in the bode-plot Figure 4.14.

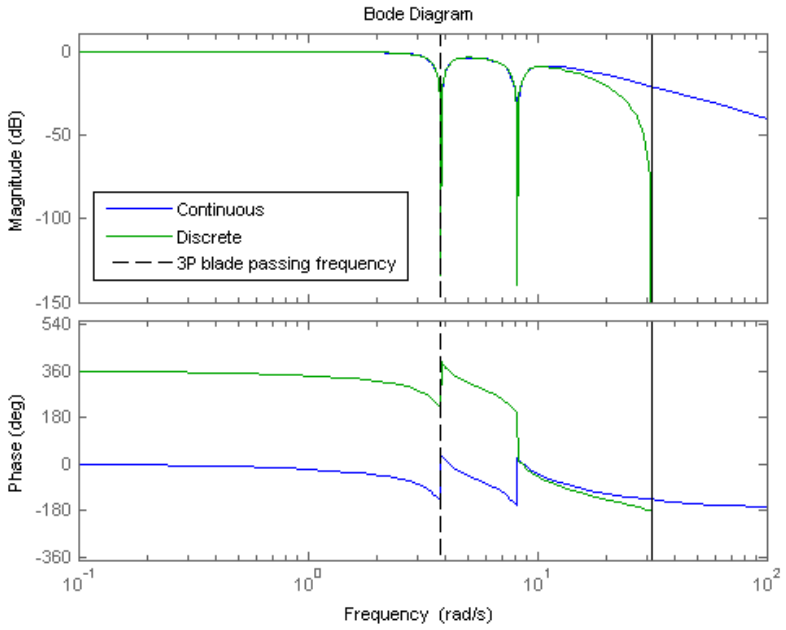

Figure 4.14: Bode plot of the UpWind pitch filter

Built upon this base for the pitch controller are a number of additional parts. First of all the torque-pitch interaction is improved, so that the pitch controller may start to activate prior to rated rotor speed if the wind speed is rising fast. This is done by including an additional PI pitch control demand, based on a power error between the current measured power at the generator and the wind turbines rated power, with gains of $K_P = 10^{-7}$ and $K_I = 5 \times 10^{-8}$.

Tower velocity damping is done through a feedback loop using an accelerometer measurement in the nacelle. This is integrated to determine the velocity of the nacelle and the blades are then pitched to increase aerodynamic damping resisting the motion. This is gain scheduled in the same way as the PI pitch control mechanism to take account of the reduced pitch action required at higher wind speeds for the same controllability. The control is also phased out so as not to operate

below rated wind speed when the loadings on the tower are not that great so as not to reduce energy capture. The open loop system of pitch motion to tower fore-aft motion is seen in Figure 4.15, with increased gains at higher wind speeds.

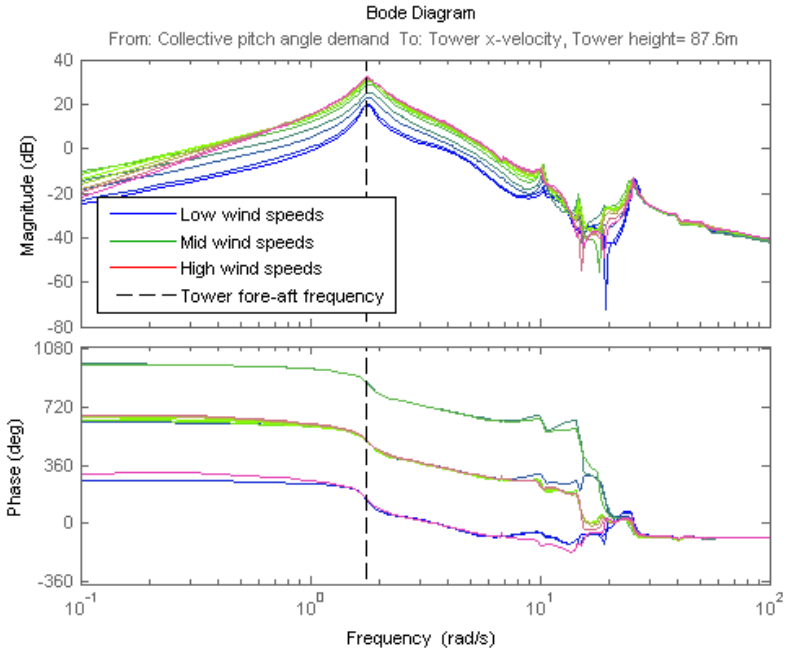

Figure 4.15: Bode plot of the open loop pitch angle to fore-aft tower motion transfer function

The low-pass filter to integrate the accelerations is a 0.8s first order lag filter. The tower velocity damping filter is shown in Figure 4.16 and is of the form

$$\frac{1 + \frac{2\zeta_1}{\omega_1^2}s + \frac{s^2}{\omega_1^2}}{1 + \frac{2\zeta_2}{\omega_2}s + \frac{s^2}{\omega_2^2}} \tag{4.13}$$

with $\omega_1 = 0.8357$, $\omega_2 = 1.3571$, $\zeta_1 = 0.69$, $\zeta_2 = 1.0$ and an overall gain of 0.0454. These values vary slightly from those described in the UpWind report, due to the natural tower frequency being lower, but has the same form.

Finally there is a non-linear pitch term to encourage pitching when the wind turbine experiences a gust. This part of the controller usually does not affect the pitch angle demand. It takes account of the generator speed error and its rate of change to determine if any additional pitch action is required, and only does so if the speed error is large, positive and increasing. A first order lag filter is included to stop the controller reacting to signal noise.

Quasi-steady results

The power curve results for this baseline controller are shown in Figures 4.17 and 4.18, comparing with both the NREL 5MW control and with the maximum power curve displayed for reference. It can be seen that the UpWind controller more closely tracks the optimum power curve, which results in better energy capture.

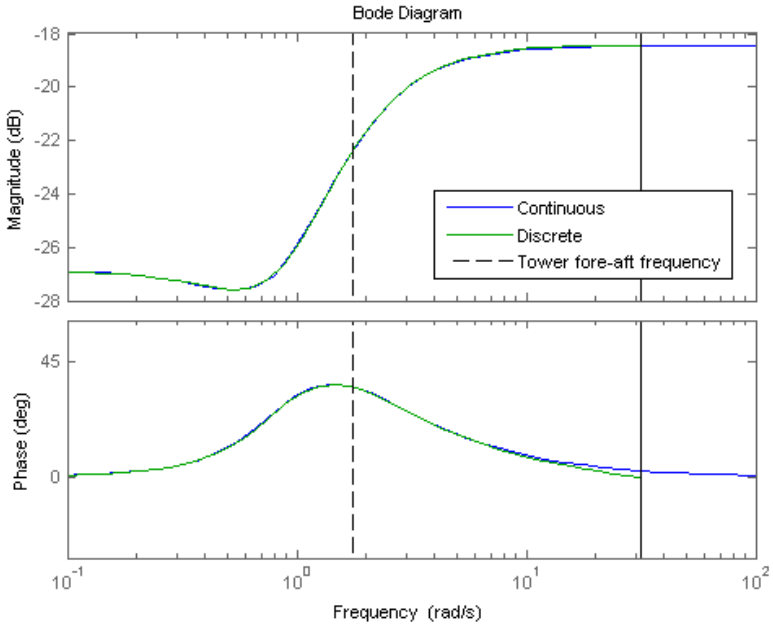

Figure 4.16: Bode plot of the UpWind tower velocity damping filter

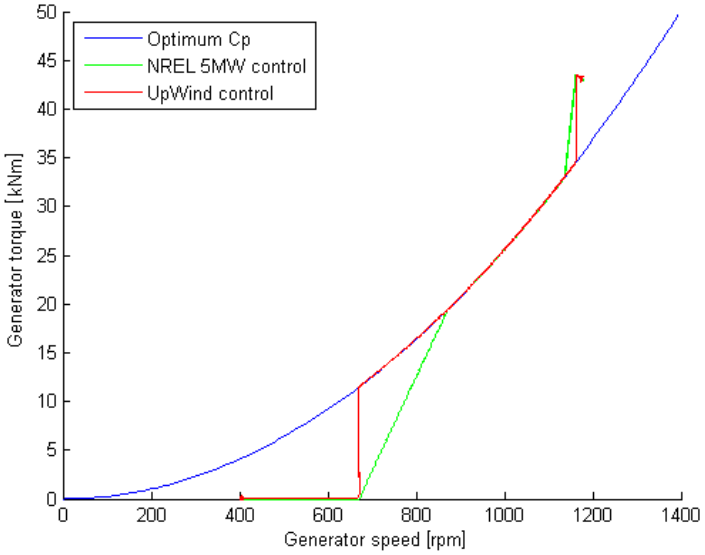

Figure 4.17: Comparison of the NREL 5MW and the UpWind torque control strategies from Bladed simulations

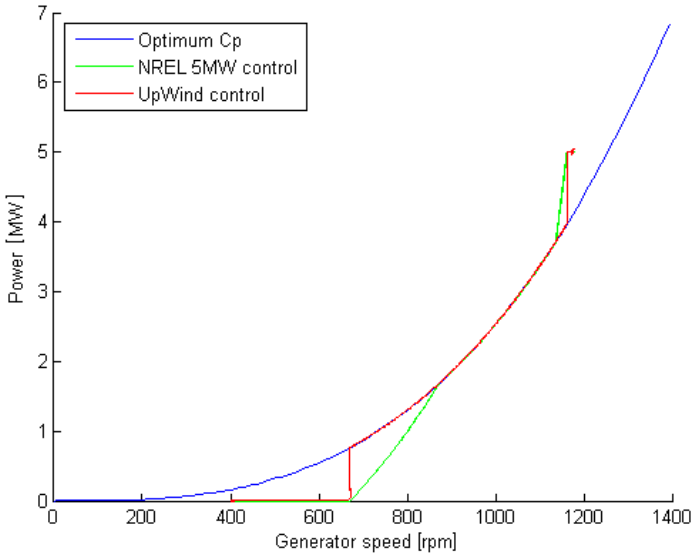

Figure 4.18: Comparison of the NREL 5MW and UpWind control power curves from Bladed simulations

The UpWind controller has been designed in a modular fashion so it is possible to pick what components of the control are active, such as the tower feedback loop or non-linear gust alleviation. The smart rotor and individual pitch controllers are also designed in a similar fashion, which helps with robustness and allows these controllers to be deployed with either the simpler NREL 5MW control or the more complex UpWind control.

4.4 Advanced load reduction control options

Two advanced load reduction control strategies are considered, which are both taken from individual pitch control research but with the control demand either being pitch angle or flap angle depending on whether individual pitch control or smart rotor control is being studied. The two strategies adopted are the dq-axis control [6] and an interpretation of the Independent Blade Control [25], both described below. These controllers are phased out below rated from 100% at rated power, to 0% action at 80% rated power. This is so as not to disrupt optimum energy capture, but also because there is less to be gained in this operating region as the loads below rated power are low. This may be adjusted dependent on a economic assessment of the trade-off between energy capture and load reduction.

4.4.1 Control using the dq-axis

The rotating out-of-plane blade root bending moment of each blade is converted to tilt and yaw moments in a stationary plane using the forward Coleman transform. The magnitude of these vectors then depict the asymmetrical yaw and tilt load components. Proportional Integral controllers then act to minimise these tilt and yaw moments, before the reverse Coleman transform is used to set the demand angle for each blade. The dq-axis control and independent control are set-up identically for both the pitch and smart rotor controls, with the exception that the demand for the actuators is switched from pitch to flap control and the gains increased by a factor of 6.3 for the smart rotor case. A visual representation of this strategy is shown in Figure 4.19.

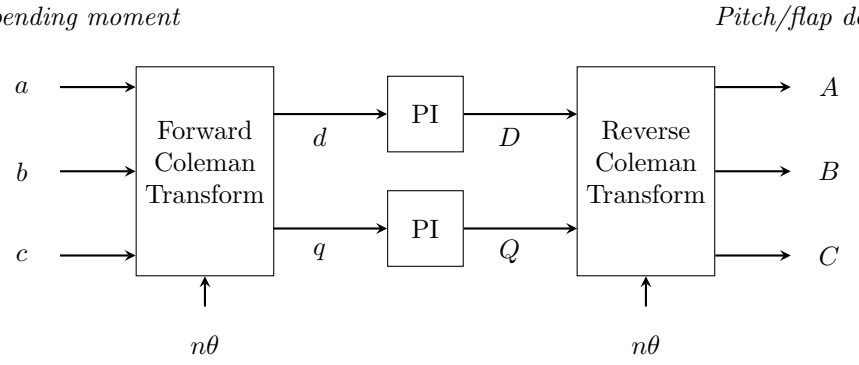

Figure 4.19: Schematic of the dq-axis control method

The forward Coleman transformation, otherwise known as the Park's or dq-0 transform, is

$$\begin{bmatrix} d \\ q \end{bmatrix} = \frac{2}{3} \begin{bmatrix} \cos(\theta) & \cos(\theta + \frac{2\pi}{3}) & \cos(\theta + \frac{4\pi}{3}) \\ \sin(\theta) & \sin(\theta + \frac{2\pi}{3}) & \sin(\theta + \frac{4\pi}{3}) \end{bmatrix} \begin{bmatrix} a \\ b \\ c \end{bmatrix} \tag{4.14}$$

where θ is the rotor azimuth angle, a, b, and c are the blade root bending moments of the each of the three blades, and d and q are the transformed fixed axis loadings, in the yaw and tilt directions

respectively. The reverse transform is

$$\begin{bmatrix} A \\ B \\ C \end{bmatrix} = \begin{bmatrix} \cos(\theta) & \sin(\theta) \\ \cos(\theta + \frac{2\pi}{3}) & \sin(\theta + \frac{2\pi}{3}) \\ \cos(\theta + \frac{4\pi}{3}) & \sin(\theta + \frac{4\pi}{3}) \end{bmatrix} \begin{bmatrix} D \\ Q \end{bmatrix} \tag{4.15}$$

where A, B and C are the demanded pitch/flap angles for each of the blades. An offset may be added to the reverse transform to account for controller delays, ωT, however this was found to have negligible impact on the load reduction potential of the controller. This controller effectively eliminates 1P loadings. Higher harmonic loadings may be reduced by altering the transform such that θ is multiplied by a factor, i.e. n to remove nP loads. To simplify analysis, reduce actuator requirements and due to the fact 1P loads cause the most significant amount of damage, only the 1P loads are targeted in this work. The maths behind this is explained in the following section.

Theory

To understand the actions of the controllers within the Coleman transform it is worthwhile looking at the underlying mathematics. This section considers the specific example of identical controllers acting on both the d and q signals, it may also be expanded to include filters within the Coleman transform. The mathematical terms used are described in Figure 4.20.

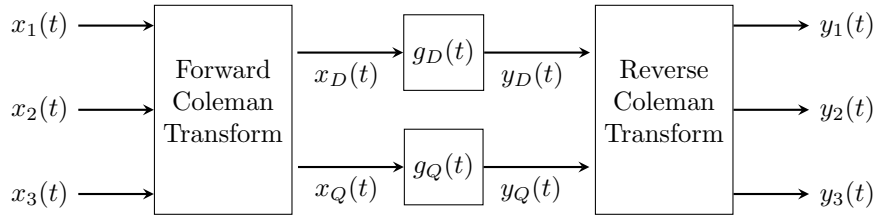

(a) Time domain

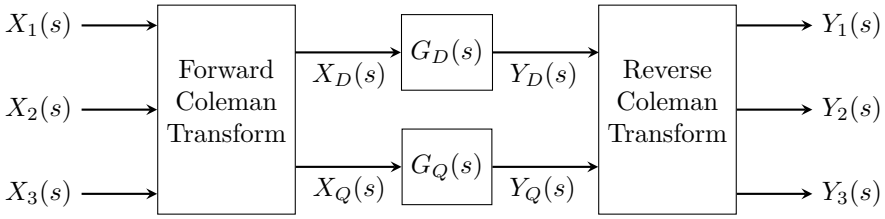

(b) Laplace domain

Figure 4.20: Coleman transform with control I/O's in time and Laplace domains

In the time domain

$$x_D(t) = \frac{2}{3}\left(x_1(t)\cos\left(\theta(t)\right) + x_2(t)\cos\left(\theta(t) + \frac{2\pi}{3}\right) + x_3(t)\cos\left(\theta(t) + \frac{4\pi}{3}\right)\right) \tag{4.16}$$

assuming a constant rotational speed $\theta(t) \to \omega t$ where ω is the constant rotational speed of the rotor and using the Laplace transform and exponential forms of the trigonometric functions

$$\mathcal{L}\left(e^{at}f(t)\right) = F(s-a) \tag{4.17}$$

$$\cos(\theta) = \frac{e^{i\theta} + e^{-i\theta}}{2} \tag{4.18}$$

and

$$\sin(\theta) = \frac{e^{i\theta} - e^{-i\theta}}{2i} \tag{4.19}$$

it can be shown that

$$X_D(s) = \frac{2}{3}\left(\frac{1}{2}X_1(s-i\omega) + \frac{1}{2}X_1(s+i\omega) + \frac{e^{i\frac{2\pi}{3}}}{2}X_2(s-i\omega) + \frac{e^{-i\frac{2\pi}{3}}}{2}X_2(s+i\omega) + \frac{e^{i\frac{4\pi}{3}}}{2}X_3(s-i\omega) + \frac{e^{-i\frac{4\pi}{3}}}{2}X_3(s+i\omega)\right) \tag{4.20}$$

and similarly

$$X_Q(s) = \frac{2}{3}\left(\frac{1}{2i}X_1(s-i\omega) - \frac{1}{2i}X_1(s+i\omega) + \frac{e^{i\frac{2\pi}{3}}}{2i}X_2(s-i\omega) - \frac{e^{-i\frac{2\pi}{3}}}{2i}X_2(s+i\omega) + \frac{e^{i\frac{4\pi}{3}}}{2i}X_3(s-i\omega) - \frac{e^{-i\frac{4\pi}{3}}}{2i}X_3(s+i\omega)\right) \tag{4.21}$$

Equivalently for $y_1(t) = y_D\cos(\theta(t)) + y_Q\sin(\theta(t))$

$$Y_1(s) = \frac{1}{2}Y_D(s-i\omega) + \frac{1}{2}Y_D(s+i\omega) + \frac{1}{2i}Y_Q(s-i\omega) - \frac{1}{2i}Y_Q(s+i\omega) \tag{4.22}$$

As $Y_D = G_D(s)X_D(s)$ and $Y_Q = G_Q(s)X_Q(s)$ this may be rewritten

$$Y_1(s) = \frac{1}{2}G_D(s-i\omega)X_D(s-i\omega) + \frac{1}{2}G_D(s+i\omega)X_D(s+i\omega) + \frac{1}{2i}G_Q(s-i\omega)X_Q(s-i\omega) - \frac{1}{2i}G_Q(s+i\omega)X_Q(s+i\omega) \tag{4.23}$$

Now from Equation 4.20 substituting in $s \to s - i\omega$ it is trivial to get

$$X_D(s-i\omega) = \frac{2}{3}\left(\frac{1}{2}X_1(s-2i\omega) + \frac{1}{2}X_1(s) + \frac{e^{i\frac{2\pi}{3}}}{2}X_2(s-2i\omega) + \frac{e^{-i\frac{2\pi}{3}}}{2}X_2(s) + \frac{e^{i\frac{4\pi}{3}}}{2}X_3(s-2i\omega) + \frac{e^{-i\frac{4\pi}{3}}}{2}X_3(s)\right) \tag{4.24}$$

and similar expressions for $X_D(s+i\omega)$, $X_Q(s-i\omega)$ and $X_Q(s+i\omega)$. These may then be used to acquire

$$\frac{1}{2}X_D(s-i\omega) + \frac{1}{2i}X_Q(s-i\omega) = \frac{1}{3}\left(X_1(s) + e^{i\frac{2\pi}{3}}X_2(s) + e^{i\frac{4\pi}{3}}X_3(s)\right) \tag{4.25}$$

and similarly

$$\frac{1}{2}X_D(s+i\omega) - \frac{1}{2i}X_Q(s+i\omega) = \frac{1}{3}\left(X_1(s) + e^{-i\frac{2\pi}{3}}X_2(s) + e^{-i\frac{4\pi}{3}}X_3(s)\right) \tag{4.26}$$

Substituting these into Equation 4.23 with $G_D(s) = G_Q(s) = G(s)$, and assuming only the real part of the exponentials are of relevance, gives

$$Y_1(s) = G(s-i\omega)\frac{1}{3}\left(X_1(s) + \frac{1}{2}X_2(s) + \frac{1}{2}X_3(s)\right) + G(s+i\omega)\frac{1}{3}\left(X_1(s) + \frac{1}{2}X_2(s) + \frac{1}{2}X_3(s)\right) \tag{4.27}$$

which, without the internal controller $G(s)$, may be simplified to

$$Y_{1_{noG}}(s) = \frac{2}{3}\left(X_1(s) + \frac{1}{2}X_2(s) + \frac{1}{2}X_3(s)\right) \tag{4.28}$$

where $Y_{1_{noG}}$ is the result when no internal controller is present. This implies

$$Y_1(s) = \frac{1}{2}\left(G(s-i\omega) + G(s+i\omega)\right)Y_{1_{noG}} \tag{4.29}$$

leading to the conclusion

$$G(s) \to \frac{1}{2}\left(G(s-i\omega) + G(s+i\omega)\right) \tag{4.30}$$

when $G(s)$ is acting within the Coleman transform compared to outside the transform. The controllers within the transform have been selected as proportional integral controllers to remove the asymmetric loadings on the rotor, in notation $G(s) = K_P + K_I/s$. It can then be shown that the transfer function for the controllers is as described in Equation 4.31, with the bode plot of this transfer function displayed in Figure 4.21. The gains chosen for this are $Kp = 10^{-8}$ and $K_I = 10^{-9}$. The effect of this controller is to essentially act as a bandpass filter, locked to the rotational frequency of the rotor, which implements a phase shift. The phase shift generated is what leads to a reduction in the cyclic loadings at the rotational frequency of the rotor.

$$Kp + \frac{K_I}{s} \to Kp + \frac{1}{2}\left(\frac{K_I}{s-i\omega} + \frac{K_I}{s+i\omega}\right) = Kp + \frac{1}{2}\frac{K_I s}{s^2+\omega^2} \tag{4.31}$$

A problem that may occur with this form of individual pitch control is excitement of the 3P modes if a 1P oscillation occurs within the transformed coordinate system. To avoid this the d and q load signals are modified using 1P notch filters, similar to the notch filters used for the standard pitch control, with $\omega = 1.2671$ and $\zeta = 1$, repeated here for convenience

$$\frac{1 + \frac{s^2}{\omega^2}}{1 + \frac{2\zeta}{\omega}s + \frac{s^2}{\omega^2}} \tag{4.32}$$

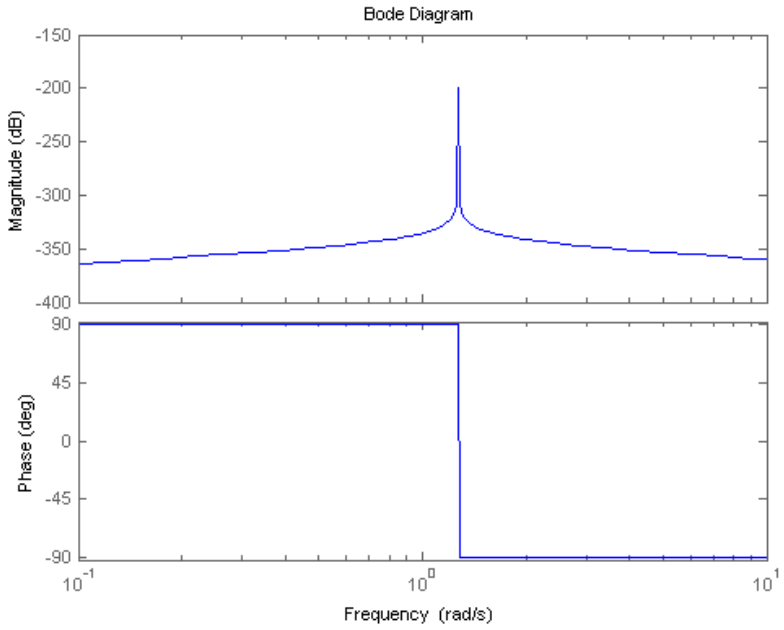

Figure 4.21: Bode plot of the IPC controller outwith the Coleman transform

4.4.2 Independent control

An alternative control approach is an independent control system [25], [26]. The collective pitch is still defined by the central controller, but then the actuator of each blade, or flap in the smart rotor design, attempts to maintain a set blade root bending moment, My_{ref}, for this pitch demand. An interpretation of this method is used in this thesis. The control method is displayed in Figure 4.22, with $My_{ref} = My_{qs} + My_{tow} + My_{nod}$, where My_{qs} is the quasi-steady out-of-plane blade root bending moment, My_{tow} the moment caused by tower fore-aft motion, and My_{nod} the moment caused by nacelle nod motion.

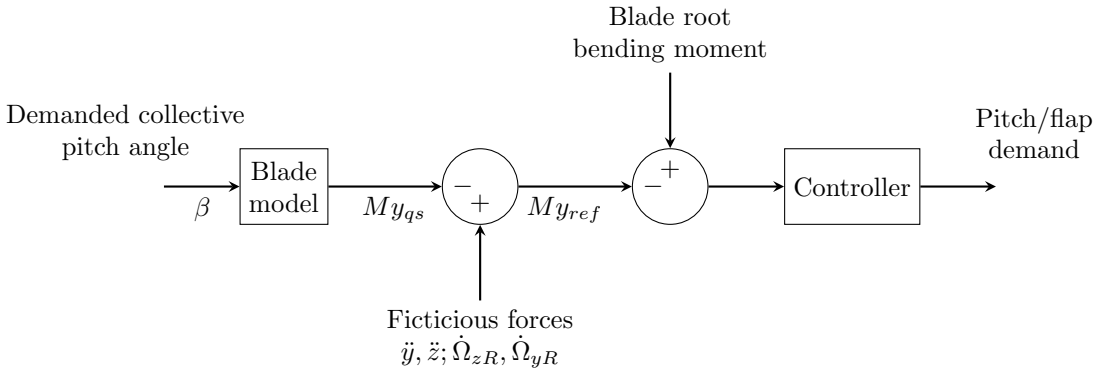

Figure 4.22: Schematic of the independent blade control method

The conversion between pitch angle and bending moment is taken into account by a blade model. In this case the blade model is produced by fitting a curve to the relationship between collective pitch angle, β in radians, and the out-of-plane blade root bending moment, My_{qs}, in MNm, during

a quasi-steady Bladed simulation of the wind turbine. This fit is shown in Figure 4.23. It is defined in the above rated region by the equation

$$My_{qs} = 32\beta^2 - 33\beta + 11 \tag{4.33}$$

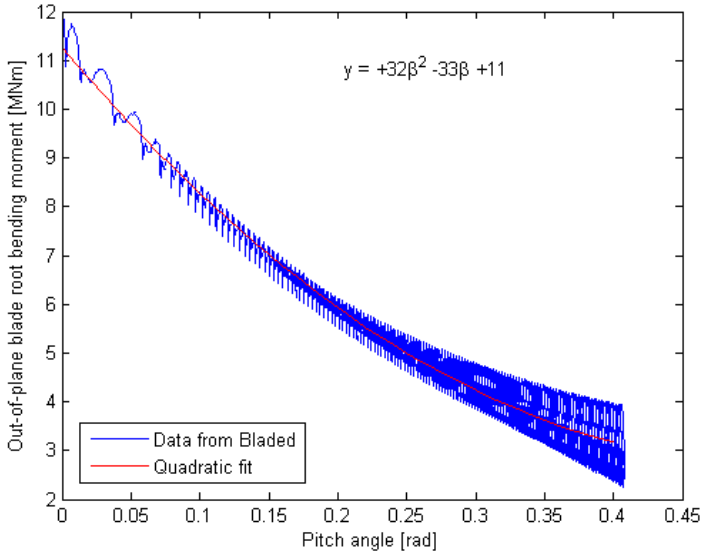

Figure 4.23: Pitch angle to out-of-plane blade root bending moment in quasi steady operation

The controller also needs to differentiate between loads caused by the wind field and those caused by the wind turbine dynamics, such as tower accelerations, $\ddot{x}_{tow}$ and $\ddot{y}_{tow}$, and nacelle nod and roll accelerations, $\dot{\Omega}_{nod}$ and $\dot{\Omega}_{roll}$, so that the blade control is decoupled from the main control system. An intuitive interpretation of the results in [25], [26] follows.

The tower accelerations cause accelerations at the blade roots. For the out-of-plane blade root bending moment, My_{tow}, only fore-aft motion is important $\ddot{x}_{tow}$. This moment is calculated based on the mass of the blade, $m_{blade} = 17732kg$, its centre of mass from the blade root $r_{com} = 20.5m$, and the tower fore-aft acceleration $\ddot{x}_{tow}$, to get

$$My_{tow} = r_{com} \times m_{blade}\ddot{x}_{tow} \tag{4.34}$$

The contribution to the blade root out-of-plane bending moment due to nacelle nod and roll accelerations is different for each blade, as it depends on their azimuthal position. The nod accelerations cause out-of-plane blade moment while roll accelerations cause in-plane moments. The out-of-plane blade root bending moments caused by nod accelerations are calculated to be

$$My_{nod} = I\dot{\Omega}_{nod}cos(\theta) \tag{4.35}$$

where I is the inertia of the blade, $363501kgm$, and θ is the azimuth angle of the blade with $\theta = 0$ determined to be in the vertical position.

The actual controller is typically designed to target specific frequencies, for example 1P vibra-

tions. This is done through the use of filters on the pitch demand from the independent controller. The control system is set up as a gain, $K_P = 10^{-9}$, and a low and high pass filter creating a fourth order band pass filter

$$\frac{s^2}{\left(1 + \frac{2\zeta}{\omega}s + \frac{s^2}{\omega^2}\right)^2} \tag{4.36}$$

with ω set to the rotational speed of the rotor at rated power and damping coefficient $\zeta = 0.15$. An additional gain is also applied to the high pass filter, allowing for switching between use of the filters and a purely proportional based controller.

4.5 Validation of baseline

Under quasi-steady conditions the baseline wind turbine controllers have been seen to correctly track the demanded path on the torque-rotor speed diagram and limit the power output to rated power. Tower velocity damping, drivetrain filter damping and the pitch filters are tested under dynamic 3D turbulent wind field cases. For this, the power spectral density for the tower acceleration, generator speed and pitch are all compared individually by running simulations with the filters either active or switched off.

4.5.1 Tower velocity damping

The tower vibrations are in fact not significant for this model and are already well damped; there is no prominent peak at the natural frequency of the tower 0.28Hz (1.76rad/s). However, using the active tower velocity damping feedback loop a reduction in loads at the desired frequency is achieved. As can be seen by the reduction in the peak at the tower frequency shown in Figures 4.24a and 4.24b. Therefore, while active tower velocity damping does not appear worthwhile for this wind turbine, it is kept as part of a state-of-the-art controller.

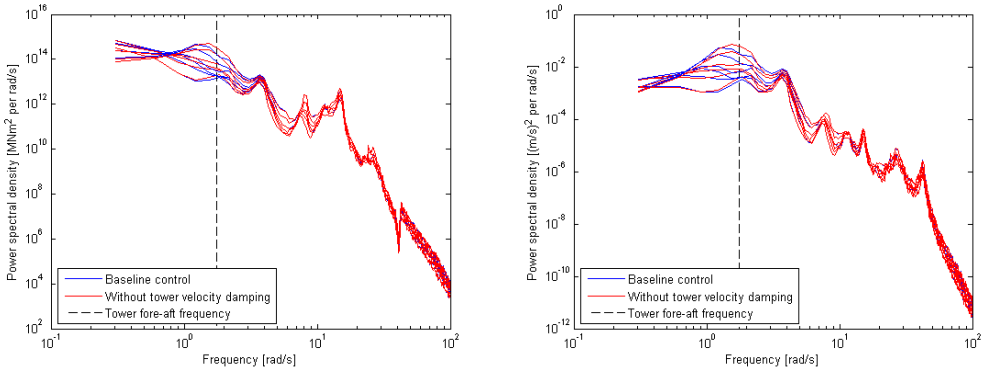

(a) Tower base fore-aft bending moment (b) Tower fore-aft velocity

Figure 4.24: Power spectral density for wind speeds 10,12,14,16,20 and 24m/s with and without the tower velocity damping loop

4.5.2 Drivetrain filter

The drivetrain filter on the other hand is an important component of the controller, without which the drivetrain frequency is excited causing oscillations in generator speed and so torque. Figure 4.25 shows the PSD of the generator speed for wind speeds from 4 to 24m/s in 4m/s steps. Across all but the lowest wind speed there is a prominent peak at 10.1rad/s. This corresponds to the first drivetrain frequency. The drivetrain filter damps out this frequency, which can also be seen in the time domain, Figure 4.26.

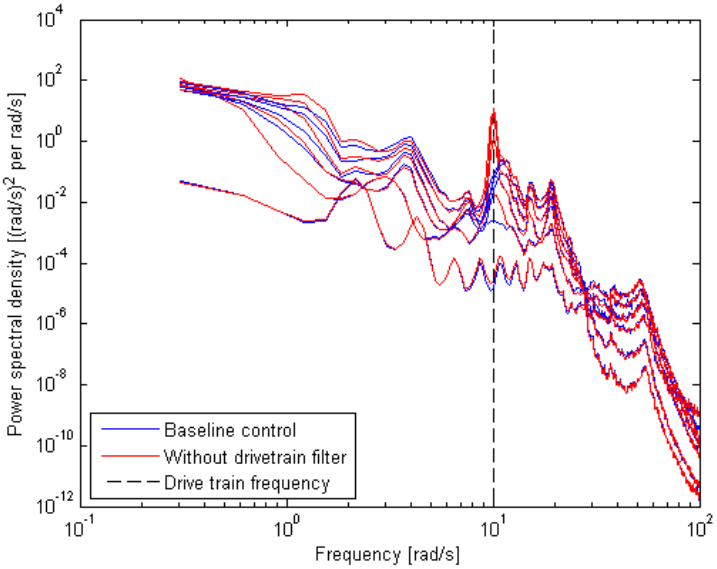

Figure 4.25: Power spectral density of the generator speed for wind speeds 4 to 24m/s in 4m/s steps, with and without the drivetrain filter. The 4m/s wind speed near cut-in is the lowest trace and exception to the rule

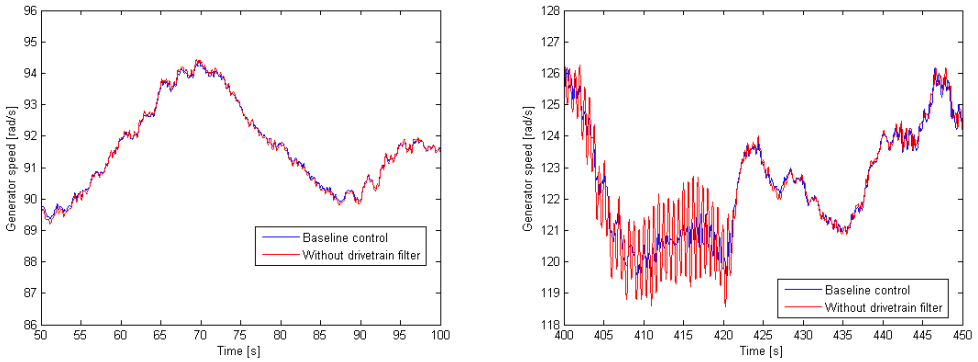

(a) 8m/s wind speed

(b) 12m/s wind speed

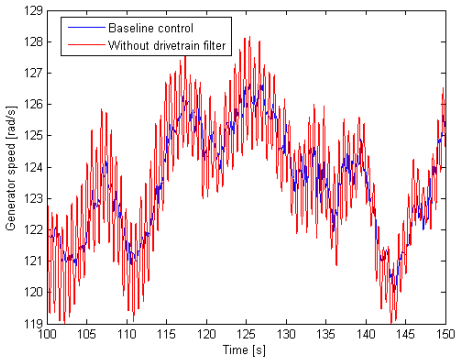

(c) 16m/s wind speed

Figure 4.26: Generator speed measurements for turbulent wind field runs, with and without the drivetrain filter

4.5.3 Pitch filters

The pitch filter works to reduce pitch action. This is done through a low-pass filter that reduces high speed pitch action, which is not beneficial in maintaining rotor speed, and by limiting pitch action at the blade passing frequency of 3.8rad/s and at the drivetrain frequency of 10.1rad/s. The result of such action is shown in Figure 4.27a. As can be seen high frequency action is reduced, as too is action about the blade passing frequency and drivetrain mode. Basic statistics show that the standard deviation of the rotor speed is not adversely affected by these filters, as can be seen in Figure 4.27b.

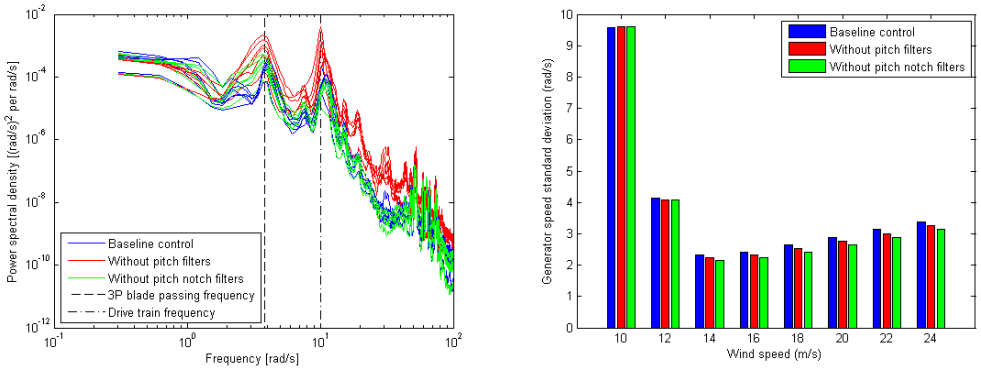

(a) Power spectral density of the generator speed (b) Generator speed standard deviation

Figure 4.27: Comparison of the baseline controller with and without pitch filters for wind speeds 4 to 24m/s in 4m/s steps

4.5.4 Advanced load reduction control options

The dq-axis control targets the rotational loadings on the wind turbine by converting the moments on the rotating blades into a fixed yaw and tilt plane. These moments are then minimised by the controller. Before converting back into the rotational plane of the rotor to set the demanded pitch angles. To confirm that the controller is working as expected a good starting point is then to look at the rotor imbalances in the tilt and yaw planes. Figure 4.28 shows that the dq-axis control effectively eliminates the yaw and tilt imbalances. The performance near rated wind speeds is less, but this is due to the controllers being phased out below rated to avoid impacting on energy capture.

Reducing rotor loads is the key objective of dq-axis control. It is then worth looking at the blade root bending moment to see whether this goal is achieved. Figures 4.29a and 4.29b show the reduction in the 1P loadings at the angular frequency of the rotor, $\omega = 1.2671 rad/s$, 0.2Hz. A linear plot exemplifies this further as seen in Figure 4.30. This result can be compared with [27], as seen in Figure 4.31 (note the frequency axis here is in Hz).

The results show that the dq-axis controllers effectively eliminate 1P loadings, but have little effect at other frequencies. A possible improvement to the dq-axis control portrayed here is the targeting of higher frequency loadings, such as at twice the rotational frequency of the rotor. Implementation of this type of control is done by multiplying the rotational position of the blades by two, on both input and output of the Coleman transform, this has the effect of targeting the 2ω

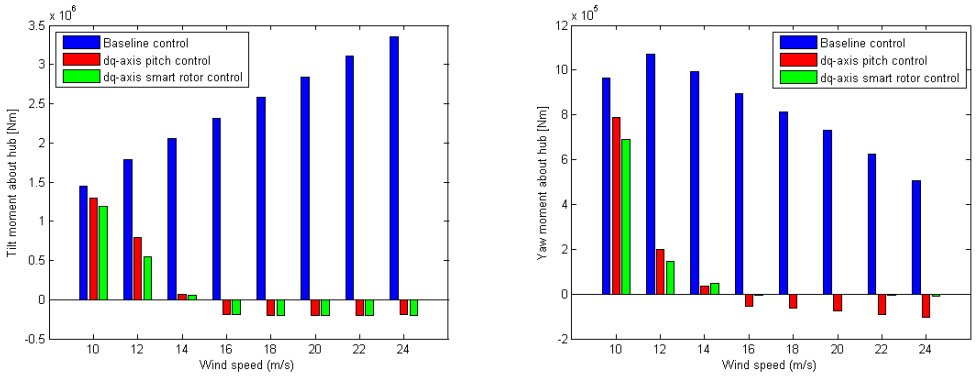

(a) Mean tilt moment (b) Mean yaw moment

Figure 4.28: Comparison of the baseline controller with the dq-axis controllers looking at the tilt and yaw moments about the hub. Higher wind speeds produce higher loads

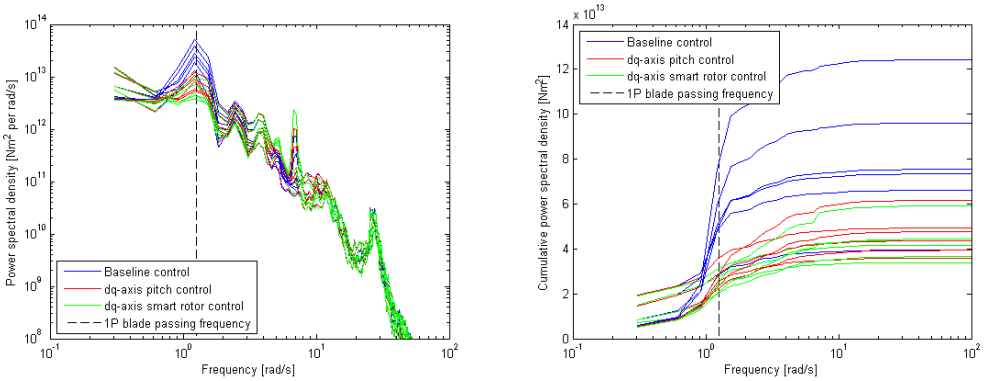

(a) PSD (b) Cumulative PSD

Figure 4.29: Comparison of the baseline controller with the dq-axis controllers looking at the blade root out-of-plane bending moment

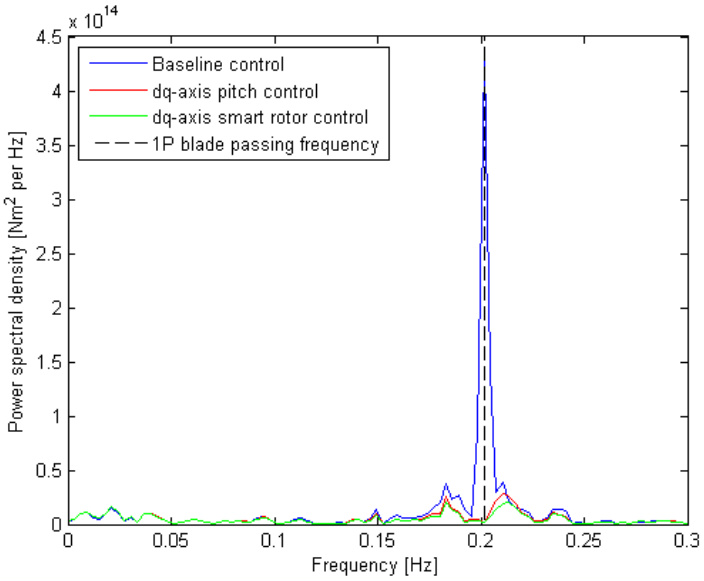

Figure 4.30: Linear plot of the PSD for the My blade root bending moment at 16m/s wind speed

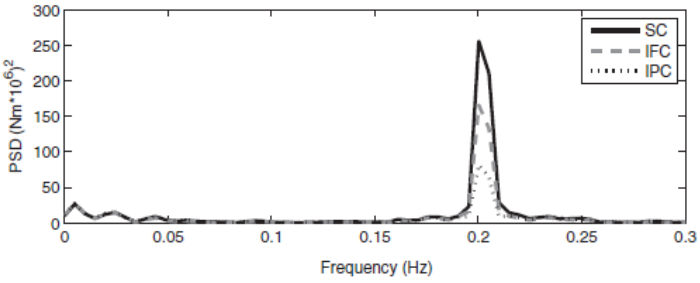

Figure 4.31: Linear plot of the PSD for the My blade root bending moment for baseline (SC), smart rotor control (IFC) and individual pitch control (IPC) [27]

loads, and higher harmonics may also be targeted in a similar manner. To simplify analysis though this enhancement is not considered in this work.

The exact load reductions and a comparison between the use of dq-axis and independent pitch control and smart rotor control for load reduction are evaluated in Chapter 8 of this thesis, and the rigorous methods for testing the performance of the wind turbine controllers are considered in the next chapter.

References

[1] B. J. Jonkman, S. Butterfield, W. D. Musial, and G. Scott, "Definition of a 5-MW Reference Wind Turbine for Offshore System Development," tech. rep., NREL, Colorado, 2009.

[2] D. G. Wilson, B. R. Resor, D. Berg, T. K. Barlas, and G. A. M. van Kuik, "Active Aerodynamic Blade Distributed Flap Control Design Procedure for Load Reduction on the UpWind 5MW Wind Turbine," in *48th AIAA Aerospace Sciences Meeting Including the New Horizons Forum and Aerospace Exposition*, (Orlando, Florida), American Institute of Aeronautics and Astronautics, 2010.

[3] T. K. Barlas and G. A. M. van Kuik, "Aeroelastic modelling and comparison of advanced active flap control concepts for load reduction on the Upwind 5MW wind turbine," in *EWEC*, (Marseille, France), 2009.

[4] P. B. Andersen, *Advanced Load Alleviation for Wind Turbines using Adaptive Trailing Edge Flaps: Sensoring and Control*. PhD thesis, Technical University of Denmark, 2010.

[5] M. A. Lackner and G. A. M. van Kuik, "The Performance of Wind Turbine Smart Rotor Control Approaches During Extreme Loads," *Journal of Solar Energy Engineering*, vol. 132, 2010.

[6] E. A. Bossanyi, D. Witcher, and T. Mercer, "Project UpWind: Controller for 5MW reference turbine," tech. rep., Garrad Hassan and Partners Limited, Bristol, 2009.

[7] D. Berg, D. G. Wilson, B. R. Resor, M. F. Barone, J. Berg, S. Kota, and G. Ervin, "Active aerodynamic blade load control impacts on utility-scale wind turbines," in *AWEA Windpower*, (Chicago, Illinois, USA), 2009.

[8] D. Berg, D. G. Wilson, M. F. Barone, B. R. Resor, J. Berg, S. Kota, G. Ervin, and D. Maric, "The impact of active aerodynamic load control on fatigue and energy capture at low wind speed sites," in *EWEC*, (Marseille, France), US Government: Sandia National Laboratories, FlexSys Inc., 2009.

[9] B. A. H. Marrant and T. van Holten, "Comparison of smart rotor blade concepts for large offshore wind turbines," in *Offshore Wind Energy and Other Renewable Energies in Mediterranean and European Seas*, vol. 31, (Civitavecchia, Italy), 2006.

[10] E. L. V. D. Hooft, P. Schaak, and T. G. V. Engelen, "Wind turbine control algorithms," tech. rep., Delft Technical University, Delft, Netherlands, 2003.

[11] A. P. Chatzopoulos, *Full Envelope Wind Turbine Controller Design for Power Regulation and Tower Load Reduction*. PhD thesis, University of Strathclyde, 2011.

[12] A. Stock and W. E. Leithead, "Providing Grid Frequency Support Using Variable Speed Wind Turbines with Augmented Control," in *EWEA*, (Copenhagen, Denmark), 2012.

[13] J. Peeringa, R. Brood, O. Ceyhan, W. P. Engels, G. de Winkel, and G. de Winkel, "Upwind 20MW Wind Turbine Pre-Design: Blade design and control," tech. rep., Energy Research Centre of the Netherlands, 2011.

[14] Areva, "Offshore Windpower M5000," 2014.

[15] REPower Systems, "REpower Systems, 5M: The 5-megawatt power plant with 126 metre rotor diameter," 2014.

[16] D. J. Malcolm and A. C. Hansen, "WindPACT Turbine Rotor Design Study," tech. rep., NREL/SR-500-32495, 2006.

[17] S. Frandsen, N. J. Tarp-Johansen, E. Norton, K. Argyriadis, B. Bulder, and K. Rossis, "Recommendations for design of offshore wind turbines," tech. rep., Risoe National Laboratory, GarradHassan & Partners Ltd., Germanischer Lloyd WindEnergie GmbH, ECN and the Greek Centre for Renewable Energy Sources, 2005.

[18] H. J. T. Kooijman, C. Lindenburg, D. Winkelaar, and E. L. V. D. Hooft, "DOWEC 6 MW pre-design: Aero-elastic modelling of the DOWEC 6 MWpre-design in PHATAS," tech. rep., ECN, Petten, Netherlands, 2003.

[19] M. Drela, "XFOIL: An analysis and design system for low Reynolds number airfoils," in *Low Reynolds number aerodynamics*, (Notre Dame, IN, Germany), 1989.

[20] D. Castaignet, T. K. Barlas, T. Buhl, N. K. Poulsen, J. J. Wedel-Heinen, N. A. Olesen, C. Bak, and T. Kim, "Full-scale test of trailing edge flaps on a Vestas V27 wind turbine: active load reduction and system identification," *Wind Energy*, vol. 17, pp. 549–564, Apr. 2014.

[21] J. Berg, B. R. Resor, J. Paquette, and J. White, "SMART Wind Turbine Rotor: Design and Field Test," tech. rep., Sandia National Laboratories, Albuquerque, New Mexico and Livermore, California, 2014.

[22] J. Berg, M. F. Barone, and N. Yoder, "SMART Wind Turbine Rotor: Data Analysis and Conclusions," tech. rep., Sandia National Laboratories, Albuquerque, New Mexico and Livermore, California, 2014.

[23] M. H. Hansen, A. Hansen, T. J. Larsen, S. Oye, P. Sorensen, and P. Fuglsang, "Control design for a pitch-regulated, variable speed wind turbine," tech. rep., Risoe, Denmark, 2005.

[24] D. J. Leith and W. E. Leithead, "Implementation of wind turbine controllers," *International Journal of Control*, vol. 66, no. 3, pp. 349–380, 1997.

[25] W. E. Leithead, V. Neilson, S. Dominguez, and A. Dutka, "A novel approach to structural load control using intelligent actuators," in *17th Mediterranean Conference on Control & Automation*, (Thessaloniki, Greece), pp. 1257–1262, 2009.

[26] W. E. Leithead and V. Neilson, "Alleviation of Unbalanced Rotor Loads by Single Blade Controllers," in *EWEC*, (Marseille, France), 2009.

[27] M. A. Lackner and G. A. M. van Kuik, "A comparison of smart rotor control approaches using trailing edge flaps and individual pitch control," *Wind Energy*, vol. 13, pp. 117–134, Mar. 2010.

Chapter 5

Performance analysis

There are numerous methods being used to determine the performance of the smart rotor concept, both as regards to the metrics for assessment and the conditions under which the control is tested. This chapter explores the various options and details the methods used for assessing the performance of the wind turbine in this thesis.

In Section 5.1 the motivation behind research into wind turbines is looked at, with consideration given to the cost of energy, control objectives, and loads. Section 5.2 then looks at the metrics used to assess the performance of the smart rotor, with reference to basic statistics, as well as specific details on using power spectral density plots, damage equivalent loads and extreme load extrapolation. Finally, the design load cases under which the turbine is tested are described in Section 5.3.

5.1 Motivation

5.1.1 Cost of Energy

The performance of a wind turbine can be measured in a number of ways. In the end though, the adoption of one design or control method over another will depend on a cost analysis. For power generation this is typically done through a levelised cost of energy analysis, which takes account of energy capture, capital costs and operations and maintenance expenditure, as well as risk through the interest rate attached to capital finance. An overview of the capital costs of a wind turbine is shown in Figure 5.1. This captures the feasible cost reductions that a smart rotor may achieve. The rotor blades, hub and bearings, as well as the shaft, yaw and pitch systems can be targeted for load reduction using the smart rotor as discussed later.

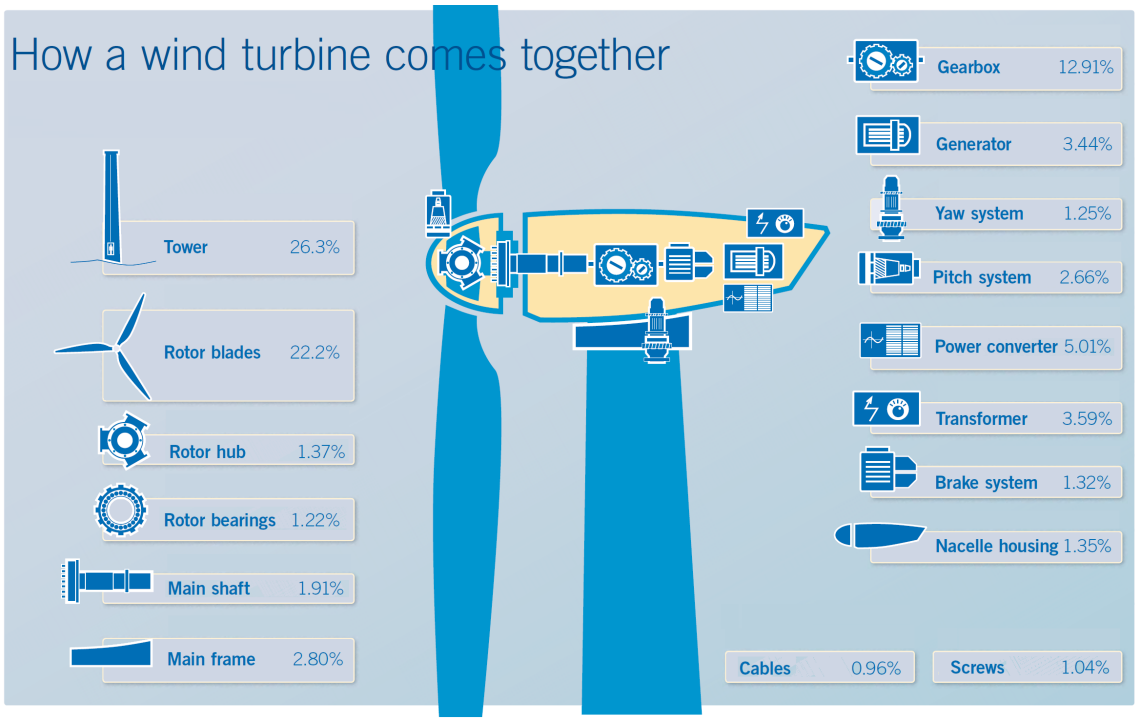

Figure 5.1: Breakdown of the capital costs associated with a 5MW wind turbine. Source [1]

More direct applications to quantify cost of energy savings using the smart rotor have focussed on the blade loads. One paper that attempts a cost analysis of the smart rotor is [2]. A conceptual 2.5MW is created based on the WindPACT 1.5MW to compare costs between a baseline and two versions of a smart rotor: one with devices capable of altering the local aerodynamics and one capable of actively extending the blades, the retractable rotor blade. Using the retractable rotor blade cost of energy could potentially be reduced by between 0.6 and 3.9%, and using active devices anything between +0.5 and -2.6%, depending on estimates for the smart rotor system costs and the operations and maintenance costs associated with it. The method is crude, using BEM aerodynamics, simple control, and rough estimates, but does nonetheless show the potential of the smart rotor when reducing structural loads.

There are also a few papers from Sandia National Laboratories looking at the cost-of-energy

benefits of the smart rotor. In [3] and [4], it is proposed that use of a smart rotor to reduce fatigue loads can allow the blades to be extended and still have the same lifetime as shorter blades. The effect of simply increasing the blade length while keeping the blade root bending load constant and the rest of the turbine the same is termed the "grow-the-rotor" concept, Figure 5.2. The extended rotor has increased energy capture below rated power, with analyses showing a 10-15% increase in energy capture for a 1.5MW wind turbine, particularly at sites of low mean wind speed. This equates to a reduction in the cost of energy of between 5 and 9%. Such approaches need to be used carefully though, as other loads, structural, electrical, mechanical or noise requirements could easily limit the possibility of increasing energy capture using this method.

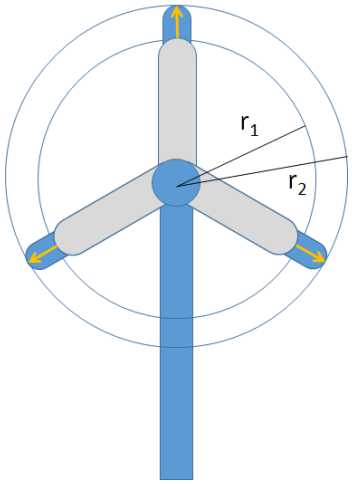

Figure 5.2: The "grow-the-rotor" concept whereby the blade length is increased until the blade root loads match those of the original wind turbine, whilst holding all other wind turbine parameters the same

While these cost analyses are useful, a detailed cost analysis is beyond the scope of this thesis and will depend highly on the specifics of the wind turbine and smart rotor system under consideration. The performance analysis described in this chapter though should aid designers in estimating the impact adoption of the smart rotor will have on the cost of energy and indeed at understanding the role the smart rotor might play. Risk on the other hand is not directly considered in this performance analysis, but is addressed separately in Chapter 10, wherein a fault of the smart rotor system is examined.

5.1.2 Controller objectives

The assessment of the wind turbine performance depends, at least partly, on the control objectives. The control objectives inform what criteria should be looked at in the evaluation. The majority of authors have looked into using the smart rotor control as a means to reduce loads and so reduce the material constraints required to build large multi-MW wind turbines. However, the smart rotor concept may also be used to target other objectives, as listed in [5], and displayed here

1. Devices may be deployed to increase lift of the blade at low wind speeds, allowing the turbine to cut-in earlier and capture additional energy

2. On downwind machines, these devices could deploy every revolution to counteract the tower wake effect
3. Active devices could aid in energy capture and load mitigation on turbines that experience array effects (e.g. to mitigate loads caused by wake from upstream wind turbines)
4. Devices could be used to prevent tower strikes, allowing for larger diameter rotors to be used and thereby increasing energy capture
5. Aerodynamic performance enhancement and noise reduction could be realized by maintaining laminar flow over the blade
6. The blade could operate higher on the lift curve with the devices protecting the blade from getting into stall

Some of these objectives have been looked at. For example using the control to mitigate the array effects such as wake from upwind turbines [6]. In the helicopter research field the smart rotor concept is being used to reduce rotor vibrations and reduce noise [7], [8], although this noise due to vortex wake reaction may not be dominant noise produced by wind turbines. Other authors have also looked at using the smart rotor as an alternative to pitch and torque control, to regulate rotor torque and power [9], [10], and in Chapter 9 of this thesis this is explored through supplementing the pitch speed control mechanism with the aim of reducing pitch actuator requirements. As an entirely separate objective, the smart rotor's inclusion of additional sensors also allows for condition monitoring of the wind turbine system [11], helping to reduce risk and potentially operations and maintenance costs.

While the use of devices to counteract tower shadow on downwind wind turbines is interesting this is outside the scope of this thesis due the choice of an upwind turbine being used. Noise reduction is also beyond the scope of this thesis, as there is no method to determine the noise output from the wind turbine in the model, additionally, on offshore wind turbines, this is less likely to be a design driver.

As regards to preventing tower strikes this is unlikely to be implemented, as although increasing clearance may be possible using smart rotor devices, the failure of such devices also needs to be taken into account. Therefore, for general performance analysis, tower clearance is neither considered as an objective nor a qualifying criterion for reducing the cost of energy.

The opportunity to increase energy capture using the smart rotor system is certainly worth looking at. Despite this, the decision has been made to focus on load reductions, building upon the work of others in the smart rotor field. Indeed, to make certain that energy capture is not affected by the smart rotor or advanced load reduction control techniques, they are purposefully phased out below rated. This simplifies the analysis to an assessment centred on load reduction potential. This is the primary focus of smart rotor research, particularly on blade root bending moment load reduction for both fatigue and ultimate loads [7], [11], [12], [13], [14], [15], [16], [17], [18], [19].

5.1.3 Loads

As regards to the loads used to assess the performance of the smart rotor concept the literature suggests various metrics and measurands. A common target for control is reduction in loads on the blade root bending moment. This might be gauged by a reduction in the standard deviation of the signal or as a reduction in the damage equivalent loads. A summary of some of the papers that use such methods is found in [20], and is displayed in Figure 5.3.

Paper	c_f [%]	dr_f/r [%]	δ [±°]	T.I. [%]	Shear exp. [–]	V_{av} [m s^{-1}]	Reduction in std of RBM [%]	Reduction in DEL [%]	Controller
Riziotis and Voutsinas[3]	10	15–47	6	—	0.2	8, 12, 16	30–35 (range)	—	PID
Andersen *et al.*[16]	10	63	8	14–18	0.14	7, 11, 18	—	36.2–47.9	HPF+inflow
Lackner and van Kuik[5]	10	20	10	NTM, ETM	0.2	8, 12, 16, 20	—	5.6–24.6	PID
Barlas and van Kuik[6]	10	20	10	NTM	0.2	8, 11.4, 16	5.7–22.4	—	PID
Andersen *et al.*[4]	10	15–30	8	—	—	11.4	—	25–37	HPF
Resor *et al.*[7]	10	24	10	6	0.2	15	26–30.9	27–31.3	PD, HPF+notch
Wilson *et al.*[8]	10	24	10	6	0.2	15	13.3	15.5	LQR
Berg *et al.*[9]	10	25	10	6	0.2	15	8.7–18.1	10.9–17	PD, LQR
This paper	10	18	8	6, NTM	0.2	7, 11.4, 15	10.9–30.7	10.9–27.3	MPC+inflow

In the column headings: c_f was the % chord width of the flap; dr_f/r the % span of blade with flaps, δ the maximum flap deflections, T.I. the turbulence intensity, V_{av} the mean wind speed, std of RBM the standard deviation of the blade root bending moment, and DEL the damage equivalent load. In the controller column: PID was a proportional integral differential controller, HPF a high pass filter, notch a notch filter, LQR a linear quadratic regressive controller, MPC a model predictive control, and inflow involves measuring the incoming flow field for feed-forward control

Figure 5.3: Comparison of different studies into the smart rotor [20]

Reductions in blade root bending moment are not the only outcome of using control focussed on this aspect though, as seen in [21] on individual pitch control. Shaft and yaw bearing loads are also affected, as too is the pitch motion. In [22], a paper on distributed blade control, energy capture and pitch actuation are also seen to be dependent on controller design. This is also reported in [23], as well as the effect their controllers have on tip deflection, tower movement and the low speed shaft torque.

The majority of papers look at similar loads when assessing the performance of the smart rotor. The choice to use the blade root bending moment as the primary measurement appears to be because the smart rotor affects this directly when active, and other loads can be considered as being indirectly affected by the action of the smart rotor control. However, that is not to say it is the most important or only load that needs to be considered. Reduction in other loads or parameters may be equally important when it comes to ascertaining the viability of the smart rotor concept. For example a reduction in mean power production affects the economically viability of the smart rotor and in [3] it is shown that although most loads are reduced, certain loads can in fact increase with the low speed shaft torque and blade root pitch moment highlighted, which may limit cost effectiveness, see Table 5.1. It seems sensible then to measure a selection of loads to gain a full picture to account for both beneficial and undesirable effects.

A study of the loads themselves also highlights where exactly the control needs to act. In [13]

Table 5.1: One-million cycle damage equivalent load (Smart rotor/Baseline [%]) with conventional trailing edge flap

Measurement	9m/s	11m/s	18m/s
Low speed shaft torque	-1.9	6.3	12.0
Blade root edge moment	1.1	1.5	-0.3
Blade root flap moment	-23.8	-11.9	-12.6
Blade root pitch moment	-2.8	1.7	14.9
Tower base side-side moment	0.3	1.8	-5.3
Tower base fore-aft moment	-16	-12.3	-3.0
Tower top yaw moment	-29.2	-19.0	-21.3

plots of the blade root bending moment damage equivalent loads, based on the load frequency and mean wind speed, highlight that most fatigue loads are at high wind speeds, low frequencies (below 5Hz) and at blade passing frequencies. This type of load analysis, along with power spectral density plots, helps resolve where the smart rotor control should focus in order to increase turbine lifetime, see Figure 5.4.

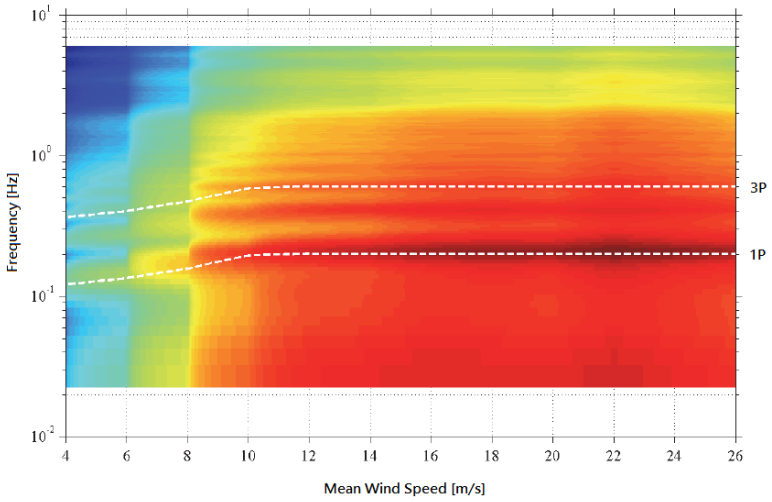

Figure 5.4: Fatigue analysis in the frequency domain of the blade flapwise root bending moment. Darker red colors indicate higher fatigue damage contributions [24]

5.2 Metrics

Different metrics may be considered useful for different purposes. A measurement of the standard deviation of certain loads may be used to quickly determine whether the control is acting as required. Power spectral density plots may be used to assess what the frequencies of the loads that need mitigating are and whether the control is acting to reduce these loads. Whereas damage equivalent loads and other load calculations help determine how cost effective using the smart rotor concept would actually be. Just looking at any one of these does not give the full picture, so it is important to consider a number of these to get a global understanding of the effect the smart rotor is having on the wind turbine.

There are three overall approaches that have been used to determine the performance of wind turbines: basic statistics, time domain load analysis and frequency analysis. Basic statistics include using the mean, recording the maximums and minimums, and calculating the standard deviation. Time domain analysis is slightly more complicated, often using rainflow counting and Miner's rule to determine damage, as per the IEC 61400-1 standard [25], or damage equivalent loads, which are preferred when specific design restraints are unknown. Then frequency domain analysis involves converting signals to the frequency domain and plotting power spectral densities.

Calculating the mean, standard deviation and extremes of the signals are a quick method to determine what effect the control strategy or any other altered parameter is having on the measurements, but it does not quantify the changes in a practical way: a 50% decrease in standard deviation for example does not necessarily correlate to a specific improvement in design life. To quantify changes in loads, calculation of damage equivalent loads (DELs) is common. Power Spectral Density (PSD) plots on the other hand aid in determining at which frequencies damping or control action is required and determining what the root cause is.

5.2.1 Power spectral density plots

Power spectral density plots display the frequencies at which most of the energy, and so damage, is focussed. The standard log-log plots can be supplemented with cumulative plots to recognise this more clearly. For example in Figure 5.5 and Figure 5.6 of the flapwise blade root bending moment, most energy can be seen to be focussed at low frequencies and at the rotational frequency of the turbine, 1.26rad/s, and harmonics thereof. While Figures 5.7 and 5.8, this time of the high speed shaft speed, highlight the influence of the first drive-train mode and the need for damping at this frequency. The drawback of the frequency analysis is that it is hard to monetise any variations and this is why damage equivalent loads are often used.

5.2.2 Damage equivalent loads

Damage equivalent loads are calculated in the time domain using rainflow counting to determine the stress cycles and then these are converted to damage using Wohler SN-curves and Palmgren-Miner's rule. The process described here is similar to that used in [26].

The procedures for rainflow counting are documented in the ASTM standard E1049-85 [27]. There are a number of different ways to conduct rainflow counting, for example in Bladed the process is to order the maxima and minima then calculate the cycles, but the process used here is

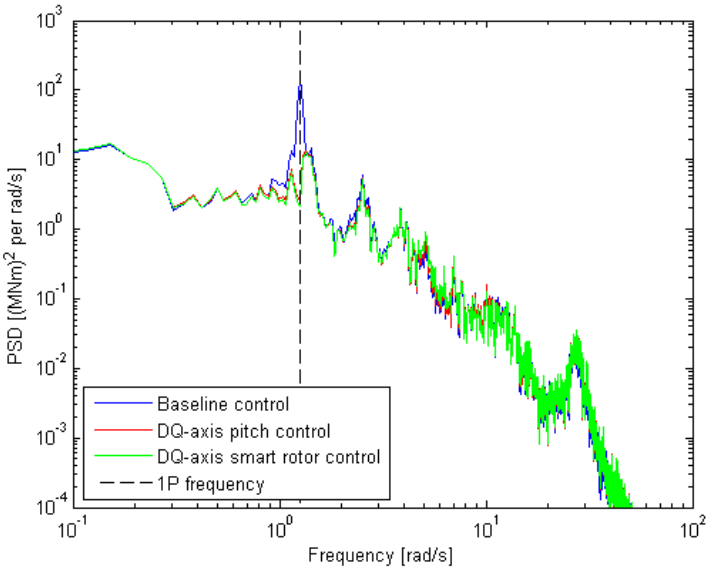

Figure 5.5: PSD of blade root bending moment

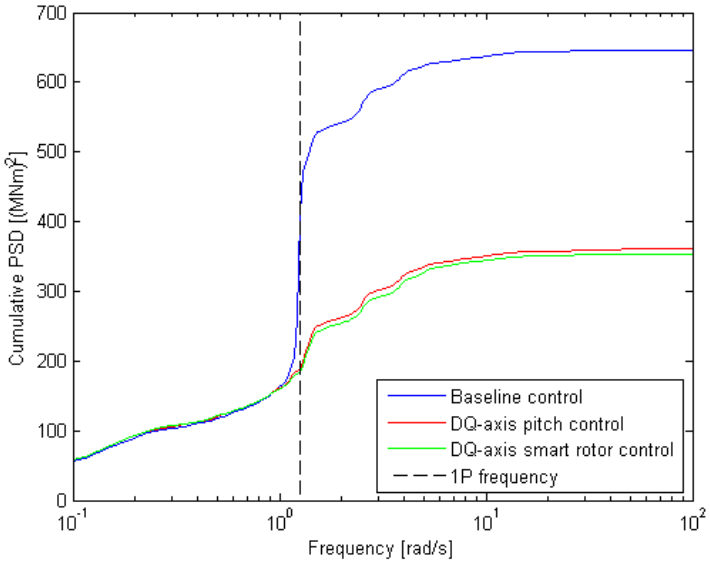

Figure 5.6: Cumulative PSD of blade root bending moment

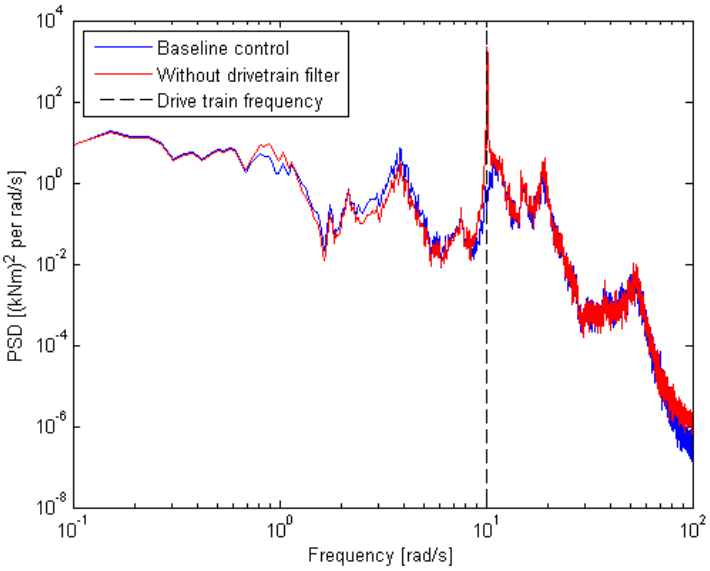

Figure 5.7: PSD of high speed shaft torque

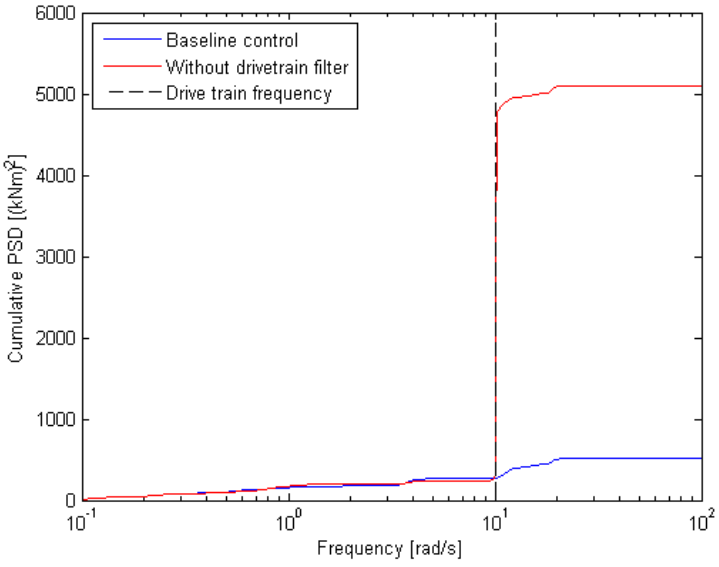

Figure 5.8: Cumulative PSD of high speed shaft torque

as described in section 5.4.4 of the ASTM standard, and is as follows: let X denote range under consideration; Y, the previous range adjacent to X, and S, the starting point in the history.

1. Read next reversal (peak or valley). If out of data, go to Step 6.
2. If there are less than three points, go to Step 1. Form ranges X and Y using the three most recent reversals that have not been discarded.
3. Compare the absolute values of ranges X and Y

   If $X < Y$, go to Step 1

   If $X >= Y$, go to Step 4.
4. If range Y contains the starting point S, go to Step 5; otherwise, count range Y as one cycle; discard the reversals of Y; and go to Step 2.
5. Count range Y as one half cycle; discard the first reversal in range Y; move the starting point to the second point in range Y; and go to Step 2.
6. Count each range that has not previously been counted as a half cycle.

The results of using this method on a time series of the blade root bending moment are shown in Figure 5.9. Note although there are higher harmonics in the spectrum, these are rarely counted as they do not result in a reversal, so do not affect the fatigue life of the component.

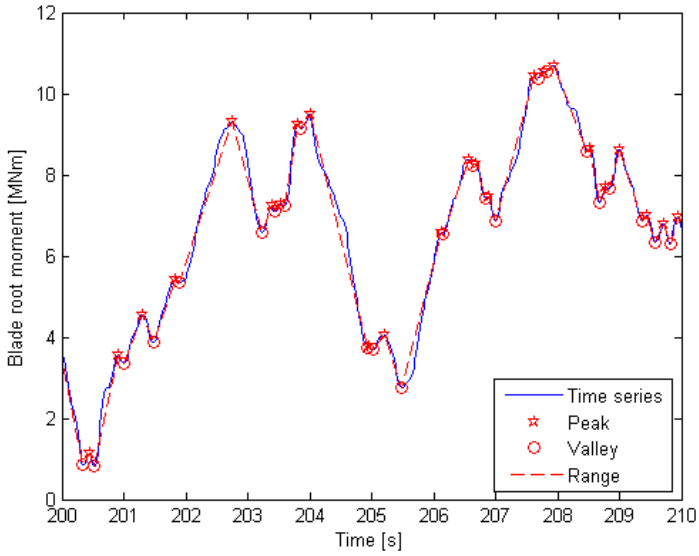

Figure 5.9: Example of the rainflow counting peak selection process

These cycles then need converting to stress ranges. To convert bending moments to stresses the required formula is

$$S = \frac{M \times y}{I_x} \tag{5.1}$$

where M is the moment about the neutral axis, y the perpendicular distance to the neutral axis, and I_x the second moment of area about the neutral axis x. At the hub, the blade section is cylindrical; the second moment of area may therefore be described by

$$I_x = \frac{\pi}{4}(r_2^4 - r_1^4) \tag{5.2}$$

where r_2 is the outer radius of the cylinder, and r_1 the inner radius. The maximum stresses will occur at the outer radius, $y = r_2$. The outer radius is given for the NREL 5MW wind turbine, $r_2 = 3.5m$, unfortunately the inner radius of the cylinder is not given, however an estimate can be made from the mass per unit length, $715kg/m$, and density of the blade assuming it is glass fibre, $2500kg/m^3$, resulting in $r_1 = 3.487m$, implying $I_x = 1.745m^4$, and the conversion factor for the root bending moment, M_{RBM}, to maximum stress at the blade root, S, is thus $S = 2.01 \times M_{RBM}$, in all directions.

Once the number of cycles at different stress ranges has been determined they can be used to calculate damage equivalent loads using Wohler S-N curves. Wohler S-N curves describe the number of sinusoidal cycles at different stress ranges before failure occurs, and are dependent on the material under consideration, for example they have different Wohler exponents and endurance limits. The formula describing the S-N curve is

$$N = N_D(S_D/S)^m \tag{5.3}$$

where m is the Wohler exponent, S_D is the endurance limit of the material and N_D the number of cycles to failure at this limit. A typical constant amplitude curve for steel and glass reinforced plastic (fibreglass) is shown in Figure 5.10, with Wohler exponents 4 and 10 for steel and fibreglass respectively. The endurance limit of steel is estimated to be $200MPa$ at 10^6 cycles and $175MPa$ for fibreglass at 10^8 cycles.

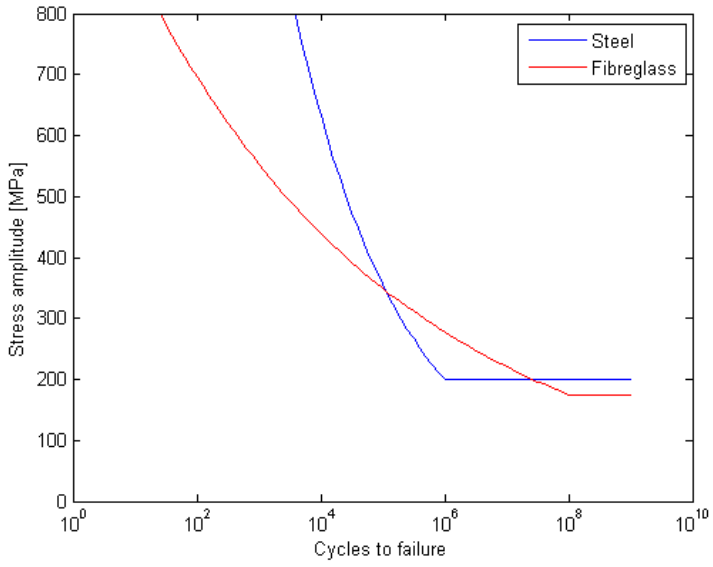

Figure 5.10: Example of constant amplitude SN-curves for steel and fibreglass

When the loads vary in amplitude, stress ranges below the endurance value may also lead to component failure, as they can extend existing cracks in the material. To take this into account the SN curve is extended. Two methods used are elementary Miner's method: whereby the curve is simply continued beyond the endurance limit; and Haibachs method: whereby the slope of the curve is modified slightly beyond the endurance limit. These are portrayed in Figure 5.11. The treatment of small cycles however has been shown to have little impact on damage prediction, so use of Elementary Miner's method is appropriate as a conservative estimate [28] (referenced in [26]).

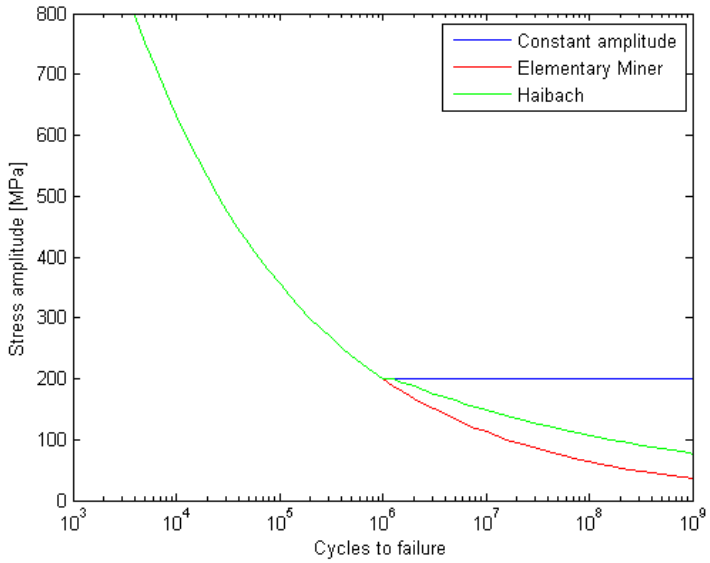

Figure 5.11: Constant and variable amplitude SN-curves for steel

Another factor affecting the number of loads to failure is the mean of the stress range. The S-N curve may be modified to take the mean stress into account using an empirical relationship. This is typically portrayed using the R value, $R = S_{max}/S_{min}$, where S_{max} and S_{min} are the maximum and minimum stresses during a cycle. The Goodman formula is a trusted relationship to account for non-zero means, defined by $\frac{S_a}{S_e} + \frac{S_m}{S_u} = 1$, where S_e is the endurance limit of the material, S_u the ultimate limit, S_m the mean stress, and S_a the adjusted S-N curve of constant life. A graph of some different options is shown in Figure 5.12 for steel, with the area below the curves being the operable life zone, and that above being the failure zone.

Unfortunately there is limited data available for the composite materials used in wind turbine blades, and the Goodman diagram is often of a non-linear nature. The mean stress is therefore typically ignored in damage calculations regarding the wind turbine blades [29], but an approach that at least accounts for the mean stress is to use an idealised Goodman curve, with the assumptions that the curve is symmetric (i.e. tensile and compressive actions are equivalent) and that fatigue strength decreases linearly from a maximum at zero mean stress to zero at the ultimate tensile and compressive strengths. A simple relationship can then be used to alter the calculated damage equivalent loads. Metals require a similar mean stress correction [26].

Miner's rule allows the calculation of the total damage, D, of partial damages, d_i, due to a finite

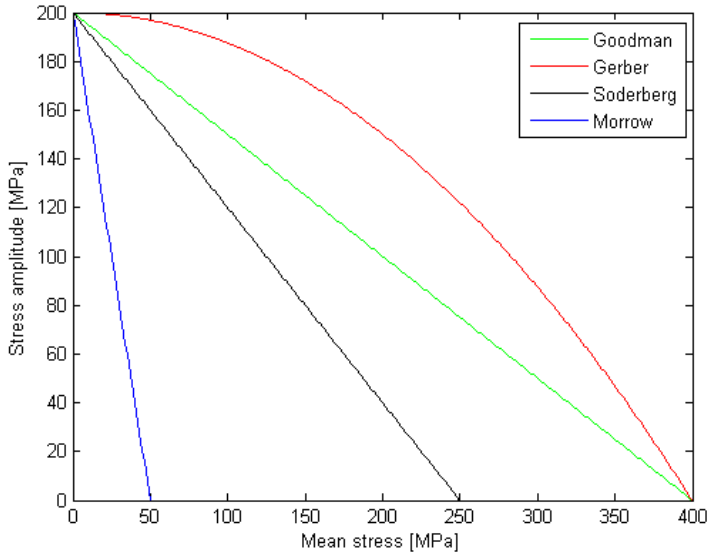

Figure 5.12: Methods to account for non-zero mean stress ranges

number of cycles, n_i, at different stress ranges with cycles to failure N_i, as follows

$$D = \sum_{i=1}^{n} d_i = \sum_{i=1}^{n} \frac{n_i}{N_i} \tag{5.4}$$

If Elementary Miner's method is used to extend the SN curve such that the SN curve is fully defined by $S = \frac{k}{N}^{\frac{1}{m}}$ then the total damage can be rewritten as

$$D = \sum_{i=1}^{n} \frac{n_i}{N_i} = \sum_{i=1}^{n} \frac{n_i}{N_{ref}} \left(\frac{S_i}{S_{ref}} \right)^m \tag{5.5}$$

where S is the stress range and the subscript $_{ref}$ denotes a reference value on the SN curve. Damage Equivalent Loads (DELs) relate the total damage to an equivalent load over a chosen number of cycles

$$D = \sum_{i=1}^{n} \frac{n_i}{N_{ref}} \left(\frac{S_i}{S_{ref}} \right)^m = \frac{N_{eq}}{N_{ref} \left(\frac{S_{eq}}{S_{ref}} \right)^m} \tag{5.6}$$

which rearranging leads to

$$S_{eq} = N_{eq}^{-\frac{1}{m}} \left(\sum_{i=1}^{n} n_i S_i^m \right)^{\frac{1}{m}} \tag{5.7}$$

If N_{eq} is set to the duration of the sampled data, i.e. 600s, then the 1Hz damage equivalent load is calculated. It then becomes possible to compare different load conditions and controller options using this metric, often called the 1Hz Damage Equivalent Load (1Hz DEL or DEQL) without detailed knowledge of the SN curve required to determine the actual damage over the wind turbines lifetime.

To determine how a given reduction affects the lifetime of the wind turbine, a simple calculation taking account of the Wohler coefficient is needed, given by, $(S_{eq,old}/S_{eq,new})^m$. Different load

scenarios may also be compared relative to each other over the lifetime of the turbine by comparing their probability of occurring and damage equivalent loads.

$$d_{rel,j} = \frac{d_j}{D} = \frac{L_j S_{eq,j}^m}{\sum_{j=1}^{n} L_j S_{eq,j}^m} \tag{5.8}$$

where L_j is the duration and $S_{eq,j}^m$ the 1Hz damage equivalent load of a particular load scenario. For example this could be used to calculate the relative loads at various wind speeds using the wind speed distribution at the site.

Finally, to account for non-zero mean oscillations, a similar process of describing the stress range caused by a non-zero oscillation with an equivalent stress range with zero mean may be used. For composites using an idealised symmetric Goodman curve this is defined by

$$S_{eq}(S_m = 0) = N_{eq}^{-\frac{1}{m}} \left(\sum_{i=1}^{n} n_i \left(\frac{S_i}{1 - \frac{|S_m|}{UTS}} \right)^m \right)^{\frac{1}{m}} \tag{5.9}$$

where UTS is the ultimate tensile strength, and S_m the mean of the stress range. An equivalent for metals is described by

$$S_{eq}(S_m = 0) = N_{eq}^{-\frac{1}{m}} \left(\sum_{i=1}^{n} n_i (S_i + 2MS_{m,i})^m \right)^{\frac{1}{m}} \tag{5.10}$$

where M is the mean stress sensitivity, which for steel is $M \approx 0.075$ and cast iron $M \approx 0.19$.

5.2.3 Extreme load extrapolation

For extreme loads it is often necessary to do a statistical extrapolation to determine the 1-in-50-year loading on a wind turbine component. In the Bladed manual to do this extrapolation fifty 40-minute simulations for each external condition, e.g. mean wind speed, are recommended for offshore wind turbines [30]. The IEC 61400-1 standard [25] on the other hand facilitates the use of the same simulations as required for fatigue load analysis. The process proposed in the IEC standard is therefore preferable for easy analysis. The process used for determining the 50 year extreme load is described below:

1. Extract extreme values from all runs at each given wind speed, v_j. The extreme values are defined as the largest value between successive upcrossings of the mean plus 1.4 standard deviations, as proposed in the IEC standard.

2. Fit a Gumbel (extreme-value) distribution to the extracted data for each wind speed, $P(F|v_j)$

3. Calculate the long term exceedance probability, $P_e(F)$, for a reference period of 10 minutes, taking account of the Rayleigh distribution of wind speeds, $P(v_j)$, and the expected number of extreme loads in 10 minutes, n_{10m},

$$P_e(F) = \sum_j \left(1 - (1 - P(F|v_j))^{n_{10m}}\right) \times P(v_j) \tag{5.11}$$

Binning is used for this calculation such that v_j is the centre of the bins extending $\pm\Delta v_j/2$, where Δv_j is the separation between mean wind speeds

4. Determine the 50-year load exceedance value, defined as F_k, found where $P(F_k) = 3.8 \times 10^{-7}$, which is the probability of a 10 minute period occurring once every 50 years

The tools for these analysis methods are developed in MATLAB and are included in Appendix D.

5.3 Design load cases

In addition to the various metrics that may be used to assess the effectiveness of the controller, different load cases may also be used. Much of the smart rotor control concepts have focussed on minimising fatigue loads and so have used the IEC standard as a reference. The IEC load cases appear the sensible choice, as it is the industry standard and so well defined, and allows comparison with some of the other works. Work has also been conducted looking into the effect of the smart rotor control in meandering wakes (produced from wind turbines upwind) [6] and during more turbulent flows (IEC extreme turbulence model) [31] and under extreme loads such as gusts [14].

The full set of load cases required for certification is described in [25]. The standard takes account of various situations: power production, faults, start up, normal shut down, and emergency shut down; amongst others. The design load cases that are most relevant are those during normal power production, although the smart rotor may also affect other design situations for example start up or emergency shut down and faults, including in the smart rotor system itself, looked at in Chapter 10.

A good analysis of the design load cases and their affect on loads is given in [13], which looks at a wide selection of design load cases to study both the extreme and fatigue loads on the NREL/UpWind 5MW reference wind turbine. Figure 5.13 shows that DLC 1.1/1.2 contributes the most to fatigue damage. This is the design load case for when the wind turbine is in normal power production, under normal turbulence wind conditions. The difference between DLC 1.1 and 1.2 is the method of post-processing used, explained in Section 5.3.1. The loads on the tower fore-aft moment are also affected by design load cases 4.1, normal shut down, and 3.1, normal start up. From these results it would appear sensible to use only DLC 1.2 for analysing the fatigue damage. Although if the effect the smart rotor control has on the tower is of importance the fatigue loads on this component should be checked with both DLC 1.2 and DLC 4.1 for completeness.

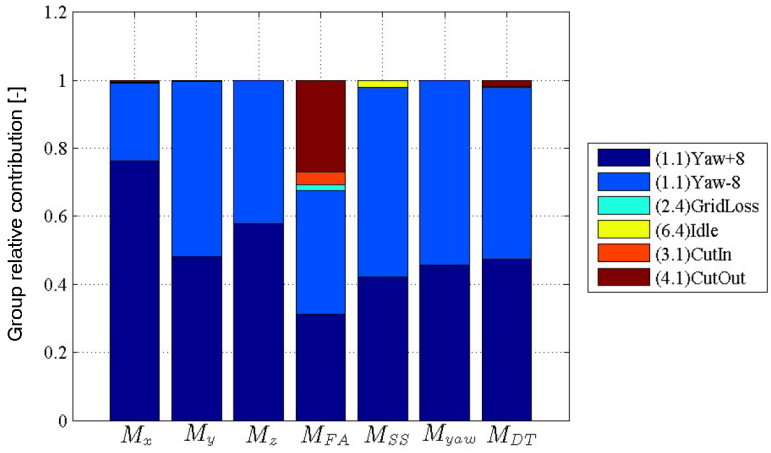

Figure 5.13: Relative contributions of fatigue damage by design load case where: M_x, M_y, M_z are the blade in-plane, out-of-plane and pitch moments respectively, M_{FA} and M_{SS} are the fore-aft and side-side tower moments, M_{yaw} the tower yaw moment, and M_{DT} the main shaft torsion [24]

DLC 1.2 is also used by a number of other authors for testing fatigue load reductions for this

reason. Examples of works that either directly cite DLC 1.2, or which follow similar cases and use the normal turbulence model (NTM), are [3], [4], [6], [11], [12], [20], [23], [31], [32], [33], [34] and [35].

The extreme loads are slightly more complex, with different design load cases causing maximum loads for different wind turbine components, as seen in the analysis of [13]: DLC 1.3, normal operation but with an extreme turbulence wind field model (ETM), causes the highest loads for main shaft torsion and tower yaw moments, and second highest on the tower side-side moment; DLC 1.4, an extreme coherent gust with direction change (ECD), results in the highest blade flap moment, and DLC 2.3, a fault during power production with an extreme operational gust (EOG), the greatest loads for the blade edge and tower fore-aft moments. The extreme loads on the tower side-side moment are caused by DLC 6.1-6.3, but these are cases when the turbine is stopped (standing still or idling) and as such these design load cases will unlikely be affected by any smart rotor control strategy. DLC 1.3, 1.4 and 2.3 are therefore used in [32] and [36] to calculate the extreme loads of the blade flap, edge and torsion moments, tower fore-aft, side-side and torsion moments, and the shaft torsion moments.

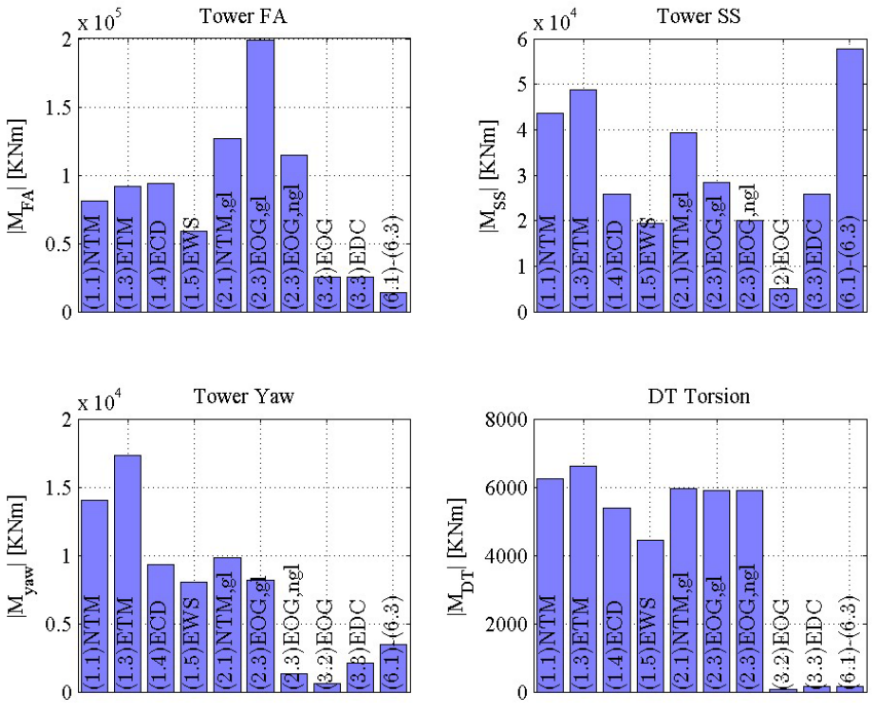

Figure 5.14: Maximum loads for various design load cases. Acronyms as in text, additionally with EWS referring to extreme wind shear [24]

DLC 1.4 and 2.3 are both operation under an extreme operational gust. The response of the smart rotor to gusts is also considered in [14]. A point that is raised is that the IEC standard gust is a global gust across the entire rotor, whereas local gusts are of more interest to the smart rotor control, because the devices on the smart rotor can react to local wind field variations.

When considering tip deflection that may cause tower strike in [37] the design load cases that are seen to be most important are DLC 2.2, 3.2 and 3.3, because these cause the largest tip deflections

as seen in Table 5.15.

Load case	Description	m
1690	DLC1.6 EOG_50 at cut-out wind with positive misalignment.	12
1350	DLC1.3 ECD, at rated wind and positive direction change.	21
2204	DLC2.2 NWP, Pitch runaway of all blades, at rated wind.	24
3383	DLC3.3 EDC_1 Start with Extreme Direction Change, max-start	25
3277	DLC3.2 EOG Start with Extreme Operating Gust, max-start.	25
2208	DLC2.2 NWP, Pitch runaway of all blades, at cut-out wind.	28

Figure 5.15: Maximum tip deflection in the out-of-plane direction for various design load cases. Acronyms as in text, additionally with NWP referring to a normal wind profile [37]

The design load case to employ during simulations depends on the control objective, which is primarily fatigue load reduction. Simulations in this thesis therefore focus on DLC 1.2 as this is most relevant to fatigue loads and simplifies analysis.

5.3.1 DLC 1.1 and 1.2

Design Load Case 1.1 and 1.2 are identical but DLC 1.1 is utilised to extrapolate for extreme loads and DLC 1.2 is utilised to calculate fatigue loads during normal power production. DLC 1.1 and 1.2 are employed to determine the loads that result from atmospheric turbulence that occurs during the normal operation of the wind turbine throughout the wind turbine's lifetime. A Normal Turbulence Model (NTM) is used to simulate the wind at a range of wind speeds. The IEC standard considers a resolution of 2m/s sufficient to account for the wind turbine operating in all wind speeds, with at least six 10-minute runs for each wind speed. Particular attention should be paid to wind speeds expected to be the most adverse for the wind turbine design. This includes testing with simulations of an 8 degree inclination to the horizontal axis of the wind turbine.

The standard categorises wind turbines into different classes depending on their suitability to different wind conditions. The wind condition parameters that need to be used for each class are shown in Figure 5.16

Wind turbine class		I	II	III	S
V_{ref}	(m/s)	50	42,5	37,5	Values
A	I_{ref} (-)	0,16			specified
B	I_{ref} (-)	0,14			by the
C	I_{ref} (-)	0,12			designer

In the table, the parameter values apply at hub height and
V_{ref} is the reference wind speed average over 10 min,
A designates the category for higher turbulence characteristics,
B designates the category for medium turbulence characteristics,
C designates the category for lower turbulence characteristics and
I_{ref} is the expected value of the turbulence intensity at 15 m/s.

Figure 5.16: Basic parameters from the IEC standard for wind turbine classes [25]

So for example a class IB wind turbine, as used in the UpWind project [19] and specified in the REpower technical data sheet [38] and so used in this work, has a 10 minute mean reference wind speed of 50 m/s, and a reference turbulence intensity at 15m/s of 0.14. These parameters are used in modelling the wind conditions detailed below.

The normal wind conditions include a wind speed distribution that has a Rayleigh distribution about the mean 10 minute wind speed at hub height, V_{hub}, given by

$$P_R(V_{hub}) = 1 - \exp\left[-\pi\left(\frac{V_{hub}}{2V_{ave}}\right)^2\right] \tag{5.12}$$

where $V_{ave} = 0.2V_{ref}$.

The wind profile is given by the power law

$$V(z) = V_{hub}\left(\frac{z}{V_{hub}}\right)^{\alpha} \tag{5.13}$$

where the power law exponent α assumed to be 0.2. This defines the average vertical wind shear.

In the normal turbulence model (NTM) the representative value of the turbulence standard deviation, σ_1, is given by the 90% quantile for the given hub height wind speed. This value for the different wind turbine classes is given by

$$\sigma_1 = I_{ref}(0.75V_{hub} + b) \tag{5.14}$$

where $b = 5.6m/s$.

Regarding the details of the normal turbulence model, it should satisfy a number of requirements:

- The turbulence standard deviation, σ_1, in the direction of the mean wind flow (longitudinal direction) should be invariant with height, and the components normal to the mean wind speed should have minimum standard deviations of:

  Lateral component (horizontal and normal to the longitudinal direction), $\sigma_2 >= 0.7\sigma_1$

  Upward component (tilted from the vertical by the mean flow inclination angle, normal to the other components), $\sigma_3 >= 0.5\sigma_1$

- The longitudinal turbulence scale parameter, Λ_1, at hub-height z, shall be given by: $\Lambda_1 = 0.7z$ when $z <= 60m$ and $42m$ when $z >= 60m$. The power spectral densities of the three orthogonal components, $S_1(f)$, $S_2(f)$ and $S_3(f)$ shall asymptotically approach the following forms as the frequency in the inertial sub range increases $S_1(f) = 0.05\sigma_1^2(\Lambda_1/V_{hub})^{-2/3}f^{-5/3}$, and $S_2(f) = S_3(f) = \frac{4}{3}S_1(f)$

- A recognised model for coherence, defined as the magnitude of the co-spectrum divided by the auto-spectrum for the longitudinal velocity components at spatially separated points in a plane normal to the longitudinal direction, shall be used.

The IEC standard recommends the Mann uniform shear turbulence model which fulfils these requirements, and also lists the Kaimal spectral and exponential coherence model as an alternative. Other models are discouraged as the choice of wind field model can affect loads significantly. Annex B in the IEC standard describes both of these models.

Bladed is capable of creating these two spectrums for use in simulations. The parameters required for the Mann wind field model are: Shear parameter, γ, Scale length, L, FFT points and the Maximum lateral/vertical wavelengths. The Kaimal model in Bladed requires the following parameters: turbulence length scales for the longitudinal, lateral and vertical directions, coherence scale parameter and coherence decay constant. TurbSim, an open source alternative from NREL, is also capable of creating the IEC Kaimal wind field spectrums. Both Bladed and TurbSim have the option of using the von Karman spectrum, which was included in the 2nd edition of the IEC standard, but excluded from the 3rd. The two software packages may also be used to create gusts or more extreme wind field profiles that may be used to test the wind turbine under additional IEC design load cases.

The IEC 61400-1 Ed. 3 Design Load Case (DLC) 1.2 accounts for the fatigue loads and uses the normal turbulence model (NTM), which is dependent on the wind turbine design class as the wind field input. The exact parameters used in the wind field synthesis and its effect on the wind turbine are explored in the following chapter.

References

[1] C. Aubrey, "Supply Chain: The race to meet demand," *Wind Directions*, pp. 27–34, Feb. 2007.

[2] T. J. McCoy and D. A. Griffin, "Control of Rotor Geometry and Aerodynamics: Retractable Blades and Advanced Concepts," *Wind Engineering*, vol. 32, pp. 13–26, Jan. 2008.

[3] D. Berg, D. G. Wilson, M. F. Barone, B. R. Resor, J. Berg, S. Kota, G. Ervin, and D. Maric, "The impact of active aerodynamic load control on fatigue and energy capture at low wind speed sites," in *EWEC*, (Marseille, France), US Government: Sandia National Laboratories, FlexSys Inc., 2009.

[4] D. Berg, D. G. Wilson, B. R. Resor, M. F. Barone, J. Berg, S. Kota, and G. Ervin, "Active aerodynamic blade load control impacts on utility-scale wind turbines," in *AWEA Windpower*, (Chicago, Illinois, USA), 2009.

[5] S. J. Johnson, C. P. V. Dam, and D. Berg, "Active Load Control Techniques for Wind Turbines," tech. rep., Sandia National Laboratories, Albuquerque, New Mexico, USA, 2008.

[6] P. B. Andersen, *Advanced Load Alleviation for Wind Turbines using Adaptive Trailing Edge Flaps: Sensoring and Control*. PhD thesis, Technical University of Denmark, 2010.

[7] T. K. Barlas and G. A. M. van Kuik, "State of the art and prospectives of smart rotor control for wind turbines," *Journal of Physics: Conference Series*, vol. 75, July 2007.

[8] Y. H. Yu, B. Gmelin, W. Splettstoesser, J. J. Philippe, J. Prieur, and T. F. Brooks, "Reduction of helicopter blade-vortex interaction noise by active rotor control technology," *Progress in Aerospace Sciences*, vol. 33, no. 97, pp. 647–687, 1997.

[9] J. G. Stuart, A. D. Wright, and C. P. Butterfield, "Considerations for an integrated wind turbine controls capability at the National Wind Technology Center: An aileron control case study for power regulation and load mitigation," tech. rep., National Renewable Energy Laboratory (NREL), Golden, CO, USA, June 1996.

[10] S. Joncas, O. Bergsma, and A. Beukers, "Power Regulation and Optimization of Offshore Wind Turbines Through Trailing Edge Flap Control," in *43rd AIAA Aerospace Sciences Meeting and Exhibit*, (Reston, Virigina), American Institute of Aeronautics and Astronautics, Jan. 2005.

[11] B. A. H. Marrant and T. van Holten, "Comparison of smart rotor blade concepts for large offshore wind turbines," in *Offshore Wind Energy and Other Renewable Energies in Mediterranean and European Seas*, vol. 31, (Civitavecchia, Italy), 2006.

[12] T. J. Larsen, H. A. Madsen, and K. Thomsen, "Active load reduction using individual pitch, based on local blade flow measurements," *Wind Energy*, vol. 8, pp. 67–80, Jan. 2005.

[13] L. Bergami, "Adaptive Trailing Edge Flaps for Active Load Reduction," in *7th PhD Seminar on Wind Energy in Europe*, (Delft University of Technology, Netherlands), 2011.

[14] M. A. Lackner and G. A. M. van Kuik, "The Performance of Wind Turbine Smart Rotor Control Approaches During Extreme Loads," *Journal of Solar Energy Engineering*, vol. 132, 2010.

[15] J.-W. van Wingerden, A. W. Hulskamp, T. K. Barlas, B. A. H. Marrant, G. A. M. van Kuik, D.-P. Molenaar, and M. Verhaegen, "On the proof of concept of a Smart wind turbine rotor blade for load alleviation," *Wind Energy*, vol. 11, pp. 265–280, May 2008.

[16] S. J. Johnson, J. P. Baker, C. P. van Dam, and D. Berg, "An overview of active load control techniques for wind turbines with an emphasis on microtabs," *Wind Energy*, vol. 13, pp. 239–253, Mar. 2010.

[17] A. W. Hulskamp, J.-W. van Wingerden, T. K. Barlas, H. Champliaud, G. A. M. van Kuik, H. Bersee, and M. Verhaegen, "Design of a scaled wind turbine with a smart rotor for dynamic load control experiments," *Wind Energy*, vol. 14, pp. 339–354, Apr. 2011.

[18] T. K. Barlas and G. A. M. van Kuik, "Review of state of the art in smart rotor control research for wind turbines," *Progress in Aerospace Sciences*, vol. 46, pp. 1–27, Jan. 2010.

[19] N. Fichaux, J. Beurskens, P. H. Jensen, and J. Wilkes, *Design limits and solutions for very large wind turbines: A 20 MW turbine is feasible*. EWEA, 2011.

[20] T. K. Barlas, G. van der Veen, and G. A. M. van Kuik, "Model predictive control for wind turbines with distributed active flaps: incorporating inflow signals and actuator constraints," *Wind Energy*, vol. 15, pp. 757–771, July 2012.

[21] E. A. Bossanyi, "Further load reductions with individual pitch control," *Wind Energy*, vol. 8, pp. 481–485, Oct. 2005.

[22] W. P. Engels, S. K. Kanev, and T. G. V. Engelen, "Distributed blade control," in *TORQUE: The Science of Making Torque from Wind*, (Heraklion, Crete, Greece), EWEA, 2010.

[23] D. G. Wilson, D. Berg, B. R. Resor, M. F. Barone, and J. Berg, "Combined individual pitch control and active aerodynamic load controller investigation for the 5mw upwind turbine," in *AWEA Wind Power Conference*, (Chicago, Illinois), 2009.

[24] L. Bergami, *Adaptive Trailing Edge Flaps for Active Load Alleviation in a Smart Rotor Configuration*. PhD thesis, Denmark Technical University, 2013.

[25] IEC, "IEC 61400-1 Ed.3: Wind turbines - Part 1: Design requirements," 2005.

[26] Dick Veldkamp, *Chances in wind energy: a probalistic approach to wind turbine fatigue design*. PhD thesis, Delft University, 2006.

[27] ASTM-standard, "ASTM E1049-85: Standard Practices for Cycle Counting in Fatigue Analysis," tech. rep., ASTM International, West Conshohocken, PA, USA, 2011.

[28] K. G. Eulitz, "Lebensdauervorhersage I - Verbesserung der Lebensdauerabschatzung durch systematische Aufarbeitung und Auswertung vorliegender Versuchsreihen," tech. rep., TU Dresden, Dresden, 1994.

[29] H. J. Sutherland and J. F. Mandell, "Updated Goodman Diagrams for Fiberglass Composite Materials using the DOE/MSU Fatigue Database," *Global Windpower*, p. 12, 2004.

[30] E. A. Bossanyi, "Bladed User Manual," tech. rep., DNV GL, Bristol, 2013.

[31] M. A. Lackner and G. A. M. van Kuik, "A comparison of smart rotor control approaches using trailing edge flaps and individual pitch control," *Wind Energy*, vol. 13, pp. 117–134, Mar. 2010.

[32] L. Bergami, M. Gaunaa, and J. Heinz, "Indicial lift response function: an empirical relation for finite-thickness airfoils, and effects on aeroelastic simulations," *Wind Energy*, vol. 16, pp. 681–693, July 2013.

[33] D. Castaignet, N. K. Poulsen, T. Buhl, and J. J. Wedel-Heinen, "Model predictive control of trailing edge flaps on a wind turbine blade," in *American Control Conference*, (San Francisco, CA, USA), pp. 4398–4403, AACC, 2011.

[34] D. Berg, D. G. Wilson, B. R. Resor, J. Berg, T. K. Barlas, A. Crowther, and C. Halse, "System ID Modern Control Algorithms for Active Aerodynamic Load Control and Impact on Gearbox," in *TORQUE: The Science of Making Torque from Wind*, (Heraklion, Crete, Greece), 2010.

[35] B. R. Resor, D. G. Wilson, D. Berg, J. Berg, T. K. Barlas, J.-W. van Wingerden, and G. A. M. van Kuik, "Impact of higher fidelity models on simulation of active aerodynamic load control for fatigue damage reduction," in *48th AIAA Aerospace Sciences Meeting Including the New Horizons Forum and Aerospace Exposition*, (Orlando, Florida), 2010.

[36] E. A. Bossanyi, B. Savini, M. Iribas, M. Hau, B. Fischer, D. Schlipf, T. G. V. Engelen, M. Rossetti, and C. E. Carcangiu, "Advanced controller research for multi-MW wind turbines in the UPWIND project," *Wind Energy*, vol. 15, pp. 119–145, Jan. 2012.

[37] J. Peeringa, R. Brood, O. Ceyhan, W. P. Engels, G. de Winkel, and G. de Winkel, "Upwind 20MW Wind Turbine Pre-Design: Blade design and control," tech. rep., Energy Research Centre of the Netherlands, 2011.

[38] REPower Systems, "REpower Systems, 5M: The 5-megawatt power plant with 126 metre rotor diameter," 2014.

Chapter 6

Wind field synthesis

Design load cases 1.1/1.2 both use the normal turbulence model as described in the IEC 61400-1 standard. The standard suggests that either the Kaimal or Mann wind field model be used for creating these 3D turbulent wind fields, but while certain parameters are defined, details such as the grid spatial and time resolution are not defined. This is likely due to the actual requirement for accurate results varying depending on wind turbine size and the modelling used. The sensitivity of simulations to these and other wind field parameters are looked at here.

This chapter describes the normal turbulence model as defined in the IEC standard in Section 6.1, determines the appropriate grid spatial and time resolutions for creating 3D turbulent wind fields to acquire accurate results in Section 6.2, and looks at the two suggested wind field models in Section 6.3. Then in Section 6.4 the sensitivity of the load reduction results to turbulence intensity, wind shear and tower shadow are considered. Finally a summary is given at the end of the chapter.

6.1 Normal turbulence model wind fields

The Design Load Cases (DLC) that are being used to assess the performance of the controllers and wind turbine are DLC 1.1/1.2, as described in the previous chapter. These are taken from the IEC 61400-1 standard, edition 3 [1]. Both of these cases use the normal turbulence model that defines wind fields likely to be present under normal operation of the wind turbine. Two models are recommended for creating these wind fields: they are the Mann model and the Kaimal model. The Mann model is described in [2], while the Kaimal model uses the Veers method for coherence [3]. Specific parameters for these two models are given in the standard, and these, along with general parameters that are used in this work, are defined in Table 6.1. Additional reasons for selecting certain parameters are noted alongside the table entries.

Table 6.1: Normal turbulence model wind field parameters for Kaimal and Mann models

General parameters	**Value**	**Reason/Recommendation**
Number of points along Y	31	NREL forum, GL standard $< 5m$ spacing
Number of points along Z	31	NREL forum, GL standard $< 5m$ spacing
Volume width Y	130m	NREL 5MW to encompass rotor
Volume height Z	130m	NREL 5MW to encompass rotor
Duration of wind file	600s	IEC/Bladed
Frequency along X (f)	≈10Hz	Bladed
Time step s (T = 1/f)	≈0.01s	Bladed
Mean wind speed U	4-25m/s	IEC
Turbulence seed	-	
Kaimal model		
Turbulence scale parameter (Λ_1)	42m	IEC/NREL 5MW hub height $> 60m$
Longitudinal ($xLu = 8.1\Lambda_1$)	340.2m	IEC
Lateral ($xLv = 2.7\Lambda_1$)	113.4m	IEC
Vertical ($xLw = 0.66\Lambda_1$)	27.72m	IEC
Coherence scale parameter ($Lc = 8.1\Lambda_1$)	340.2m	IEC
Coherence decay parameter (H)	12	IEC
Mann model		
Shear parameter (γ)	3.9	IEC
Scale length ($L = 0.8$ or 0.7Λ)	33.6	IEC
FFT points in lateral/vertical direction	128	Bladed > 32
Max lateral/vertical wavelength	168m	Bladed $> widthY or Z$

The 3D turbulent wind fields used in this work are created using Bladed [4]. The wind field outputs from Bladed are 4-dimensional matrices describing wind speed deviations in the longitudinal, lateral and vertical directions for every point in a 3D space encompassing the rotor in the vertical and lateral directions and stretching longitudinally for a length defined by the mean wind speed and duration of the wind file. The deviations have the dimensionless form $\delta = \frac{V-V_0}{IV_0}$ where V is the point wind speed, V_0 is the mean wind speed and I the turbulence intensity.

This turbulent wind field can then be used, assuming Taylor's frozen wake hypothesis, as the input file to full wind turbine simulations, with the wind speed being calculated at the rotor by the formula

$$V(r, \phi, t) = V_0 F_{s0}(F_s + I\delta(r, \phi, t))F_t F_w \tag{6.1}$$

where F_{s0} is the wind shear factor from the reference height (for mean wind speed V_0) to the hub height; F_s is the wind shear factor from the hub height to the point defined by polar coordinates

(r, ϕ), with r the radius from the centre of the rotor and ϕ the azimuth angle; F_t is the tower shadow factor for the point (r, ϕ); and, F_w is the upwind turbine wake factor for point (r, ϕ). This is as presented in [5]. A cubic interpolation is used between data points.

6.2 Grid resolution

The grid resolution required for accurate simulations is determined by running simulations with the NREL 5MW wind turbine and baseline controller with a variety of grid sizes. Six fully independent wind field seeds are used at 16m/s mean wind speed to quantify uncertainty that is naturally present due to the stochastic nature of the wind. For determining the required spatial resolution, a 61×61 grid wind field is created in TurbSim using the Kaimal model [6], with an along wind frequency of 20Hz, equating to spacings of 2.16m in the horizontal and vertical directions and 0.8m in the along wind direction. TurbSim is used here due to it being capable of creating larger data files than Bladed.

Data is then removed from the wind field to achieve wind files with grid points at the same positions but with fewer evenly spaced points, i.e. factors of 60 plus one (e.g. 31×31, 21×21, 16×16, 13×13 etc. grids). This is achieved by manipulating the turbulent wind field files using a MATLAB script adapted from NREL's TurbSim package, see Appendix E.

Power production runs are conducted for each of these corrected wind fields, with wind shear and tower shadow disabled to simplify analysis. The results of these runs are shown in Figure 6.1. As can be seen from the figure the uncertainty between different seeds mean a grid resolution of approximately 13m is acceptable, as the standard deviation between runs is much greater than the uncertainty due to the grid resolution. The 13m grid resolution equates to a grid size of 11×11 points for the 130m×130m spatial field required of the NREL 5MW wind turbine.

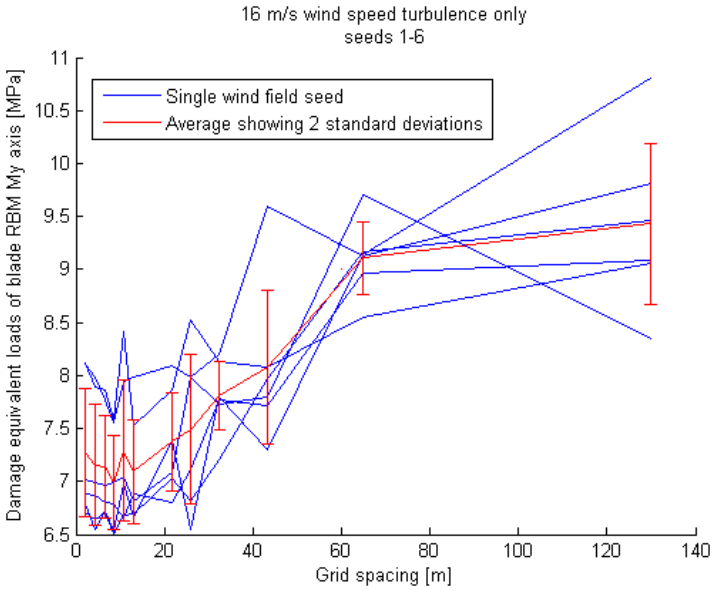

Figure 6.1: Damage equivalent loads for various wind field spatial resolutions

A similar sensitivity study for time resolution is conducted, using a 31×31 spatial grid and starting with a 0.01s time step (100Hz, 0.16m spacing). Points are then removed to create resolutions of multiples of this time step. The results are shown in Figure 6.2. The damage equivalent load converges linearly with smaller time steps (increased resolution), and compared to the standard deviation between wind field seeds, a time step of even 1s appears reasonable.

The resolutions suggested by GL certification are grid spacings of less than 5m in the rotor

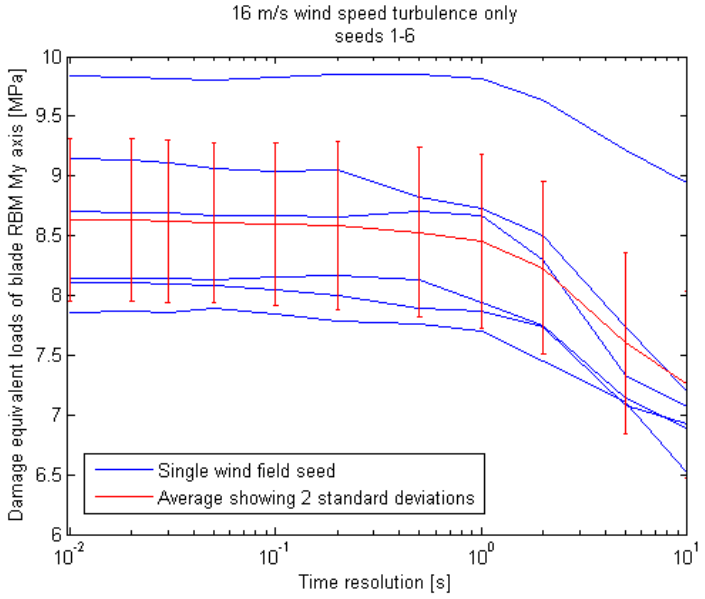

Figure 6.2: Damage equivalent loads for various wind field time resolutions

plane and time resolution greater than 10Hz. From the results above these are seen to be more than adequate. As such, to conform with both the certification guidelines and take a conservative approach, the grid size used in this thesis is 31x31, with a time resolution of greater than 10Hz.

The IEC standard specifies two wind field models that may be used, and so the next step, having verified the suitability of the wind field resolutions, is to look at the sensitivity of the wind turbine simulations to these models.

6.3 Wind field model: Kaimal and Mann

As the Mann and Kaimal models are recommended by the IEC standard and the models and the programmes employed to create these wind fields are widely used in research and industry, the loads should be accurate enough at least for standard wind turbine control. This is supported in [7] and verified here for the dq-axis implementation of the smart rotor wind turbine. The wind fields from now on are all produced using Bladed.

The Kaimal spectrum model provides consistent results and, as according to the Kolmogorov law, approaches the asymptotic limit proportional to $n^{-5/3}$ at high frequencies, see Figure 6.3. On the other hand the Mann model drops off quicker than expected by this law, showing deficiency at high frequencies. Whilst this has been justified as the averaging over a sizeable area for each point in the wind field [2], it is something to bear in mind as it reduces the overall turbulence intensity and so affects results, as commented upon in the next section.

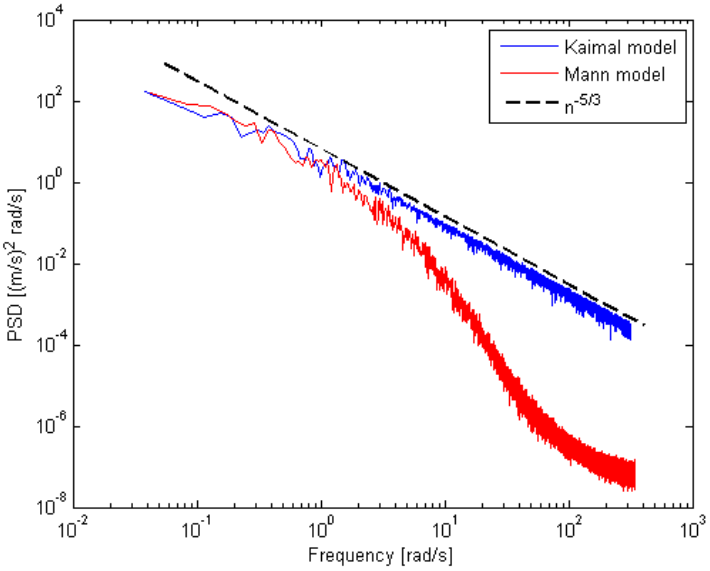

Figure 6.3: PSD of the along wind component of the wind field at the hub for both Kaimal and Mann models

This roll-off at high frequencies can be mitigated by increasing the resolution of the model parameters, as shown in Figure 6.4. In this case the number of FFT points in the vertical/lateral domain are altered showing that these affect the high frequency component of the spectra. Clearly more points are preferable, but there are limits that become clear when considering that arrays can quickly stretch beyond a gigabyte in size, e.g. the top resolution explored here was over 400MB ($= 8192 \times 3 \times 128 \times 128$), and the wind field synthesis occurs in the RAM of the computer. The roll-off may also have some physical basis, as the turbulence spectrum progresses from the inertial to dissipation range. The narrower range in frequency in Figure 6.4 compared to Figure 6.3 is simply due to a lower data sampling rate being used.

Ultimately what is important is that the smart rotor control is accurately represented or that uncertainties in the results are known. Comparing the 1Hz blade root damage equivalent loads for a 16m/s mean wind speed with class B turbulence the results are not statistically significant, as

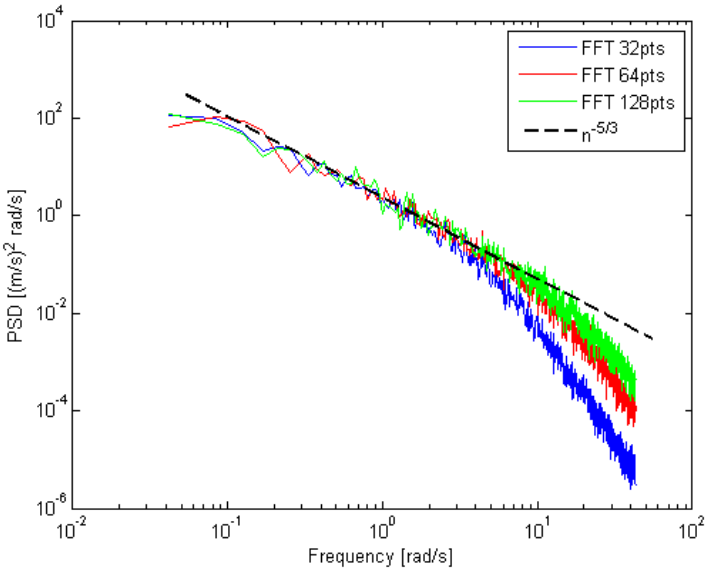

Figure 6.4: PSD of the x component of wind speed at the hub for the Mann model with a varying number of FFT points in the lateral/vertical directions

shown in Table 6.2. Also in the table it can be seen that the differences in the wind field model are similar across the control strategies. So that although lower loads are seen for the simulations run with the Mann model, these are represented across all strategies, and indeed the difference between the individual pitch control and smart rotor control are negligible when using the same wind field. This lends credibility to the argument that either wind field may be used for analysis of the smart rotor.

Table 6.2: 1Hz blade root bending moment DEL at 16m/s mean wind speed

Wind field model	CPC	IPC	SRC
Kaimal	9.1 ± 0.6	7.6 ± 0.7	7.5 ± 0.7
Mann	8.6 ± 0.3	7.2 ± 0.5	7.2 ± 0.5

The decision to use only the Kaimal model for evaluation in this thesis is then for expediency, consistency and to avoid the uncertainty that exists over the selection of the Mann model parameters, rather than because of a perception that it is more realistic or better than the Mann model.

6.4 Sensitivity study

6.4.1 Turbulence intensity

Turbulence can have a significant effect on the loads which a wind turbine experiences. While a class IB turbine has been chosen for study, it is worth examining the sensitivity of loads and load reductions a smart rotor wind turbine can achieve based on the other classes of turbulence. To this end six ten-minute runs are conducted as per the IEC standard DLC 1.2 at a wind speed of 16m/s, a speed at which significant fatigue load damage occurs [8], for each of the turbulence classes.

The damage equivalent loads are similar for both the Kaimal and Mann models, with increased turbulence causing increased damage to the wind turbine. The Mann model accounts on average for 94.3% of the turbulence intensity in the lateral direction, and so this may account for the small reduction in damage equivalent loads observed in Figure 6.5 for the Mann model.

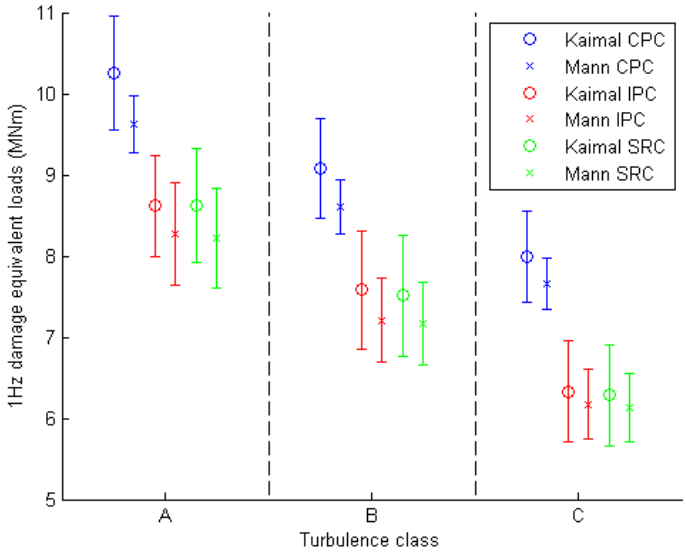

Figure 6.5: A comparison of 1Hz DEL for class A, B and C turbulence

The effect of increased turbulence intensity is not only to increase loads though, but also to alter the perceived effectiveness of the advanced controller techniques. The reason for this is that the dq-axis load reduction controllers perform best at reducing cyclic loads on the wind turbine, which turbulence has a limited effect on. So while a similar load reduction is achieved regardless of turbulence intensity, the percentage load reduction is much less when higher turbulence intensities are used, Table 6.3. This makes it vital for fair comparisons of advanced load reduction controllers to know at what turbulence intensity the controllers are being tested. The table also highlights that the percentage load reduction is also affected by the model used. The choice of the Kaimal model may therefore lead to slightly optimistic load reductions despite conservative damage equivalent load values.

Table 6.3: 1Hz DEL blade root bending moment load reduction compared to the collective pitch control case [%]

Turbulence class (turbulence intensity)		Kaimal		Mann	
		IPC	SRC	IPC	SRC
A	(17.6%)	16.0	15.9	14.0	14.5
B	(15.4%)	16.5	17.3	16.2	16.8
C	(13.2%)	20.8	21.5	19.4	19.9

6.4.2 Wind shear

Bladed allows creation of wind shear using either the power-law or log-law, or a user defined wind shear. The IEC standard suggests using the power-law, $V(z) = V_{hub}(z/z_{hub})^{\alpha}$, with $\alpha = 0.2$. However, it is worth considering how appropriate it is to use this value considering studies have shown it to vary considerably. For example [9] has values from 0.3 to 0.45 for a single site varying each month throughout the year, while [10] and [11] show the dependency of fatigue damage on wind profile to be considerable. A look at the effect of the wind shear exponent is therefore important.

Varying the exponent from 0 to 0.5 shows that damage accumulates extremely rapidly with increased wind shear, see Figure 6.6. This plot also clearly demonstrates the advantages of using load reduction techniques, which reduce the damage equivalent loads considerably. Indeed even at high wind shears the damage equivalent load is below the baseline case with a shear exponent of 0.2 when operating either individual pitch or smart rotor control. This suggests that these advanced load reduction techniques would likely be best suited to situations where the standard collective pitch control is unable to satisfy design restraints. An example of this sort of situation are offshore low level jets, whereby low turbulence but extreme wind shear results in highly damaging cyclic loads. Independent blade control may then be used to significantly reduce loads, even to below those of the collective pitch controlled IEC operational load case [12].

The advantage of using advanced control strategies in environments of increasing wind shear are displayed in Table 6.4. This also demonstrates the requirement again to carefully compare systems using the same environment, else load reduction potentials could easily be exaggerated to the preference of one system over another.

Table 6.4: 1Hz DEL blade root bending moment load reduction compared to the collective pitch control case [%]

Control strategy	Wind shear exponent					
	0.0	0.1	0.2	0.3	0.4	0.5
IPC	6.1	9.8	16.5	23.8	29.8	34.1
SRC	6.6	10.3	17.3	24.4	30.0	34.4

6.4.3 Tower shadow

Finally tower shadow is considered, assessing its impact on loads and potential load reductions using the smart rotor and individual pitch control. A potential flow theory is implemented in Bladed with a tower dimension correction factor of 1.2, and compared with simulations without tower shadow present.

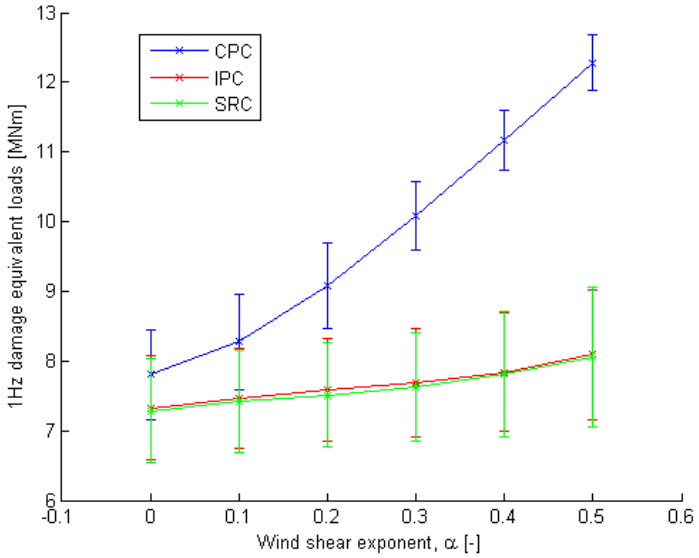

Figure 6.6: 1Hz DEL at 16m/s wind speed with class B turbulence intensity and various wind shear exponents using collective pitch control (CPC), individual pitch control (IPC) and smart rotor control (SRC)

The change in 1Hz damage equivalent loads is as much as 2% for the collective pitch controlled baseline case, while load reductions are increased as a result of tower shadow when individual pitch and smart rotor control are active, and these are of approximately one percent. See Table 6.5 for the actual loads. Tower shadow is therefore an area where smart rotor control can help, though gains to be had are much smaller than when operating in a strong wind shear.

Table 6.5: 1Hz DEL blade root bending moment load [MNm]

Control strategy	No tower shadow	Potential tower shadow
CPC	8.94	9.08
IPC	7.58	7.58
SRC	7.50	7.51

6.5 Discussion

The synthesis of wind fields is a highly complex and uncertain area of research with the results in this chapter helping to clarify the influence various aspects have on the loadings on wind turbines and the ability to mitigate these using advanced load reduction techniques.

A grid spatial resolution of 31×31 points spread over the 130m×130m square area of the rotor is seen to accurately produce results while also fulfilling the GL certification standard, requiring less than 5m grid spacing. A time resolution of greater than 10Hz has also been seen to produce results that are accurate, with natural stochastic disturbances contributing much more to the uncertainty in results than the size of the discrete time steps, even with second long intervals.

Both the Kaimal and Mann wind field models are tested, with the Kaimal model selected for use due to less uncertainty as to the model parameters, but with the understanding that both models elicit similar responses from the wind turbine. So the choice here is one of pragmatism rather than an endorsement of the Kaimal model's suitability over the Mann model.

Sensitivity studies show that turbulence intensity, wind shear and tower shadow all affect both loads on the wind turbine and the load reductions seen when operating advanced control strategies. Low turbulence intensities result in low loads but conversely higher percentage reductions using individual pitch or smart rotor control. While high wind shears cause both higher loadings and the ability to mitigate these using either of the advanced load reduction strategies, resulting in high load reductions.

This highlights the importance of fair comparisons, as it is easy to bias results using the environmental conditions. Either way, an important result is that the smart rotor control operates just as effectively as the individual pitch control in all these scenarios. Suggesting the wind field synthesis method used, if assumed to work for testing individual pitch control, can equally be used for testing smart rotor control.

References

[1] IEC, "IEC 61400-1 Ed.3: Wind turbines - Part 1: Design requirements," 2005.

[2] J. Mann, "Wind field simulation," *Probabilistic engineering mechanics*, vol. 13, pp. 269–282, Oct. 1998.

[3] P. Veers, "Three-dimensional wind simulation," tech. rep., Sandia National Laboratories, Albuquerque, New Mexico and Livermore, California, 1988.

[4] E. A. Bossanyi, "Bladed User Manual," tech. rep., DNV GL, Bristol, 2013.

[5] E. A. Bossanyi, "Bladed Theory Manual," tech. rep., DNV GL, Bristol, 2013.

[6] N. D. Kelley and B. J. Jonkman, "Overview of the TurbSim stochastic inflow turbulence simulator," tech. rep., NREL, Golden, CO, USA, 2005.

[7] Dick Veldkamp, *Chances in wind energy: a probalistic approach to wind turbine fatigue design.* PhD thesis, Delft University, 2006.

[8] L. Bergami, "Adaptive Trailing Edge Flaps for Active Load Reduction," in *7th PhD Seminar on Wind Energy in Europe*, (Delft University of Technology, Netherlands), 2011.

[9] R. Farrugia, "The wind shear exponent in a Mediterranean island climate," *Renewable Energy*, vol. 28, pp. 647–653, Apr. 2003.

[10] A. Sathe and W. Bierbooms, "Influence of different wind profiles due to varying atmospheric stability on the fatigue life of wind turbines," *Journal of Physics: Conference Series*, vol. 75, July 2007.

[11] A. J. Eggers, R. Digumarthi, and K. Chaney, "Wind Shear and Turbulence Effects on Rotor Fatigue and Loads Control," *Journal of Solar Energy Engineering*, vol. 125, no. 4, p. 402, 2003.

[12] D. Robb, C. Gonzalez, P. Clive, W. E. Leithead, and A. Giles, "Offshore Low Level Jets - Mitigating the Damage with Lidar and Individual Blade Control," in *EWEA Offshore*, no. 2003, (Messe Frankfurt, Germany), 2013.

Chapter 7

Trailing edge flap devices

Whilst there are a large number of aerodynamic devices to choose between for the smart rotor control, as seen in Chapter 3, trailing edge flaps have been selected for use in this thesis as they are one of the most developed and promising devices. The baseline wind turbine is designed with flaps that constitute 20% of the chord width of the blade and 20% of the rotor diameter.

This chapter explores this choice. In Section 7.1 the motivation behind exploring different configurations is given. In Section 7.2 thin aerofoil theory is used to explore the aerodynamic characteristics, before using XFOIL to test flaps of 10, 20 and 30% chord in Bladed simulations. The result of these Bladed simulations are given in Section 7.3 with regard to the flap actuator requirements. Finally conclusions to this research are made at the end of the chapter.

7.1 Motivation

There are numerous devices being considered for smart rotor control as explained in Section 3.3 of the technical review. Trailing edge flaps are one of the most promising and developed technologies, but there are a variety of types and sizes that can be considered. Research is ongoing in development of flexible trailing edges so as to achieve a smooth aerofoil profile when deployed and prevent separation [1], however, rigid trailing edge flaps, like the ailerons on planes, have been implemented on the two smart rotor wind turbine demonstration plants. For the Sandia wind turbine the integration, construction and dimensions of the flaps are catalogued in a number of reports [2], [3], [4], [5], and it is the dimensions of these flaps that act as a starting point for the work here.

Whilst others have also looked at the ideal placement for trailing edge flaps and their span [6], this work looks at the effect of changing the flap chord width. This further aids in the selection of trailing edge flaps and in understanding the theory behind them. The blade structure and method of actuation is important, but both are beyond the scope of this work. It is important though to recognise what the requirements of such actuators are, and this is considered by looking at the motions the flaps undergo, the torque requirements and the cause of these: flap inertia, aerodynamic pressures, gravity and friction, and the aerodynamic characteristics. This facilitates future selection of the devices.

7.2 Aerodynamic characteristics

The NACA 64618 aerofoil profile is used across the entire span where the flap is located, referenced in Appendix B. It is therefore used in all the calculations that follow. To assess the impact of the flap's chord width, three flap sizes are selected of 10, 20 and 30% of the chord extending forward from the trailing edge. All other dimensions and limits are kept the same. To determine the effect of the chord width on the aerodynamic characteristics, and indeed control of the wind turbine, thin aerofoil theory is used to give an overview of the effect that changing the chord width can have. XFOIL is then used for the three selected flap sizes, with further analysis to support the conclusions drawn from thin aerofoil theory. Finally the way this data is used in Bladed is described.

7.2.1 Thin aerofoil theory

From thin aerofoil theory, for example as described in [7], a cambered aerofoil's lift coefficient is determined by

$$C_L = 2\pi \left[\alpha + \frac{1}{\pi} \int_0^\pi \frac{dz}{dx} (\cos\theta_0 - 1) d\theta_0 \right] \tag{7.1}$$

where α is the angle of attack of the aerofoil, $\frac{dz}{dx}$ the gradient of the camber along the chord, and θ_0 corresponds to the distance along the chord, x, given by

$$x = \frac{c}{2}(1 - \cos\theta_0) \tag{7.2}$$

The deployment of a rigid trailing edge flap alters the gradient of the camber by a set amount from the hinge location to the end aerofoil. This can be approximated, using the small angle approximation, as β ($\tan\beta \approx \beta$ for small β). Such that

$$\Delta\frac{dz}{dx} = \begin{cases} 0 & \text{if } x < x_f \\ \beta & \text{if } x \geq x_f \end{cases} \tag{7.3}$$

where β is the angle of the flap and x_f the hinge position of the flap. This alters the lift as follows

$$\Delta C_L = 2 \int_{\theta_f}^\pi \beta(\cos\theta_0 - 1) d\theta_0 \tag{7.4}$$

where θ_f is determined through rearrangement of Equation 7.2 for x_f as

$$\theta_f = \cos^{-1}\left(1 - \frac{2x_f}{c}\right) \tag{7.5}$$

Substituting this into Equation 7.4 and integrating this then leads to

$$\Delta C_L = -2\beta\left(\sin\theta_f + (\pi - \theta_f)\right) \tag{7.6}$$

Immediately it can be seen that the change in lift is a linear function of the flap angle, β, whose gradient depends on the location of the flap hinge along the chord. This dependency is shown in Figure 7.1 for a trailing edge flap, showing the change in lift coefficient per degree of flap deployment.

This figure shows the decreasing returns for trailing edge flaps of increasing chord, indicating that a trailing edge flap need not extend too far forwards to achieve good controllability.

The baseline model includes a flap of 20% chord, based on the Sandia smart rotor demonstration wind turbine [3]. To assess whether this is the ideal size three flap hinge positions are highlighted as representative of what might be expected for use on a smart rotor wind turbine. These are for trailing edge flaps with 10%, 20% and 30% chord lengths. The resulting change in lift coefficients for these flaps are 0.043, 0.060 and 0.072 per degree of flap deployment. Due to the linear relationship between lift and flap angle, this means, comparing to the 20% chord length flap, the 10% would have an increased deflection of 39%, and the 30% chord flap reduced deflections of 27%. Controller gains therefore need to be adjusted accordingly if a fair comparison is to be made.

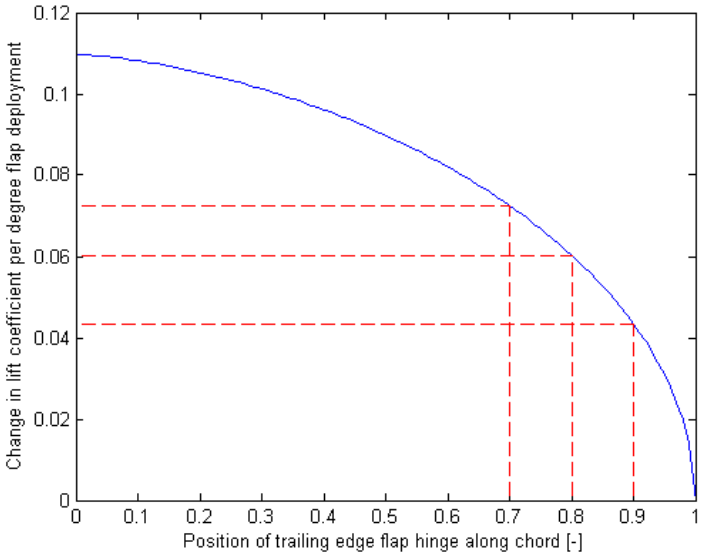

Figure 7.1: Lift coefficient for a trailing edge flap deflection to the pressure side for various hinge positions along the chord

The expected lift coefficient from the NACA 64618 aerofoil can also be calculated using Equation 7.1. NACA 6-series aerofoils are defined by their lift, thickness and location of minimum pressure, rather than a set camber line. It is possible though to work back from the co-ordinates of the NACA 64618 aerofoil to determine the camber line and fit a polynomial to it. This polynomial can then be used to calculate the lift.

For a polynomial

$$p(x) = \sum_{n=0}^{N} p_n x^n \tag{7.7}$$

the lift equation can be reduced to

$$C_L = 2\pi \left[\alpha + \sum_{n=1}^{N} p_n \left(1 + \Gamma_{(n-1)} \right) \right] \tag{7.8}$$

where $\Gamma_0 = 0$, and otherwise defined for positive integers as

$$\Gamma_n = \sum_{j=1}^{n} \prod_{k=1}^{j} \frac{2k-1}{2k} \tag{7.9}$$

Figure 7.2 shows a 12th order polynomial fit to the camber line of the aerofoil profile. Whilst higher order polynomials create a better fit and so should better represent the actual camber line, they can become ill conditioned and lead to numerical errors. The calculated lift as a function of polynomial order is shown in Figure 7.3. Excluding the extreme values for low and high order polynomial fits (i.e. for polynomials of order 4 to 34), the lift coefficient averages 0.53, with a standard deviation of 0.03. This is close to the result from XFOIL, discussed in the following section, of 0.5259, and demonstrates that thin aerofoil theory is a good estimate to the expected lift of an aerofoil profile.

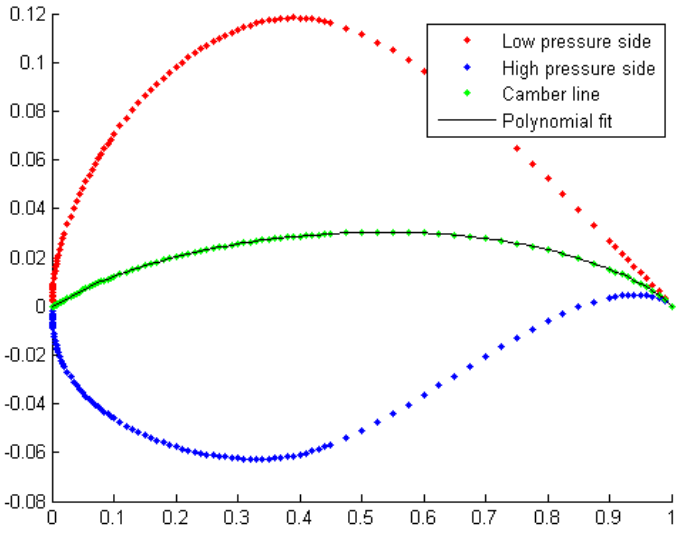

Figure 7.2: 12th order polynomial fit to the calculated camber line of the NACA 64618 profile

Similar calculations can be done for the pitching moment produced by deployment of the trailing edge flap, using Equation 7.12

$$C_{M,\frac{c}{4}} = \frac{\pi}{4}\left[A_2 - A_1\right] \tag{7.10}$$

where

$$A_n = \frac{2}{\pi}\int_0^{\pi} \frac{dz}{dx}\cos(n\theta_0)d\theta_0 \tag{7.11}$$

Inserting the flap profile as described in Equation 7.3 leads to the simple relationship

$$C_{M,\frac{c}{4}} = \frac{\beta}{\pi}\left(\sin(2\theta_f) - \sin(\theta_f)\right) \tag{7.12}$$

which demonstrates a linear relationship between the pitching moment and the flap angle, β, so that the larger the flap angle, the larger the pitching moment created. As the blade is not rigid,

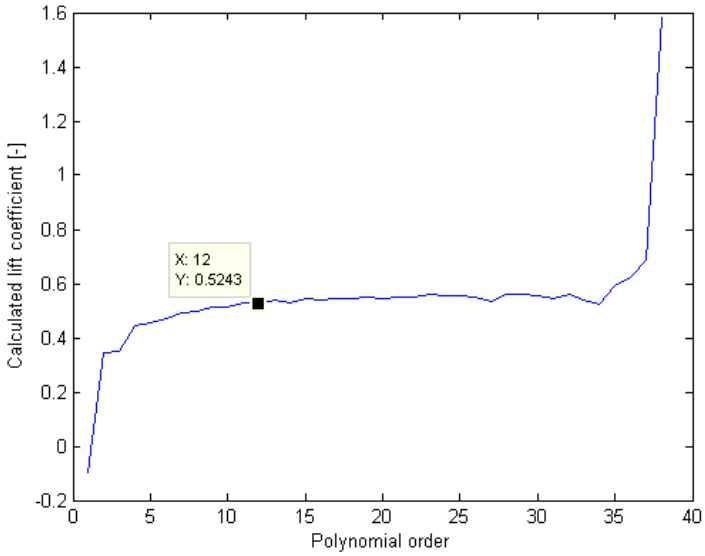

Figure 7.3: Lift coefficient as a function of the polynomial order, with the 12th order polynomial data point highlighted

this can lead to twisting and in extreme cases control reversal, whereby the trailing edge flaps are activated to increase lift, but force the blades to twist reducing the angle of attack and so also the lift. Figure 7.4a shows a plot of the pitching moment per degree flap angle for various flap hinge locations. As can be seen the three trailing edge flaps that are being looked at all produce similar pitching moments upon deployment. However, it should be remembered that the larger flaps require less deflections to achieve the same lift, so the pitching moment to lift ratio is actually reduced for flaps of greater percentage chord, Figure 7.4b. If blade torsional rigidity is a problem this suggests that larger chord width flaps should be used.

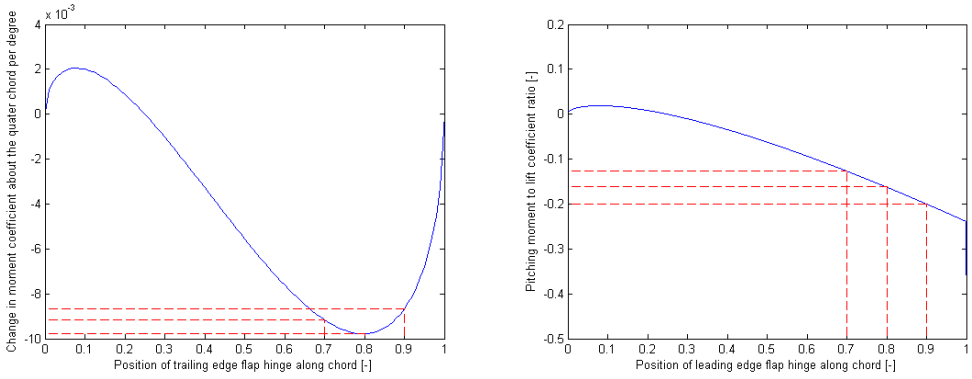

(a) Quarter chord pitching moment (b) Ratio of pitching moment to lift coefficient

Figure 7.4: Pitching moments for the trailing edge flaps with 10%, 20% and 30% chord length

Additionally the thin aerofoil theory can be used for leading edge flaps. Figure 7.5 highlights that these are not suitable for altering the lift coefficient, as only very minor changes in lift are possible unless the leading edge flap extends far back towards the trailing edge, where most of

the change in lift is possible. As such leading edge flaps are not usable for active adjustment of loads. There is an exception to this when operating close to stall, as leading edge flaps can extend the lift curve beyond its usual operation, but for pitch to feather wind turbines this is not relevant. Interestingly there is one other advantage, and that is the pitching moment produced from deployment of a leading edge flap would positively affect control, such that the pitching moment produced, causing twisting of the blade, would reinforce the desired change in lift, see Figure 7.6. This may also be used to counteract the adverse pitching moment produced by trailing edge flaps.

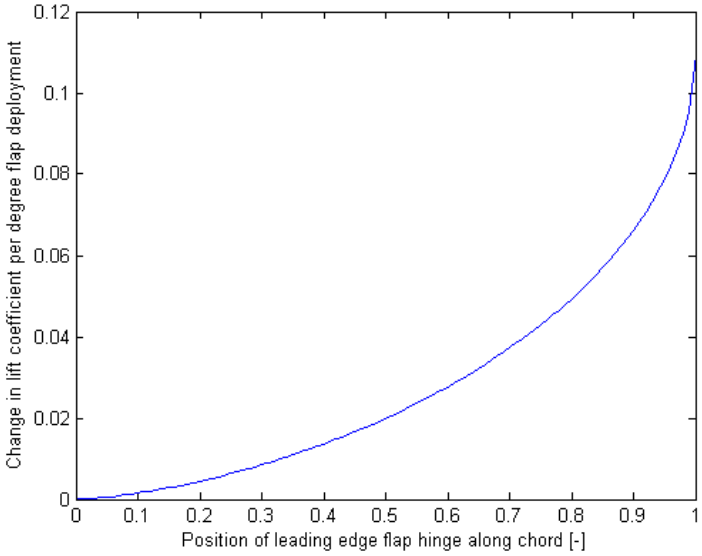

Figure 7.5: Lift coefficient for a leading edge flap deflection to the suction side for various hinge positions along the chord

7.2.2 Modelling the flaps using XFOIL

The aerodynamic characteristics for the three trailing edge flaps are obtained using XFOIL [8], which allows rapid calculation of the lift, drag and pitching moments for 2D aerofoil shapes. The flaps are modelled internally in XFOIL hinged to the NACA 64618 aerofoil at the specified chord, 0.7, 0.8 and 0.9c. The hinge is placed at the camber line, i.e. half way between the top and bottom surfaces, and is assumed to create a smooth attachment. Examples are plotted in Figure 7.7 for each of the flaps.

The lift coefficients are plotted in Figure 7.8 for the flaps set at various angles, in the range of attacks -20 to 20 degrees. At high angles of attack, or with high flap deflections, separation occurs reducing the lift achieved, as can be seen in the tail ends of the graphs and by the bunching of the curves at top and bottom where the flap angles are highest. XFOIL does not best represent this region and indeed empirical or semi-empirical results are preferable at these high angles. At high angles of attack the data from XFOIL is therefore not used, and instead the data is extended using the original data supplied with the NREL model [9].

Due to the wind turbine control being pitch-to-feather regulated though, $\pm 20°$ is within the angle-of-attack operating region of the turbine. So in reality the modelled data is the data used

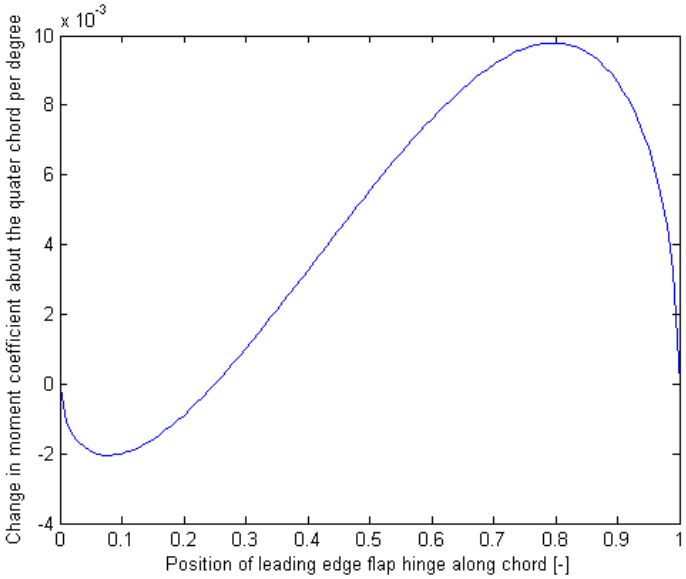

Figure 7.6: Quarter chord pitching moment per degree of leading edge flap angle for various locations of the flap hinge along the chord

and during normal operation the angle of attack remains in the linear part of the lift curves. Any excursions are rare, negative in nature, and occur only at high wind speeds and near the tip of the blades. At 24m/s mean wind speed for example, the angle of attack of the blade tips are within the above limits over 99% of the time.

The flap deflections required also reduce for the larger flap sizes, as it is the change in lift coefficient that really matters, such that separation is also avoided with regards to this.

An interesting result can be seen in the plots of the aerodynamic characteristics seen in Figure 7.9. While lift and drag are higher for the larger chord width flaps, Figure 7.9a and Figure 7.9b, the lift to drag ratio is only marginally affected by the chord width, Figure 7.9d, and the same is true of the pitching moment induced, Figure 7.9c. This suggests that as regards to aerodynamic performance, any of these flaps may be used.

7.2.3 Device modelling in Bladed

Bladed uses look up tables to calculate the lift, drag and pitching moments on the blades for each time step. Therefore Bladed does not know the profile of the blade, or indeed differentiate between what devices are being used. It simply recognises a change in aerodynamic coefficients based on the angle of attack and "aileron angle" assigned by the controller.

Up to 20 data sets may be used for each flap section, with interpolation done between data points. As such, the data for flap angles 0, $\pm 2, \pm 4, \pm 6, \pm 8, \pm 10, \pm 12, \pm 14, \pm 18$ and ± 22 degrees are used. Structurally, no changes are made to the blades. Although this is not realistic, when comparing the different methods of control this is beneficial, especially since the main objective is to reduce loads such that the blades can be redesigned to be cheaper. As an example, the actual data input is plotted for the 20% chord flap, at a deflection angle of 0 degrees in Figure 7.10, compared to the original data that comes with the NREL 5MW model [9]. As can be seen there is a slight

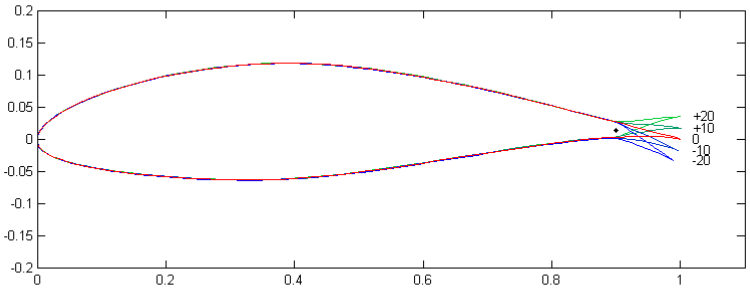

(a) 10% chord

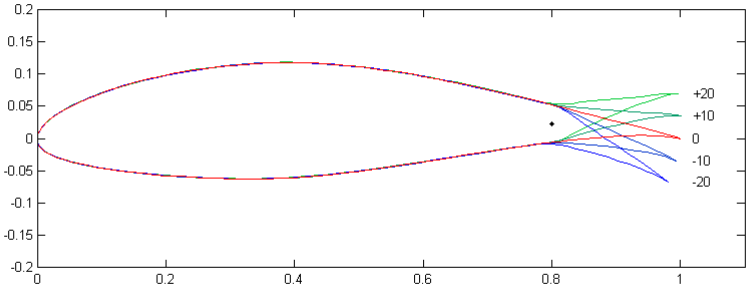

(b) 20% chord

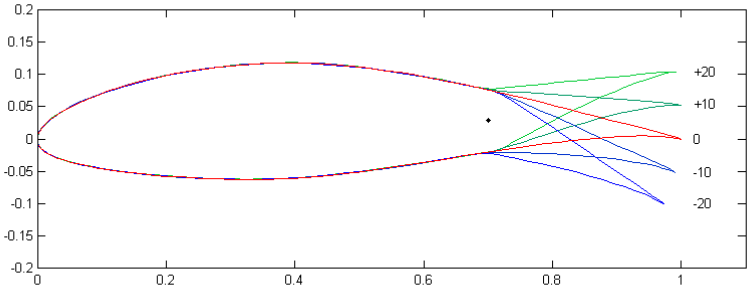

(c) 30% chord

Figure 7.7: Aerofoil profiles of the NACA 64618 with trailing edge flaps of various chord lengths

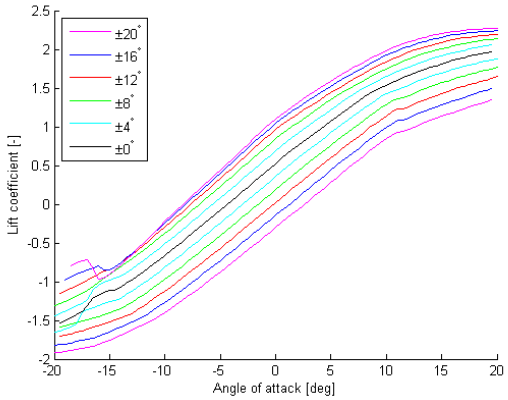

(a) 10% chord

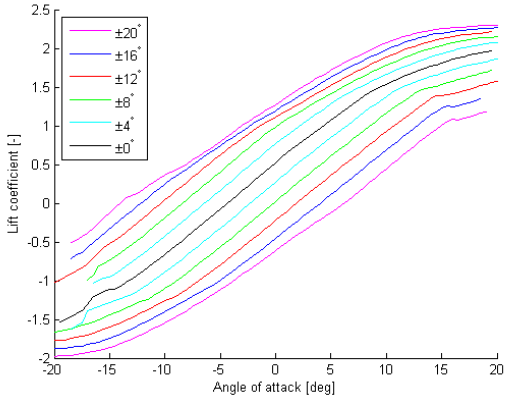

(b) 20% chord

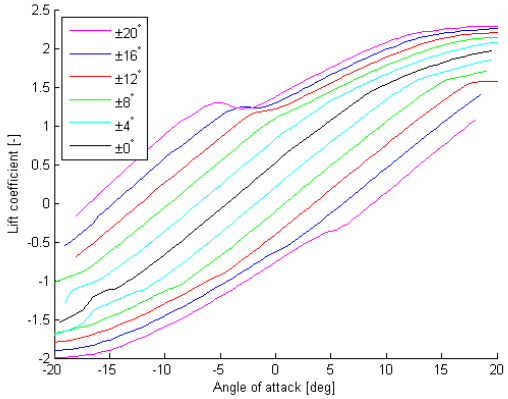

(c) 30% chord

Figure 7.8: Lift coefficient for each of the flaps at various deployment angles and angles of attack

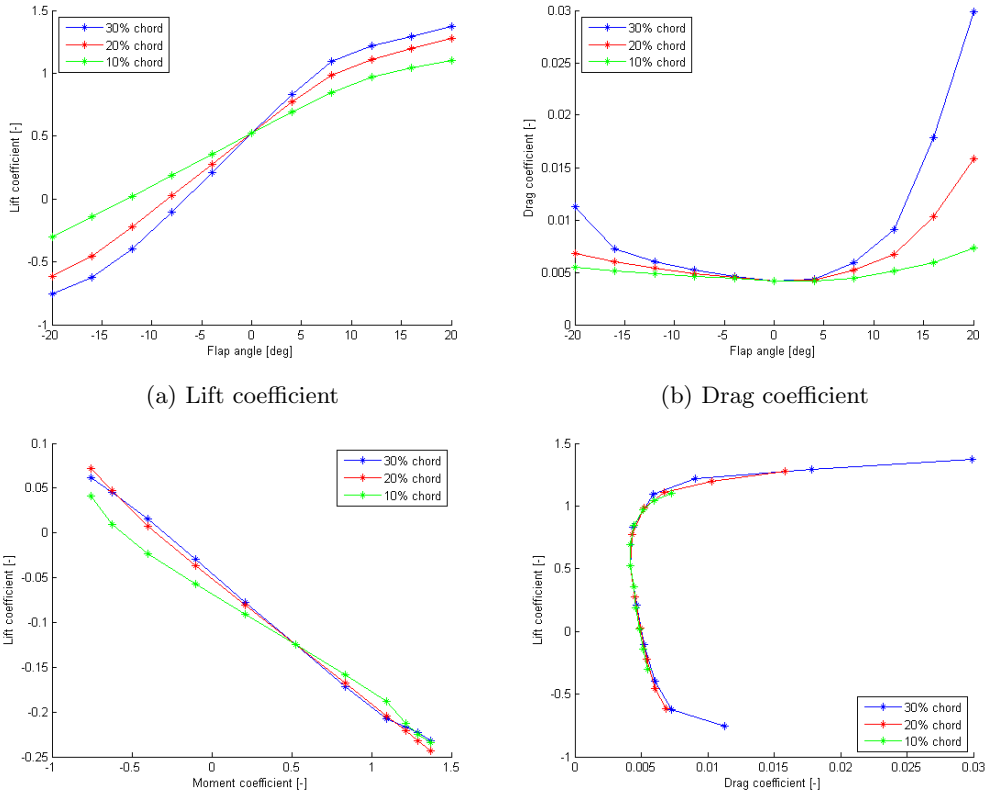

(a) Lift coefficient

(b) Drag coefficient

(c) Lift versus pitching moment

(d) Lift versus drag

Figure 7.9: Lift, drag and pitching moment polars

discontinuity between the data sets, with higher drag seen in the original data, and a reduced peak in the lift coefficient. It is therefore suggested that in future studies extrapolation from XFOIL for the entire 360 degrees should be done using QBlade [10], AirfoilPrep [11], RFoil [12] or similar, as done for the NREL 5MW original data [9], to better represent the aerodynamic characteristics of the devices. As mentioned though, due to the wind turbine being pitch regulated, angles of attack outside ±20 degrees are very unlikely.

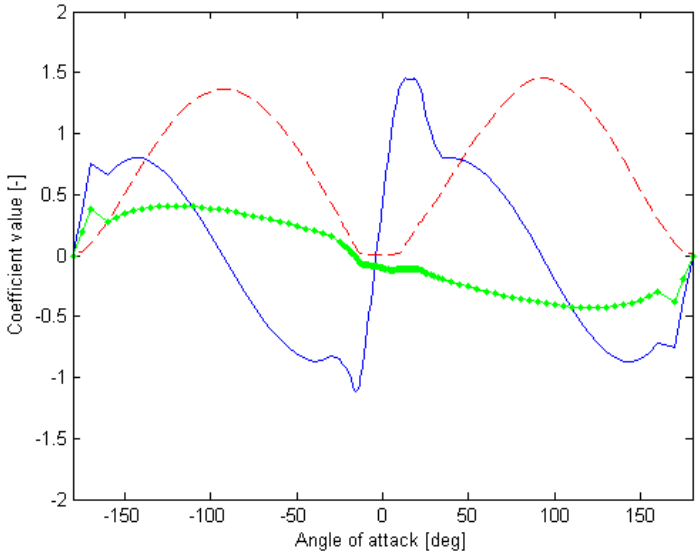

(a) Original

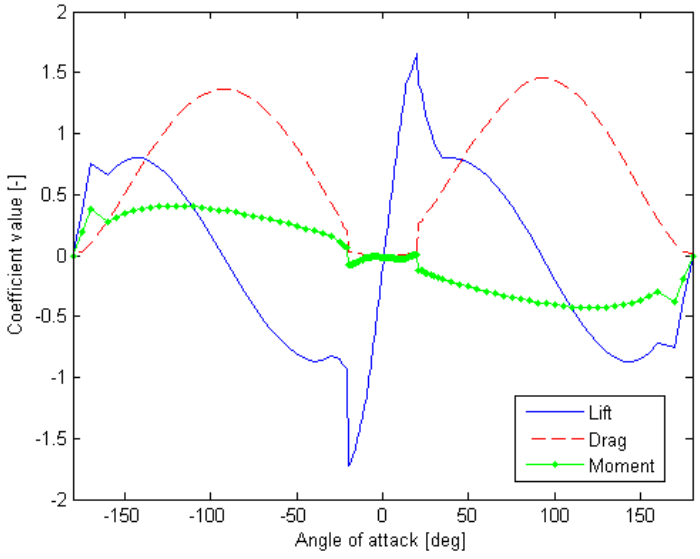

(b) With a 20% chord flap deployed at 0 degrees

Figure 7.10: Lift, drag and pitching moment polars ready for input into Bladed

7.3 Actuator requirements

As demonstrated in the previous section, the aerodynamic characteristics for each of the trailing edge flaps being considered are very similar and no one chord length is preferable as regards to this. The aerodynamics are just one aspect of the problem when selecting suitable devices though. Actuation of the devices also needs to be considered. The flap actuators will have varying requirements depending on the chord of the flaps used. The first thing to look at, as suggested by the reduced change in lift coefficient for the shorter chord flaps, is the flap motion.

7.3.1 Motion

Maximum deflections, travel, rates and accelerations that the flap undergo are displayed in Table 7.1, alongside the out-of-plane blade root bending moment standard deviation, which is representative of the loads on the blade root. The motion required of the flap actuators can be considered in combination with the differences in lift coefficient for each of the flaps, as discussed previously.

While the change in lift coefficient per degree of flap deployment are 0.043, 0.060 and 0.072, according the ratio 1.39:1:0.83 for the 10%, 20% and 30% flaps respectively, the change in flap motions is slightly different. In fact the ratio is closer to 1.48:1:0.78. This positive bias towards flaps with greater chord is likely due to the non-linear nature of the lift coefficient at extreme values, leading to a reduction in the effectiveness of the flaps at high flap angles. This is due to separation occurring and since high angles are naturally avoided for flaps with greater chord this is to their benefit. This is also exemplified by the three wind speeds, as even greater motions are required by the shorter chord width flaps as the wind speed increases. Indeed if the limits applied to the Sandia plant are reproduced here, which has maximum deflection limits of ± 20 degrees, this can also lead to saturation of the devices, resulting in a loss of control and so increased loads.

When considering the flap deflections that may be required in 1-in-50-year extreme wind cases, saturation would become all too clear a problem for the shorter flaps, and in fact flaps that are greater than 30% of the chord may actually be needed to operate optimally in all wind conditions. However, there is of course a trade off between making the system operate optimally in all conditions, and the costs associated with implementing such a system. Assuming that the Sandia flap is optimally designed at 20% chord width, for a similar probability of saturation the deflection limits of the 10% chord flap would have to be extended to ± 31 degrees, whilst for the 30% chord flap these could be reduced to ± 15 degrees. Another area that may lead to increased costs is the torque rating required of the actuator and so is discussed in the following section.

7.3.2 Torques

The torques required depend upon a number of factors: gravity loads, inertia, aerodynamic loads and friction. For the pitch actuator, these outputs are supplied by Bladed, using a pitch actuator friction model with set parameters. For the flap actuator the torques required for each of these needs to be calculated manually, and is done so as follows with the assumption the mass of the flap is simply the mass/span of the blade multiplied by the chord width:

- Gravity loads: the centre of mass is calculated for the flap, the offset in the out-of-plane direction from the pivot point is then taken, and this is multiplied by the weight of the

Table 7.1: Flap actuator demands of the dq-axis controller for the various flap chord widths at 12, 16 and 24m/s mean wind speeds. The absolute results are shown for the 20% chord flap. While, excluding the first result, the other two flaps are shown as a percentage of the 20% results

Metric	10% flap	20% flap	30% flap
Flap deflection 1-in-50-year extreme event (°)	39.36	25.34	19.5
12m/s			
Max flap deflection (°)	138.1%	9.96	76.8%
Flap travel ($°s^{-1}$)	135.0%	3.45	77.0%
Flap rate std ($°s^{-1}$)	136.9%	4.86	76.9%
Flap acceleration std ($°s^{-2}$)	125.4%	18.34	73.9%
Blade root out-of-plane bending moment std (MNm)	101.0%	1.97	100.3%
16m/s			
Max flap deflection (°)	149.6%	11.02	77.3%
Flap travel ($°s^{-1}$)	150.0%	5.02	78.3%
Flap rate std ($°s^{-1}$)	149.0%	6.16	77.9%
Flap acceleration std ($°s^{-2}$)	131.5%	17.84	74.8%
Blade root out-of-plane bending moment std (MNm)	102.0%	1.65	100.4%
24m/s			
Max flap deflection (°)	152.3%	12.97	77.3%
Flap travel ($°s^{-1}$)	159.1%	6.48	78.3%
Flap rate std ($°s^{-1}$)	157.2%	7.83	78.0%
Flap acceleration std ($°s^{-2}$)	135.2%	20.10	74.8%
Blade root out-of-plane bending moment std (MNm)	103.3%	1.82	100.2%

flap to calculate the torque, $\tau_{gravity}$. The out-of-plane displacement from the pivot point is calculated by taking into account the centre of mass of the flap, d_{flap}, the azimuth of the rotor, θ_{azi}, the pitch of the blade, θ_{blade} and the angle of the flap, θ_{flap}, such that $r = d_{flap}\cos(\theta_{azi})\sin(\theta_{blade}+\theta_{flap})$, and $\tau_{gravity} = r \times m_{flap}$, where m_{flap} is the mass of the flap. The flap mass is assumed to be the mass per unit span of the blade multiplied by the percentage chord of the flap.

- Inertial loads: the inertia of the flap, I_{flap}, is calculated assuming a triangular flap profile. The inertia is then multiplied by the angular acceleration of the flap, $\ddot{\theta}_{flap}$, to find the torque, $\tau_{inertia} = I_{flap}\ddot{\theta}_{flap}$

- Aerodynamic loads: the hinge moment per unit span of the flap at different flap angles and angles of attack, $C_m(\alpha, \theta_{flap})$, is calculated in XFOIL. This data is tabulated in a look-up table so that the aerodynamic torque on the flap may be calculated for various flap angles. The aerodynamic torque is also dependent on the chord length of the blade, c_{blade}, and the velocity of the perceived wind, v. The equation used to calculate the aerodynamic moment on the flap hinge is then, $\tau_{aero} = \frac{1}{2}C_m(\alpha, \theta_{flap})\rho v^2 c_{blade}^2$, where ρ is the density of air.

- Friction: friction opposes the motion of the flap and is dependent on the type of bearing and actuator used. For example it might consist of a component of constant friction, friction coefficient proportional to the forces being applied and friction coefficient proportional to the rate of motion. As the type of bearing and actuator are not been considered in this work, the frictional component is not considered here. It may however be significant and would increase

both torque requirements and power consumption.

Table 7.2 shows the various components and the maximum torques required of the flap actuators for the three chosen flap chord lengths. It can be seen that the torques required of the flap's actuators are dominated by the aerodynamic term when friction is ignored, which is a similar result to [4]. Gravity and inertial loads are insignificant in comparison. It should be noted the total maximum torque is not just the sum of the maximum of all three components, as the torques sum both constructively and destructively.

Table 7.2: Maximum contributions to torque demands of the actuators across all simulation runs (Nm)

	10% flap	20% flap	30% flap
Torque 1-in-50-year extreme event	859	3436	7511
12m/s			
Gravity	4	16	35
Inertia	1	11	50
Aerodynamic	372	1451	3390
Total	369	1441	3367
16m/s			
Gravity	4	16	35
Inertia	1	10	44
Aerodynamic	394	1515	3504
Total	391	1505	3482
24m/s			
Gravity	4	16	35
Inertia	1	7	28
Aerodynamic	429	1599	3659
Total	426	1588	3635

It is also important to recognise the rapidly increasing torques required of larger flaps, as whilst reductions have been observed in the flap motion, the increase in torque may be more of a concern when selecting actuators and indeed looking at the power requirements of the flaps, the increase in torque drives the power demand.

7.3.3 Power

The power demands for the three different flap sizes are shown in Table 7.3. As the wind speed increases, the power requirements also increase, this is down to both the increased motion at higher wind speeds and increased torques. The root mean square (rms) power consumption is low though. More significant are the 1-in-50-year power requirements that are considerably higher than the mean values. This is in part due to the sinusoidal motion of the flaps, which means even for normal operation the actuators will need to be rated higher than might be suggested by the rms values. Additionally it is clear that as the chord width of the flaps increase the power requirements also increase, this is due to the increased torques far outweighing the benefit of reduced motion.

Friction has however been ignored. A comparison of the power dissipated by constant friction can be made assuming constant friction across all three flap designs. The greatest power consumption due to friction will then be from the smallest of the flaps as friction opposes the motion and the

Table 7.3: Power requirements of the flap actuators (W)

	10% flap	20% flap	30% flap
Power 1-in-50-year extreme event	297	755	1378
12m/s rms power	20	71	141
16m/s rms power	27	86	172
24m/s rms power	38	111	220

smallest flap undergoes the greatest travel, see Table 7.1. However, friction is also likely to be considerable due to forces acting on the bearings of the flaps, radially, axially and due to bending moments, and this will depend highly on the structural design of the flaps. A detailed model is therefore required to accurately determine the contribution of both torques and power requirements from friction.

7.4 Discussion

The aerodynamic characteristics of trailing edge flaps has been looked at through a thin aerofoil theory analysis and through use of XFOIL. The changes in motion required of the flaps is predicted and observed in the results from simulations run in Bladed using the 10, 20 and 30% chord width flaps, with the change in lift coefficient per degree of flap deployment shown to directly affect the required flap motion.

The torques that are required of the flap actuators due to the inertia of the flap, aerodynamic pressure and gravity are also considered. The torques increase more rapidly than the decreased motion, leading to increased power requirements for flaps with longer chord widths.

There is a risk however with shorter flaps that saturation can occur or a loss in performance due to flow separation, it therefore seems reasonable to select the same chord width as the Sandia demonstration wind turbine, that is 20% chord width, so as to avoid saturation, reduce the chances of separation, which is not accurately modelled in XFOIL, and on the other hand not to demand high torques and powers. This is also likely a size that eases with construction and integration into wind turbine blades.

As regards to the flap actuator the low torque and power requirements are desirable as a smaller actuator may then be used, which would facilitate their integration into the limited space available in the blade. There is also the ability to trade increased torque for decreased movement through use of flaps with larger chord and span lengths, so an optimum may be found here with a possible trade off between torque and motion. Equally leverage or gearing may be used.

Friction has not been taken into account and this will add to both torque and power requirements, but to include friction a detailed structural model of the blade, flap and actuator will be required. Such a model would also be useful in analysing changes to the blade dynamics, such as the blade frequency, its flexibility and the effect that a flexible blade has on the flaps and their design. This level of detail is beyond the scope of this thesis, but will need to be considered. Additionally, although the detailed study of flaps of three different chord widths may suggest trends, additional flap sizes are needed to properly quantify these results.

References

[1] S. Daynes and P. M. Weaver, "Design and testing of a deformable wind turbine blade control surface," *Smart Materials and Structures*, vol. 21, Oct. 2012.

[2] D. Berg, J. Berg, J. White, B. R. Resor, and M. Rumsey, "Design, Fabrication, Assembly and Initial Testing of a SMART Rotor," in *49th AIAA Aerospace Sciences Meeting including the New Horizons Forum and Aerospace Exposition*, vol. 4-7, (Reston, Virigina), American Institute of Aeronautics and Astronautics, Jan. 2011.

[3] J. Berg, D. Berg, and J. White, "Fabrication, Integration and Initial Testing of a SMART Rotor," in *50th AIAA Aerospace Sciences Meeting including the New Horizons Forum and Aerospace Exposition*, (Reston, Virigina), American Institute of Aeronautics and Astronautics, Jan. 2012.

[4] J. Berg, B. R. Resor, J. Paquette, and J. White, "SMART Wind Turbine Rotor: Design and Field Test," tech. rep., Sandia National Laboratories, Albuquerque, New Mexico and Livermore, California, 2014.

[5] J. Berg, M. F. Barone, and N. Yoder, "SMART Wind Turbine Rotor: Data Analysis and Conclusions," tech. rep., Sandia National Laboratories, Albuquerque, New Mexico and Livermore, California, 2014.

[6] P. B. Andersen, L. C. Henriksen, M. Gaunaa, C. Bak, and T. Buhl, "Deformable trailing edge flaps for modern megawatt wind turbine controllers using strain gauge sensors," *Wind Energy*, vol. 13, pp. 193–206, Mar. 2010.

[7] J. D. Anderson, *Fundamentals of Aerodynamics*, vol. 48. Maryland, USA: McGraw-Hill, fifth ed., Dec. 2011.

[8] M. Drela, "XFOIL: An analysis and design system for low Reynolds number airfoils," in *Low Reynolds number aerodynamics*, (Notre Dame, IN, Germany), 1989.

[9] B. J. Jonkman, S. Butterfield, W. D. Musial, and G. Scott, "Definition of a 5-MW Reference Wind Turbine for Offshore System Development," tech. rep., NREL, Colorado, 2009.

[10] D. Marten and J. Wendler, "QBLADE: an open source tool for design and simulation of horizontal and vertical axis wind turbines," *International Journal of Emerging Technology and Advanced Engineering*, vol. 3, no. 3, pp. 264–269, 2013.

[11] C. Hansen, "NWTC Computer-Aided Engineering Tools (AirfoilPrep)," 2014.

[12] F. Grasso, "Usage of Numerical Optimization in Wind Turbine Airfoil Design," *Journal of Aircraft*, vol. 48, pp. 248–255, Jan. 2011.

Chapter 8

Direct comparison of individual pitch and smart rotor control

Both individual pitch control and smart rotor control are being considered for load reduction on large multi-megawatt wind turbines. While individual pitch control involves adjusting the pitch of each blade individually to reduce the cyclic loadings on the rotor, smart rotor control involves activating control devices distributed along the blades to alter the local aerodynamics of the blades. In this chapter, two distinct advanced load reduction control strategies are implemented, as described in Section 4.4 of this thesis. These are the dq-axis centralised controller and the Independent controller.

The approach used is to attain equal load reductions, assigned as the out-of-plane blade root bending moment, using both individual pitch and smart rotor control. This allows other parameters to be compared side-by-side for both control methods. The effectiveness of the control strategies is determined through measurement of fatigue and extreme load reductions, Section 8.2 and Section 8.3, the pitch and flap actuator requirements, Section 8.4 and Section 8.5, and the rotor speed variability, Section 8.6.

8.1 Motivation

Trailing edge flaps have been shown to demonstrate load reduction potential by a number of authors with results comparable to those of individual pitch control e.g. [1], [2]. The question then arises though, as to whether this complex smart rotor system is of merit when similar results can be achieved using individual pitch control. One method to avoid this question is to simply make the smart rotor an extension of individual pitch control, i.e. supplementing it to achieve greater load reductions. This has been tried with promising results [3], [4], but load reduction gains can also be achieved simply by making the pitch actuators work harder. This has not been considered by other authors and has resulted in assertions that the smart rotor control is beneficial as regards to the costs, when indeed the alternative may be a cheaper option. This work therefore attempts to quantify some of the advantages and disadvantages of each system based on a fatigue load reduction that would result in similar cost savings regarding the blade design. The fatigue loads that are affected by the control strategies are therefore looked at in detail. The controllers described in Chapter 4 of this thesis are used for this purpose.

The results highlight that the loads of the smart rotor are very closely aligned to those of individual pitch control and that the advanced control strategies used, while important to the loads affected, do not favour either the smart rotor or individual pitch control. Therefore either individual pitch or smart rotor control may be used to achieve similar load reductions. This is a similar result to what others have found, e.g. [3], although previously no direct comparison with equal load reductions has been made. This is evidence that there need to be other reasons to favour one system over another than fatigue load reduction.

Although fatigue loads are often the design driver behind large wind turbine blades [5], extreme loads are also considered as these too can also affect the design [6]. They, like the fatigue loads, are reduced equally by either smart rotor or individual pitch control, though the advanced controllers implemented have less of an effect on these extreme loads. Other advanced controllers may specifically target extreme loads though [7]. This makes it clear that load reduction is not the deciding factor in selecting either smart rotor or individual pitch control, as the cost of energy reduction as regards to loads could be made equal. Instead other criteria, which ultimately result in cost savings, need to be considered to encourage the adoption of the smart rotor.

While it is clear that blade designs have to be altered considerably to accommodate smart rotor devices, the pitch actuator and pitch bearing is also placed under higher demands when individual pitch control is active [8]. The demands of using the various control strategies on the pitch actuator are one reason why individual pitch control may not be adopted and is therefore of interest in this comparison. Pitch travel, rates and accelerations are all increased as a result of operating individual pitch control, which can lead to increased wear on the bearings, increased maintenance requirements, increased failures, or simply the requirement of higher cost actuators that are more capable of sustained activity and the additional cooling that would be required for heat dissipation. For reference, the pitch actuator and bearings contribute approximately 3% to the capital cost of a 5MW wind turbine [9], and cause approximately 10% of the downtime due to failures [10], [11]. On the other hand, the smart rotor can achieve the load reductions of the individual pitch control without adversely effecting the pitch actuator, potentially leading to cost reductions.

The actuator requirements of the smart rotor control are also shown to highlight that these

may be of a significantly lower power rating than the pitch actuators, though these would likely be harder to install, power and maintain. An idea is proposed though, that should blades with smart rotor devices be created that are cheaper than standard blades due to the reduced blade loads, these could replace blades on current wind turbines with only the additional need to supply a small amount of power to them, without any other changes to the turbine being required. This could facilitate fairly rapid testing of the smart rotor once the blades are constructed. The blades themselves currently contribute approximately a fifth to the overall cost of the wind turbine [9], so there is some room for manoeuvre.

The rotor speed variability is also considered, as it was felt that using the pitch for both speed control and load reduction could adversely effect one another. This effect is negligible though. A look at using smart rotor control to supplement rotor speed control is given in the next chapter.

The comparison that follows highlights the differences between the smart rotor and individual pitch control systems, as well as the dq-axis and independent control strategies, to aid in the understanding of what should be implemented on future wind turbines.

8.2 Fatigue load reductions

The objective of the individual pitch and smart rotor control techniques is to reduce blade root out-of-plane loads. However, the goal of this work is to compare the two control methods. By making the blade root out-of-plane load reductions deliberately similar for both the individual pitch and smart rotor control methods, a direct comparison can be made between the two in other areas. This avoids bias that can occur simply by selecting favourable gains for one control type over another, or by confusing the argument through supplementing one with the other. Whilst the initial study suggested a pitch to flap angle gain of 4.6, described in Section 4.2, a lower gain of 4.15 was found to be close to optimal for equivalent load reductions using either flap or pitch control.

Some interesting results can immediately be seen, even within the remit of loads. The lifetime fatigue load reductions are shown in Table 8.1. These are calculated based on the IEC standard as described in Chapter 5.

Table 8.1: Lifetime damage equivalent loads as a percentage (%) of the collective pitch controlled case

	Baseline	dq-axis control		Independent control	
Load metric	1Hz DEL [MNm]	Pitch	Smart rotor	Pitch	Smart rotor
Blade root Mx	7.05	97.3	97.7	96.1	96.2
Blade root My	7.74	84.2	84.4	89.5	89.5
Rotating hub My	5.35	77.1	76.7	84.1	83.5
Rotating hub Mz	5.34	77.3	76.7	84.3	83.9
Yaw bearing My	3.49	97.1	97.7	101.9	102.2
Yaw bearing Mz	3.44	96.2	96.5	102.1	102.6
Tower base Mx	5.39	99.3	99.6	101.4	100.9
Tower base My	14.84	100.5	100.8	102.1	102.6

The control methods reduce not only the targeted out-of-plane blade root bending moment (blade root My), but also slightly reduce in-plane blade root bending moment (blade root Mx) and loads on the shaft (rotating hub My and Mz). Yaw bearing moments on the other hand may either increase or decrease marginally depending on the control strategy used, and tower loads exhibit a similar response, though with the fore-aft tower moment (tower base My) undergoing a small increase in loads regardless of the control strategy. The differences between the dq-axis and independent control strategies are interesting, as this shows that the control strategies are not necessarily limited to one key objective.

In this work however, the important comparison is between use of smart rotor control and individual pitch control. When comparing load reductions for both the individual pitch and smart rotor control they are all very similar, regardless of control strategy. This suggests either the smart rotor or individual pitch control method may be used to achieve similar fatigue load reductions. It is worth however exploring the differences some more to confirm this really is the case.

The blade root out-of-plane lifetime loads are shown in Figure 8.1. All the load reduction occurs in the above rated region as the advanced control strategies are phased out below rated. This can be justified simply by looking at the below rated lifetime loads, which already contribute significantly less to the lifetime damage than at higher wind speeds.

Looking at the load reduction achieved by the control strategies at each mean wind speed, as

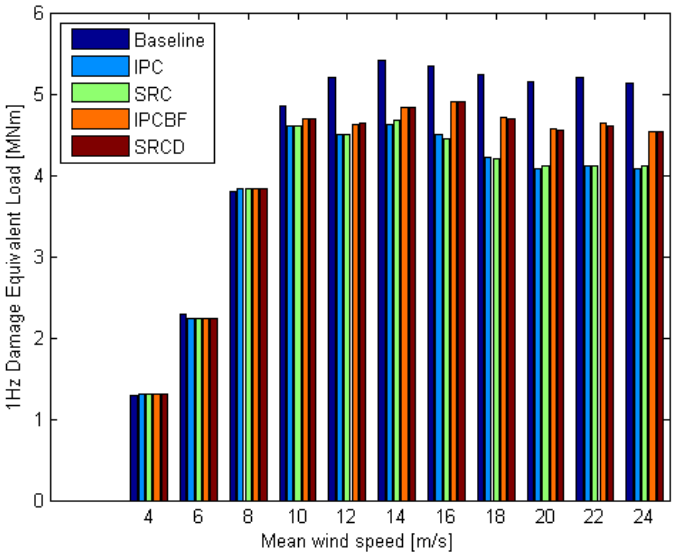

Figure 8.1: Contributions to lifetime 1Hz damage equivalent loads for the blade root out-of-plane bending moment for the wind turbine with collective pitch control (baseline), individual dq-axis pitch control (IPC), dq-axis smart rotor control (SRC), and independent blade control (IPCBF) and independent smart rotor control (SRCD)

seen in Figure 8.2, there may however be a benefit of additional action at the near rated wind speeds, where load reductions of around 5%, rather than load reductions of 10 to 15%, are achieved. What is clear though, is that regardless of wind speed, both individual pitch and smart rotor control perform equally well, and that a much larger variation in loads is caused by the controller design, rather than the use of different actuators. The small differences between smart rotor and individual pitch control at different wind speeds are most likely due to chance, rather than one having an advantage over the other at different wind speeds.

The variation in loads due to controller design can also be seen in the mean tilt and yaw moments on the hub, Figure 8.3. Whilst the dq-axis controller specifically targets imbalances in these moments, the independent controller in-directly helps to reduce these moments. Interestingly, the dq-axis controller in fact results in small negative tilt and yaw moments, while the independent controller shifts the imbalances but does not eliminate them. At 10 and 12m/s mean wind speed, it is also clear that the controllers are not fully active, as the reductions are much less than at higher wind speeds.

Comparing between the smart rotor and individual pitch control in Figure 8.3, a slight systematic difference can be perceived. This is likely due to the gain not being perfect, as it shows itself across all wind speeds and both dq-axis and independent control strategies. Nevertheless, across all wind speeds, both the smart rotor and individual pitch achieve similar load reductions. This suggests that no saturation of the flaps, which are limited to $\pm 20°$, occurs and that smart rotor control is interchangeable with individual pitch control across the entire operating range of the wind turbine.

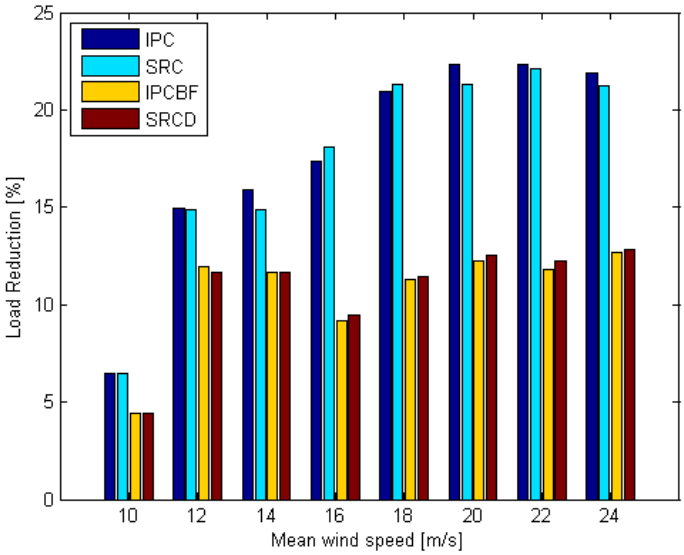

Figure 8.2: Comparison of non-lifetime weighted 1Hz damage equivalent loads for the blade root out-of-plane bending moment at different mean wind speeds

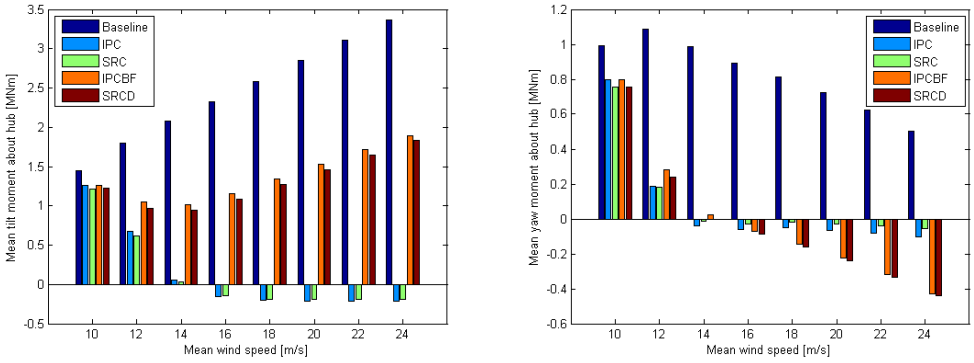

(a) Mean tilt moment

(b) Mean yaw moment

Figure 8.3: Average tilt and yaw moments about the hub at above rated wind speeds

8.3 Extreme load reductions

The 1-in-50-year occurrence extreme loads from the normal turbulence model design load case (DLC 1.1), may also be compared between the different control methods. These are shown in Table 8.2. These load results come with the caveat that DLC 1.1 is not always the design-driving load case, and indeed in cases like emergency shutdown higher loads may result for the advanced load reduction strategies than for the collective pitch controlled case unless suitable safety systems are adopted [12] [13].

Table 8.2: Extreme loads compared to collective pitch control as a percentage (%)

	Baseline	dq-axis control		Independent control	
Load metric	Extreme load [MNm]	Pitch	Smart rotor	Pitch	Smart rotor
Blade root Mx	13.4	100.3	105.1	95.7	96.2
Blade root My	25.7	97.2	96.4	96.7	96.7
Rotating hub My	20.3	78.2	78.6	89.8	90.0
Rotating hub Mz	21.8	74.5	74.9	84.7	84.9
Yaw bearing My	20.0	72.7	75.1	91.5	91.6
Yaw bearing Mz	16.5	90.2	91.5	94.5	95.1
Tower base Mx	54.1	91.5	94.5	95.8	97.1
Tower base My	191.5	99.9	101.8	99.2	100.1

It can be seen from comparing the smart rotor and individual pitch control methods that similar load reductions are again achieved when it comes to extreme loads. This comes with the proviso that the dq-axis control blade root in-plane moment and tower fore-aft moment show exceptional results, with a higher extreme load with the smart rotor than for the individual pitch controlled case. This then requires that extreme loads are also considered when designing the blades for either smart rotor or individual pitch control.

Apart from this exception, the results support the argument that load reductions, and so savings to the construction of the blades, may be had either through use of pitch control or through smart rotor control. To quantitatively value the cost benefits of one system over the other, additional criteria are therefore required to differentiate the two. To this extent, the actuator requirements are described in the following two sections.

8.4 Pitch actuator requirements

A comparison is made of the pitch motion, torque and power requirements for the pitch actuator at three above rated wind speeds, 12, 16 and 24m/s, for each control strategy, Table 8.3. The increased travel and pitch rates over the baseline case will result in increased wear of the actuator and pitch bearing. As can be seen the independent controller does not increase the motion as much as the dq-axis controller, but as seen earlier with the current tuning does not achieve as great a load reduction. This supports the hypothesis that for greater load reductions, actuator requirements are indeed greater, which is a conclusion found in [14] where load reductions are achieved through a combination of pitch and smart rotor control. The study however is limited to one wind speed and actuator requirements measured purely by travel.

Pitch accelerations are also seen to increase, though not by as much. The average torques required of the pitch actuator do increase though, by approximately 10%. The increase in both average torques and rates results in a higher mean power demand of the actuators. This would result in more power loss in the system, but is small compared to the rating of the wind turbine. It would though require the pitch actuator to have better thermal dissipation.

Control using the smart rotor on the other hand reduces the torque on the pitch actuators, and whilst the pitch motion is marginally altered, the power requirement as a result of the reduced torques is also decreased. These are both positive results, as it suggests no change, or even a de-rating, of the pitch actuator is required when implementing the smart rotor wind turbine.

Based on this criterion, the pitch system would need to be upgraded to operate an individual pitch control strategy. In contrast, it can be seen that when using a smart rotor control strategy, the motion required of the pitch actuator can be held close to the baseline case. The cost to upgrade the pitch system versus the cost of implementing a smart rotor system is key to the decision of one system over another, but equally it is vital to compare the cost of implementing either system to the savings made from reduced loads.

Focussing on the pitch rate it is also evident that at higher wind speeds increased pitch action is required, particularly for the dq-axis controller, but also for the baseline which means for speed control, see Figure 8.4. Indeed the percentage increase in pitch rate standard deviation is similar from 16-24m/s for the dq-axis controlled case. Therefore there may be some trade-off between the rating of the pitch actuator and load reductions at high wind speeds which occur less often.

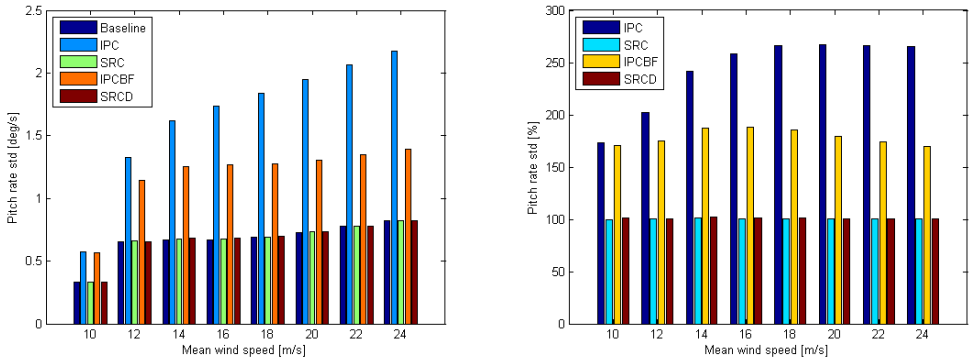

(a) Absolute (b) Percentage of baseline

Figure 8.4: Standard deviation of the pitch rate at above rated wind speeds

Table 8.3: Comparison of pitch actuator motion as a percentage (%) of the baseline collective pitch controlled wind turbine pitch actuator at 12, 16 and 24 m/s mean wind speed

		dq-axis		Independent	
12m/s	Baseline	Pitch	Smart rotor	Pitch	Smart rotor
Pitch travel	$0.442°s^{-1}$	215.1	100.3	183.7	100.5
Pitch rate std	$0.657°s^{-1}$	201.9	100.3	174.6	100.1
Pitch acceleration std	$3.884°s^{-2}$	128.1	100.1	98.0	98.0
Pitch torque std	137 kNm	113.7	89.6	111.8	89.5
Pitch power mean	1.11 kW	262.5	84.0	220.0	83.9

		dq-axis		Independent	
16m/s	Baseline	Pitch	Smart rotor	Pitch	Smart rotor
Pitch travel	$0.582°s^{-1}$	270.1	100.5	193.0	101.5
Pitch rate std	$0.671°s^{-1}$	258.4	100.6	188.6	101.6
Pitch acceleration std	$3.714°s^{-2}$	142.3	100.1	107.3	100.1
Pitch torque std	112 kNm	114.2	87.8	111.4	87.6
Pitch power mean	0.98 kW	338.5	84.8	233.1	84.8

		dq-axis		Independent	
24m/s	Baseline	Pitch	Smart rotor	Pitch	Smart rotor
Pitch travel	$0.654°s^{-1}$	277.8	100.7	172.3	100.5
Pitch rate std	$0.820°s^{-1}$	265.1	100.6	169.7	100.5
Pitch acceleration std	$4.793°s^{-2}$	130.7	99.2	104.6	99.3
Pitch torque std	89 kNm	100.8	85.4	103.2	85.7
Pitch power mean	0.91 kW	307.0	82.0	191.7	81.8

With regards to the smart rotor, what is very clear though from these tables and figures is that use of the smart rotor barely affects the pitch actuator motion, regardless of wind speed. This implies that use of the smart rotor would not require any change to the pitch actuator for implementation. Supposing naively that the entire benefit of load reduction is found through decreased cost of the blade construction (rather than longer blades or similar), this would then allow a blade manufacturer to produce blades for any wind turbine, assuming a power supply can be suitably supplied to the smart rotor actuators, without any major alterations to the rest of the turbine or central controller. This could then, at least in theory, be simpler than altering the hub and pitch actuators to facilitate individual pitch control.

As well as the average rates, accelerations, torques and power demands, the actuator also needs to perform to the extreme conditions. To this end the lifetime 1-in-50-year extreme values are displayed in Table 8.4. Again the extreme rates are higher for the pitch controlled case, whilst the smart rotor control is similar to the baseline with regards to both pitch rates and accelerations. Strangely, the extreme pitch acceleration for the independent controller is significantly lower than the baseline or other control strategies. No obvious reason exists for this anomaly, though it could be down to the method for extreme load extrapolation. Also of interest is the fact that although the mean torques are lower for the smart rotor, as seen in Table 8.3, the extreme torques are in fact higher than for the pitch controlled case, and baseline. This is of slight concern as it may mean larger actuators are required. However, as regards to peak power requirements, again the smart

rotor requires similar to the baseline, while the individual pitch control requires peak ratings of 50-60% more than the baseline collective pitch controlled case.

Table 8.4: Comparison of pitch actuator motion as a percentage (%) of the baseline collective pitch controlled wind turbine pitch actuator

		dq-axis		Independent	
Metric	Baseline	Pitch	Smart rotor	Pitch	Smart rotor
Pitch rate extreme	$8.48°s^{-1}$	156.5	100.2	134.1	98.6
Pitch acceleration extreme	$60.7°s^{-2}$	100.2	99.3	82.7	100.6
Pitch torque extreme	910.1 kNm	100.6	106.3	100.8	107.0
Pitch power extreme	30.6 kW	162.2	99.2	151.1	96.0

Due to the increased motion of the individual pitch control the power consumption is higher than for the collective or smart rotor control cases. This increase will require better thermal dissipation and an actuator with a higher rated power. Bearing and pitch actuator wear is a complex issue though. Whilst additional motion may increase wear, lower torques can reduce it, suggesting that a thorough analysis needs to be conducted into the exact causes and constraints on both the actuator and the bearings, as depending on the conditions and control strategy, wear might either increase or decrease and this will depend highly on the type of actuator and bearings under consideration. This will have a direct impact on the cost of adopting an individual pitch control strategy.

8.5 Flap actuator requirements

For the smart rotor, we also need to consider the flap actuator. Although it is possible to reduce loads through higher bandwidth devices, both pitch and flap actuators are set with the same actuator model: a second order passive transfer function with a frequency of 1Hz and damping factor of 0.7. This allows the actuator motion, torque and power required to be directly compared, without having to significantly adjust the controllers to achieve similar load reductions.

The flap angular motion is of a higher order than the pitch actuator motion. This is because a 4.15 degree change in flap angle is only equivalent to a 1 degree change in pitch angle. Indeed, this is why the gains are adjusted from the pitch to flap control, with a factor of 4.15 found to take account of the reduced span of the flap and the reduced gradient of lift coefficient versus pitch. This of course is for this particular flap design and as seen in Chapter 7 a trade can be made between flap motion and flap torques. There is also the possibility of using multiple actuators on each blade to further reduce the torques required, though rates would stay the same.

As can be seen by comparing the results of Table 8.5 with Table 8.3, the travel required of the flap is higher than for the pitch actuator. However, direct comparisons with the pitch actuator should not be drawn, as the flap does not provide speed control and because the space available in the blade is substantially less than in the hub. Comparisons between the two controllers should also be avoided, as the differences are down to tuning rather than one being better than the other. The requirements are therefore not only different as regards to the motions, torques and power requirements, but also to the physical constraints to which such an actuator would need to conform. Low torques and power requirements are therefore not only desirable, but necessary.

Table 8.5: Flap actuator demands of the dq-axis and independent controllers

Metric	dq-axis	Independent
Flap deflection extreme	24.80°	23.43°
12m/s		
Flap travel	$3.48°s^{-1}$	$2.92°s^{-1}$
Flap rate std	$0.74°s^{-1}$	$0.63°s^{-1}$
Flap acceleration std	$2.78°s^{-2}$	$1.30°s^{-2}$
16m/s		
Flap travel	$5.12°s^{-1}$	$3.50°s^{-1}$
Flap rate std	$0.99°s^{-1}$	$0.69°s^{-1}$
Flap acceleration std	$2.69°s^{-2}$	$1.13°s^{-2}$
24m/s		
Flap travel	$6.73°s^{-1}$	$3.76°s^{-1}$
Flap rate std	$1.27°s^{-1}$	$0.75°s^{-1}$
Flap acceleration std	$3.06°s^{-2}$	$1.22°s^{-2}$

The 1-in-50-year maximum deflections are also shown. That these exceed the maximum allowed flap deflection implies that at times the control system will saturate and so lose some of the ability to control the loadings. However, this is not limited to the smart rotor control, the extreme pitch rate also exceeds the $8°s^{-1}$, see Table 8.4. Extreme conditions should therefore be studied to assess the impact that these conditions would have on the wind turbine.

8.6 Rotor speed variability

The final criterion for comparison here is the rotor speed variability. Above rated pitch control is used to maintain rated rotor speed, whilst the torque is adjusted to hold power output constant. It is possible that the advanced control strategies may interfere with the central controller, particularly the rotor speed control when individual pitch control is active as both systems will be utilising the pitch actuators. It is found however that rotor speed variability is similar regardless of the control strategy: baseline, dq-axis, independent, smart rotor or individual pitch control. This is a positive result as it shows that the advanced control strategies are not to the detriment of the central controller, Figure 8.5.

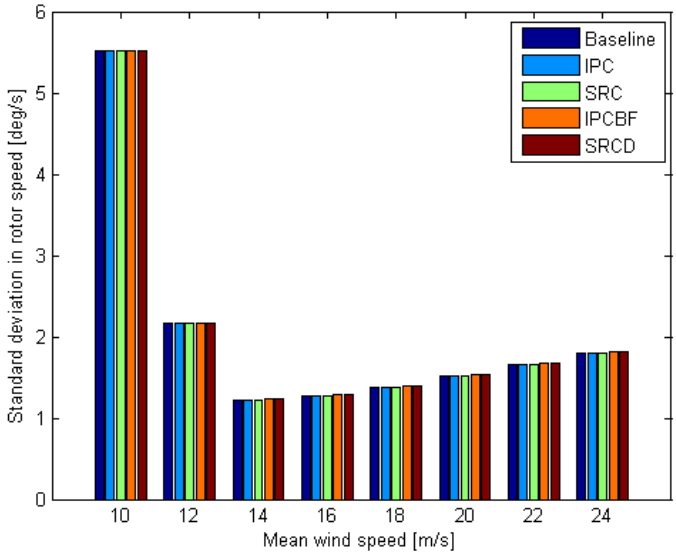

Figure 8.5: Standard deviation of the rotor speed at above rated wind speed

8.7 Discussion

This study verifies that it is possible to achieve similar load reductions with trailing edge flaps as it is by pitching the entire blade. This was shown using two different control techniques: a dq-axis centralised controller and a distributed Independent controller. It is also shown that while load reductions are similar for the smart rotor and individual pitch, the style of the controller does have an effect on a variety of other variables, including components that are not the direct target of the controller, for instance tower loading and hub tilt and yaw imbalance.

For individual pitch control, load reductions come at a cost of increased actuator duty and power requirements. Any requirement to upgrade the pitch actuator and bearings will come at a cost and it is these potential costs that need to be compared with the price attached to implementing a smart rotor in deciding which to adopt, if either.

From the results it is clear that use of trailing edge flaps can achieve the same load reductions as individual pitch control without any alteration to the pitch actuator. Indeed use of the smart rotor can reduce both the motion and rates of the pitch actuator, creating potential savings. The real concern here is whether a suitable actuation system can be found that is both reliable and cost effective in comparison to upgrading the pitch system.

This direct comparison of both individual pitch and smart rotor control encourages future work to look at the possibility of using the smart rotor to supplement collective pitch control for roles other than out-of-plane blade root bending moment load reduction as the upgrade to the pitch actuator is one of the main detractors to implementing individual pitch control it suggests that further reduction to the pitch actuator requirements may be of further benefit, and this is explored in Chapter 9.

References

[1] P. B. Andersen, L. C. Henriksen, M. Gaunaa, C. Bak, and T. Buhl, "Deformable trailing edge flaps for modern megawatt wind turbine controllers using strain gauge sensors," *Wind Energy*, vol. 13, pp. 193–206, Mar. 2010.

[2] T. K. Barlas, G. van der Veen, and G. A. M. van Kuik, "Model predictive control for wind turbines with distributed active flaps: incorporating inflow signals and actuator constraints," *Wind Energy*, vol. 15, pp. 757–771, July 2012.

[3] M. A. Lackner and G. A. M. van Kuik, "A comparison of smart rotor control approaches using trailing edge flaps and individual pitch control," *Wind Energy*, vol. 13, pp. 117–134, Mar. 2010.

[4] D. G. Wilson, D. Berg, B. R. Resor, M. F. Barone, and J. Berg, "Combined individual pitch control and active aerodynamic load controller investigation for the 5MW upwind turbine," in *AWEA Wind Power Conference*, (Chicago, Illinois), 2009.

[5] P. S. Veers, T. D. Ashwill, H. J. Sutherland, D. L. Laird, D. W. Lobitz, D. A. Griffin, J. F. Mandell, W. D. Musial, K. Jackson, M. Zuteck, A. Miravete, S. W. Tsai, and J. L. Richmond, "Trends in the Design, Manufacture and Evaluation of Wind Turbine Blades," *Wind Energy*, vol. 6, pp. 245–259, July 2003.

[6] M. A. Lackner and G. A. M. van Kuik, "The Performance of Wind Turbine Smart Rotor Control Approaches During Extreme Loads," *Journal of Solar Energy Engineering*, vol. 132, 2010.

[7] H. Yi and W. E. Leithead, "Alleviation of Extreme Blade Loads by Individual Blade Control during Normal Wind turbine Operation," in *EWEA*, (Copenhagen, Denmark), 2012.

[8] M. Shan, J. Jacobsen, and S. Adelt, "Field Testing and Practical Aspects of Load Reducing Pitch Control Systems for a 5 MW Offshore Wind Turbine," in *EWEA*, (Vienna, Austria), 2013.

[9] C. Aubrey, "Supply Chain: The race to meet demand," *Wind Directions*, pp. 27–34, Feb. 2007.

[10] P. J. Tavner, J. Xiang, and F. Spinato, "Reliability analysis for wind turbines," *Wind Energy*, vol. 10, Jan. 2007.

[11] J. Ribrant and L. M. Bertling, "Survey of Failures in Wind Power Systems With Focus on Swedish Wind Power Plants During 1997–2005," *IEEE Transactions on Energy Conversion*, vol. 22, pp. 167–173, Mar. 2007.

[12] E. A. Bossanyi, B. Savini, M. Iribas, M. Hau, B. Fischer, D. Schlipf, T. G. V. Engelen, M. Rossetti, and C. E. Carcangiu, "Advanced controller research for multi-MW wind turbines in the UPWIND project," *Wind Energy*, vol. 15, pp. 119–145, Jan. 2012.

[13] C. L. Bottasso, A. Croce, C. E. D. Riboldi, and M. Salvetti, "Cyclic pitch control for the reduction of ultimate loads on wind turbines," *Journal of Physics: Conference Series*, vol. 524, June 2014.

[14] L. C. Henriksen, L. Bergami, and P. B. Andersen, "A model based control methodology combining blade pitch and adaptive trailing edge flaps in a common framework," in *EWEA*, (Vienna, Austria), 2013.

Chapter 9

Supplementary control

Pitch actuator requirements are increased when individual pitch control is activated, and the avoidance of such increased demands may be seen as a benefit of smart rotor control. The smart rotor though is capable of more than just reducing the loads on the wind turbine, and can in fact supplement the overall pitch control system to reduce pitch demands.

In this chapter the smart rotor control is used to supplement the pitch rotor speed control. The motivation for this is explained in Section 9.1, followed by a description of rotor speed control in Section 9.2. The method of supplementing the pitch control with smart rotor control and the tuning of the controller are then described in Section 9.3. Results from using the smart rotor control to just supplement the pitch control and to supplement the pitch control while also achieving load reductions are then presented in Sections 9.4 and 9.5, before finishing off the chapter with conclusions.

9.1 Motivation

The idea of supplementing the pitch control with smart rotor control is not new. It has already been considered in the case of supporting individual pitch control and thus enhancing load reductions [1], [2], [3]. As raised in the previous chapter though, this is merely an alternative to upgrading the pitch actuator. The motivation behind this chapter is then to see the smart rotor as an opportunity to support the pitch actuator in a variety of roles, as opposed to purely advanced load reduction. A similar study has been conducted in [4] that has shown this to have potential.

Historically aerodynamic devices have been considered as an alternative to pitch control to regulate rotor torque, and in particular for over-speed protection [5], [6], [7]. Rather than replacing pitch control though, this work looks at supplementing it so as to reduce the pitch actuator demands while maintaining controllability. While this is not seen as the main purpose of smart rotor control it may be a useful enhancement to the remit of smart rotor control.

Although this work implements the system on a trailing edge flap smart rotor, different devices may be used implementing the strategies suggested. Equally, although it is rotor speed control that is supplemented here, in fact the method used to split the signal between the smart rotor and pitch actuator may be used for the overall pitch demand to fully supplement the pitch control, including when individual pitch control is active. The smart rotor control then has the ability to not only reduce loads, but also pitch actuator demands and so pitch actuator and bearing requirements.

9.2 Rotor speed control

The baseline controller described in Chapter 4 is implemented here. To aid in understanding, the rotor speed control is described again here with use of a block diagram shown in Figure 9.1.

Rotor speed above rated is controlled by adjusting the collective pitch angle of the blades. To reduce the aerodynamic torque on the rotor the blades are pitched to feather, reducing the angle of attack and thus lowering the lift produced. This is done here using a Proportion Integral (PI) controller based on rotor speed error, and additionally a term to take account of the difference between actual power and rated power, to encourage pitching in rising wind speeds in the region just below rated.

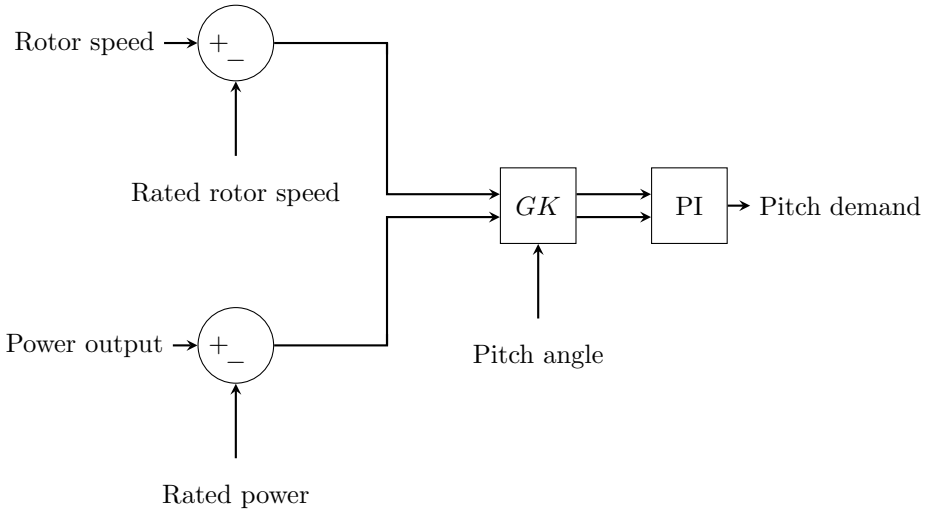

Figure 9.1: Rotor speed control system diagram

The two controllers share the same integrator and anti-windup limits, which are imposed on the integral in the form of minimum and maximum pitch angles and maximum rates. For the rotor speed error a proportional gain of 0.0135 and integral gain of 0.00453 are used and for the power error a proportional and integral gain of 10^{-7} and 5×10^{-8} are used respectively. A gain schedule is used to account for the fact that at lower wind speeds more pitch action is required to achieve the same controllability. This gain scheduling uses the current pitch angle to adjust the gain and is of the form $GK = 1/(1.0 + \theta/12.5)$, with the pitch angle, θ, in degrees, and a minimum gain imposed of 1/3.5.

9.3 Supplementary control design

Supplementation of the pitch speed control is done through splitting the demanded pitch angle from the PI speed controller based on frequency. High frequency variations are controlled by the smart rotor, which is considered more than capable of rapid response, and low frequency variations are left to be controlled by the pitch mechanism. Single pole low and high pass filters are found to be adequate for this role, implemented as recursive filters, with the same corner frequencies. This method is portrayed in Figure 9.2. As the filters are complementary, the high pass filter can be implemented as the original demand minus the low pass filtered demand. A gain is required to make the demanded flap angle equivalent to the demanded pitch angle, GK_{flap}, as described in Section 4.2 of the Baseline Chapter and in Chapter 7 on trailing edge flaps. In this case the value chosen is 4.15, so as to compare directly with the smart rotor controlled case in the previous chapter.

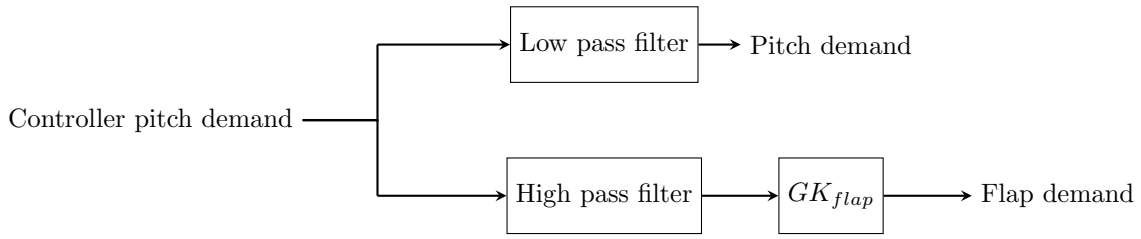

Figure 9.2: Control system diagram showing how the controller demand is split between the pitch and flap actuator demands

Whilst in this chapter this method is implemented solely on the PI rotor speed control, the method could equally be applied to the tower vibration damping feedback loop or indeed the overall pitch demand. The focus on rotor speed control is done for clarity and simplicity in making comparisons, and demonstrates the effect that using smart rotor control to supplement pitch control can have.

9.3.1 Tuning the filters

A series of filter cut-off frequencies are trialled to determine the optimum cut-off frequencies for the supplementary control, taking account of the impact on the pitch actuator, flap actuator and rotor speed.

For these results two 10 minute runs using Kaimal 3D turbulent wind fields are run for each wind speed between 10-24m/s in 2m/s intervals, and the maximum pitch rates and accelerations, flap deflections and rotor speed variations are found for each different cut-off frequency. This allows an initial analysis of what effect the supplementary control has on the wind turbine and a discovery of what filter cut-off frequency is preferable.

At high frequencies the filters are pushed to their limits due to the 10Hz sampling rate of the pitch controller, as seen in Figure 9.3. However, at these high cut-off frequencies the benefit of supplementing the pitch control with the smart rotor is already diminished, and so high cut-off frequency filters are not too important. This can be seen in Figures 9.4a and 9.4b, wherein the maximum pitch rates and accelerations approach those of the base case where the supplementary smart rotor speed control is inactive.

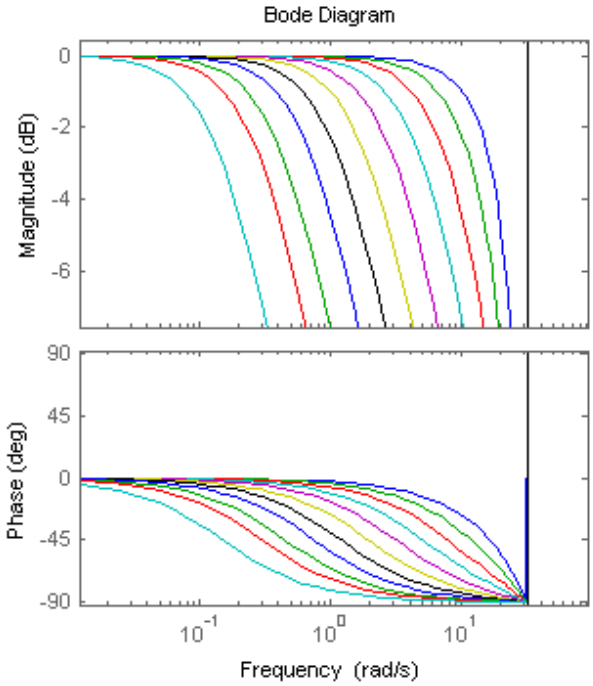

Figure 9.3: Bode plot of low pass discrete filters with increasing cut-off frequencies

Setting the cut-off frequency too low also causes problems, again as seen in increases in the maximum pitch rates and accelerations, Figures 9.4a and 9.4b. This occurs because the flap actuator saturates, as can be seen in Figure 9.4c, which portrays the maximum flap angle reached during the simulations. When this occurs the ability to control the system is reduced, which leads to larger oscillations in rotor speed, as can be seen in Figure 9.4d. It is therefore clear from this result that trailing edge flaps are not capable of fully supplanting pitch control as they lack full controllability due to saturation at 20 degrees in either direction.

These results suggest a cut-off frequency of approximately 1.95rad/s would be effective. As this maintains the same rotor speed stability as the baseline case, while achieving the highest possible benefit for the pitch actuator rates and accelerations. The maximum flap angle reached is also less than half the value at which the flap saturates and so will also help avoid aerodynamic uncertainties due to separation.

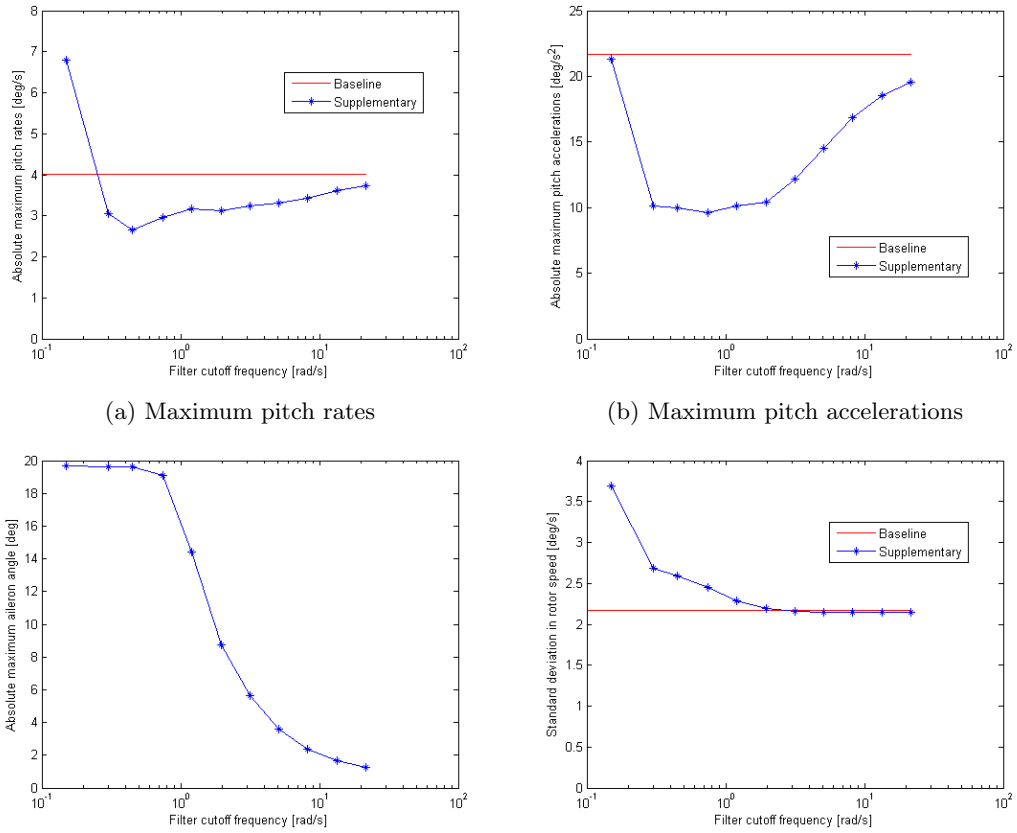

(a) Maximum pitch rates

(b) Maximum pitch accelerations

(c) Maximum flap angles reached

(d) Mean standard deviation in rotor speed

Figure 9.4: The effect of supplementary control cut-off frequencies on various parameters across all above rated wind speeds

9.4 Supplementary speed control

To analyse the specific case of a 1.95rad/s cut-off frequency in more detail the IEC 61400 standard is used for a class IB turbine [8]. Six runs at each wind speed from 10-24m/s in 2m/s steps are used; below 10m/s no pitch action occurs as the wind turbine remains below rated so these simulations are the same as the base case.

The first thing to analyse is the rotor speed variability as the smart rotor control is designed to supplement the pitch speed control to maintain constant rotor speed above rated. In Table 9.1 the supplementary control is seen to actually slightly increase the variability of the rotor speed, by upto a couple of percent. An increased pitch to flap gain, e.g. greater than 4.15, would decrease this, while a lower pitch to flap motion gain would increase the variability. So that a comparison can be made with the smart rotor control assessed in the previous chapter an equalisation of the rotor speed variability has not been implemented. This can be justified when looking across the wind speeds, as the increased variability using the supplementary control is negligible in comparison to the fluctuation in variability due to mean wind speed. Whilst the supplementary control is designed to maintain constant rotor speed, the objective of supplementing the pitch control is to reduce the pitch actuator motion, this reduction can be seen by looking at the pitch actuator requirements.

Table 9.1: Above rated rotor speed variability assessed as the standard deviation in rotor speed

Mean wind speed [m/s]	Baseline [deg/s]	Supplementary [deg/s]	Supplementary compared to baseline [%]
10	5.51	5.52	100.1
12	2.16	2.18	100.5
14	1.21	1.23	101.7
16	1.27	1.29	101.6
18	1.37	1.39	101.2
20	1.51	1.53	101.2
22	1.65	1.67	101.3
24	1.80	1.82	101.5

The pitch actuator travel across different wind speeds is displayed in Table 9.2, which shows increased benefit of using supplementary control at increased wind speeds. The extreme 1-in-50-year actuator demands for both the flap and pitch actuator are shown in Table 9.3. As can be seen pitch actuator demands are reduced considerably when smart rotor supplementary speed control is active. The reduction in the pitch rate is 32% and in the pitch acceleration 75%. These are to be expected due to the high frequency control demands being dealt with by the flap actuator. The torque demands on the other hand increase marginally, by approximately 4%.

It should also be noted that the pitch rate is normally limited to an absolute maximum of 8 degrees per second, this is exceeded approximately once every 16 years for the baseline controller, leading to occasional saturation of the pitch actuator. This will cause a slight loss in control, but only very rarely. Contrastingly when the supplementary control is used the chance of saturation is reduced to a probability of roughly once every 100,000 years, which would appear to suggest the actuator would be overrated for this use.

The flap deflections on the other hand are limited to an absolute deflection of 20 degrees. The

Table 9.2: Above rated travel of the pitch actuator

Mean wind speed [m/s]	Baseline [deg/s]	Supplementary [deg/s]	Supplementary compared to baseline [%]
10	0.1101	0.0925	84.0
12	0.4420	0.3674	83.1
14	0.5116	0.4267	83.4
16	0.5282	0.4270	80.8
18	0.5490	0.4285	78.0
20	0.5809	0.4446	76.5
22	0.6173	0.4622	74.9
24	0.6540	0.4821	73.7

Table 9.3: Extreme 1-in-50-year actuator demands

Variable	Baseline	Supplementary control
Pitch rates [deg/s]	8.5	5.8
Pitch acceleration [deg/s^2]	60.6	15.4
Pitch torque [kNm]	910.1	944.0
Flap deflection [deg]	-	12.0
Flap rates [deg/s]	-	48.9
Flap acceleration [deg/s^2]	-	433.5

likelihood of saturating the flap angle limit though is minuscule, with a probability of occurring only once every few million years of standard operation. This therefore suggests ample room for the smart rotor to take on more control functions. The flap rates and accelerations though also need to be considered. In Table 9.3 these are displayed and can be compared with those of the Sandia demonstration plant, which has rates of 200 to 330 degrees per second [9]. Assuming sinusoidal oscillations of plus/minus 20 degrees, this equates to accelerations of 2000 to 5545 degrees per second squared. The values observed therefore appear well within the realm of possibility.

Supplementing the main pitch control mechanism with smart rotor control is clearly feasible from this investigation, and facilitates a reduction in the pitch actuator requirements. This is the trivial case though and the smart rotor will likely need to offer something more than just a reduction in the pitch actuator requirements. The case where the smart rotor reduces loads, as well as the pitch actuator requirements, is therefore considered. It is termed here 'consolidated smart rotor control.'

9.5 Consolidated smart rotor control

The dq-axis smart rotor control is adopted as described in Section 4.4.1 and combined with the supplementary control strategy. In the previous chapter individual pitch control was compared directly with smart rotor control with regard to load reduction and actuator requirements. Here the focus is on use of smart rotor control for both load reduction and supplementing the overall pitch control system to reduce pitch demands.

Again an initial look at the rotor speed variability shows this is only mildly affected by the supplementary control (sup), smart rotor load reduction control (SRC), and by the consolidated smart rotor control (SRC + sup).

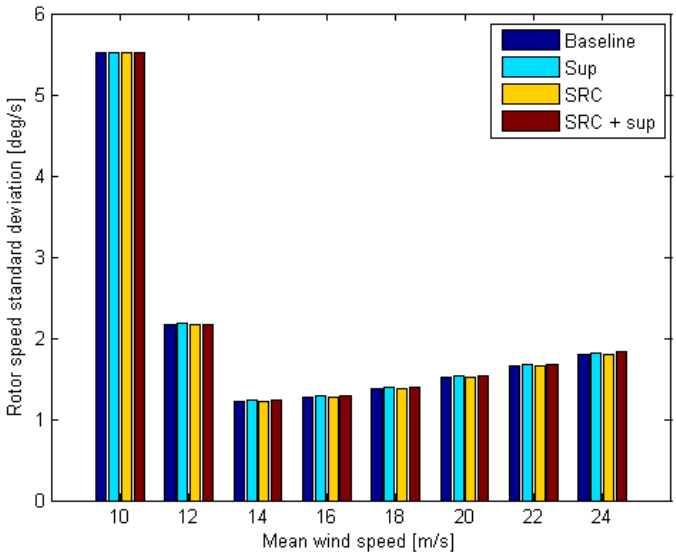

Figure 9.5: Above rated rotor speed variability

Fatigue load reductions are achieved of a similar level to those normally achieved by smart rotor control, as can be seen in Table 9.4, with only slightly worse results than the purely smart rotor controlled case. By increasing the smart rotor controller gains, which would increase flap demands, equivalence between the results is likely possible. The individual pitch control (IPC) load reductions are displayed as well to show the similarity of the load reduction potential of all three methods, demonstrating that as close to a fair comparison as possible is being made when implementing the consolidated controller.

Intriguingly, the tower loads are increased when using the supplementary control. This is likely due to extra thrust variations near the tower frequency, which is reduced in the collective pitch controlled case by the tower velocity feedback loop. A coordinated controller design could benefit this system, limiting interference with the tower vibration damping and so reduce these loads [10]. It should be noted there is no real variation in thrust as a result of using flaps instead of pitch control, the reason being the thrust on the rotor is in large part due to the lift the blades produce, as the torque is held constant, the thrust varies only a small amount.

The benefit of the consolidated controller is the reduction in pitch actuator demands, as shown

Table 9.4: Lifetime damage equivalent loads compared to the baseline [%]

Variable	sup	IPC	SRC	SRC + sup
Blade root Mx	100.2	97.4	97.6	97.6
Blade root My	101.0	83.4	83.1	84.5
Rotating hub My	100.2	77.2	76.7	76.9
Rotating hub Mz	100.3	77.1	76.5	76.7
Yaw bearing My	100.6	95.8	96.4	96.9
Yaw bearing Mz	100.6	95.7	96.1	96.5
Tower base Mx	102.1	97.8	98.6	100.7
Tower base My	102.6	99.2	99.8	102.8

in Figure 9.6 for the pitch travel and Table 9.5 for the extreme demands. This result is similar to [4], with evidence of the trade between pitch and flap travel and load reductions.

In the work done here, the extreme loads are considered too. Activation of the smart rotor load reduction control barely alters the pitch demands over the collective pitch controlled (CPC) baseline, apart from an increase in the extreme pitch torque. Supplementary control on its own drastically reduces the pitch rates and accelerations, as displayed in the previous section. When both smart rotor control for load reduction and the supplementary control are active, load reductions and pitch demand reductions similar to the purely supplementary control occur, with rate and acceleration reductions of 33% and 75% respectively, though again with an increase in the extreme pitch torque demand.

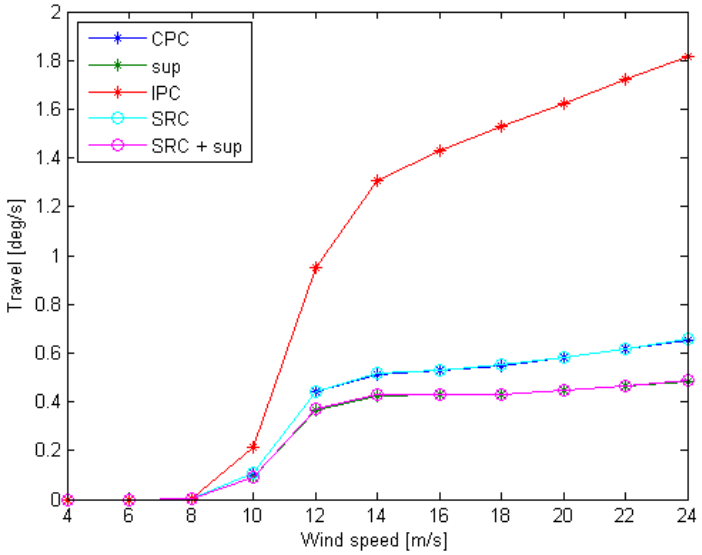

Figure 9.6: Pitch travel for the various control strategies. The results for the collective pitch control and smart rotor control are very similar, as too are the results for the supplementary and consolidated controllers

There is of course a cost to these benefits, and that is that the flap actuator has to work harder when both smart rotor load reduction control and the supplementary speed control are active.

Table 9.5: Extreme 1-in-50-year pitch actuator demands

Variable	CPC	sup	IPC	SRC	SRC + sup
Pitch rates [deg/s]	8.5	5.8	13.3	8.5	5.7
Pitch acceleration [deg/s^2]	60.6	15.4	60.7	60.2	15.4
Pitch torque [kNm]	910.1	944.0	916.0	967.5	994.0

Indeed extreme deflections, rates and accelerations all increase. This in fact leads directly to an increase in the risk of the flap reaching its maximum flap angle, from on average about four times a year, to over 8 times a year. This may be mitigated by increasing the filter cut-off frequencies and so reduce the flap deflections contributed by the supplementary speed control, but clearly this will impact on the pitch actuator reductions achievable, as seen in the initial design study.

Table 9.6: Extreme 1-in-50-year flap actuator demands

Variable	sup	SRC	SRC + sup
Flap deflection [deg]	12.0	25.7	27.5
Flap rates [deg/s]	48.9	69.3	79.8
Flap acceleration [deg/s^2]	433.5	622.4	761.5

This consolidated controller demonstrates that there is a trade to be had between the various aspects that smart rotor control influences: pitch demands, flap demands and load reductions. Previously, work has focussed rather on the load reductions achievable using smart rotor control, but it is the trade-off between these three aspects that should be considered when designing and implementing a smart rotor wind turbine to effectively lead to cost of energy reductions.

9.6 Discussion

Smart rotor control research has been focussed on load reduction, but in fact additional benefits can be had from adopting such a system. While smart rotor control devices are generally not capable of fully replacing pitch control, as seen by the saturation of the flaps when a low cut-off frequency is selected for the filters, they can help alleviate the pitch demands. This is achieved through filtering the pitch demand such that high frequencies are dealt with by the smart rotor devices while the low frequencies are dealt with by pitching the blades. It is also shown that this may be achieved while also using the smart rotor control for load reduction, suggesting that in the design of smart rotor wind turbines, supplementary control should be considered to reduce pitch actuator requirements.

The consolidated control example supports this proposition by achieving similar load reductions to both standard smart rotor control and individual pitch control while extreme pitch rates and accelerations are reduced by 33% and 75% respectively. This comes at the cost of increased demands on the flap actuator. A trade between pitch actuator demands, flap actuator demands and load reductions is therefore considered appropriate when designing and implementing a smart rotor wind turbine.

References

[1] M. A. Lackner and G. A. M. van Kuik, "A comparison of smart rotor control approaches using trailing edge flaps and individual pitch control," *Wind Energy*, vol. 13, pp. 117–134, Mar. 2010.

[2] W. P. Engels, S. K. Kanev, and T. G. V. Engelen, "Distributed blade control," in *TORQUE: The Science of Making Torque from Wind*, (Heraklion, Crete, Greece), EWEA, 2010.

[3] D. G. Wilson, D. Berg, B. R. Resor, M. F. Barone, and J. Berg, "Combined individual pitch control and active aerodynamic load controller investigation for the 5MW upwind turbine," in *AWEA Wind Power Conference*, (Chicago, Illinois), 2009.

[4] L. C. Henriksen, L. Bergami, and P. B. Andersen, "A model based control methodology combining blade pitch and adaptive trailing edge flaps in a common framework," in *EWEA*, (Vienna, Austria), 2013.

[5] W. W. Jr., M. Snyder, and J. T. Calhoun, "Feasibility Studies of Spoiler and Aileron Control Systems for Large Horizontal-Axis Wind Turbines," *Journal of Energy*, vol. 5, pp. 281–284, Sept. 1981.

[6] P. Jamieson, A. Bowles, A. Derrick, W. E. Leithead, and M. C. M. Rogers, "Innovative concepts for aerodynamic control of wind turbine rotors," *Journal of Wind Engineering and Industrial Aerodynamics*, vol. 39, pp. 395–404, Jan. 1992.

[7] J. G. Stuart, A. D. Wright, and C. P. Butterfield, "Considerations for an integrated wind turbine controls capability at the National Wind Technology Center: An aileron control case study for power regulation and load mitigation," tech. rep., National Renewable Energy Laboratory (NREL), Golden, CO, USA, June 1996.

[8] IEC, "IEC 61400-1 Ed.3: Wind turbines - Part 1: Design requirements," 2005.

[9] J. Berg, M. F. Barone, and N. Yoder, "SMART Wind Turbine Rotor: Data Analysis and Conclusions," tech. rep., Sandia National Laboratories, Albuquerque, New Mexico and Livermore, California, 2014.

[10] W. E. Leithead, S. Dominguez, and C. Eee, "Coordinated Control Design for Wind Turbine Control Systems," in *EWEC*, (Athens, Greece), 2006.

Chapter 10

Faults

A smart rotor wind turbine is able to reduce fatigue loads by deploying active aerodynamic devices along the span of the blades, which can lead to a reduced cost of energy. However, a major drawback is the complexity and potential for unreliability of the system. Faults can cause catastrophic damage and without compensation would require shut down of the turbine, resulting in lost revenue. This chapter looks at a fault tolerant solution to avoid shut down of the turbine and lost revenue during a fault, while keeping additional damage to a minimum.

A worst case scenario of a jammed flap with no direct knowledge of its occurrence is considered, while operating a dq-axis smart rotor wind turbine. A method for detecting the fault using 1P cyclic loadings is presented, as well as a method to correct for the fault by adjusting the remaining active flaps to the same angle as the jammed flap. As the actual angle at which the flap is jammed is unknown, this is done through monitoring and removing the imbalance in the out-of-plane blade root bending moment between all three blades. These scenarios are analysed using IEC standard load cases to assess both loads and the impact on energy capture.

It is found that detection of faults is vital for smart rotor controllers to avoid highly damaging cyclic loads caused by rotor imbalance, but that fault correction is fairly simple to implement and this allows the load benefits of the smart rotor to be accessible even with long fault periods.

10.1 Motivation

For the smart rotor, micro-tabs, jets, vortex generators, plasma fields, active twist, inflatable structures and many other control devices are being considered, along with a variety of sensors and actuators [1]. However, concerns over the implementation of these more novel control devices and the depth of knowledge already associated with trailing edge flaps, have led the two demonstration plants in operation to minimise risk and opt for these traditional control surfaces, which are similar to ailerons on an aircraft wing [2] [3]. Nevertheless, the conditions under which an aircraft and wind turbine operate are quite different. The regular maintenance and no-expense-spared safety requirements of aircraft are quite different to the repetitive continuous operation and cost-effectiveness requirements of devices on wind turbines. Reliability and maintenance are therefore key issues, especially on offshore machines [4] where the smart rotor concept may be most beneficial because the high costs of foundations, cabling, maintenance etc., help weigh optimal size analysis towards larger machines [5].

Fears over the reliability of the devices have not yet been addressed though. Shut down should the smart rotor system fail is undesirable due to lost revenue, and swift corrective maintenance is likely to be costly when considering the conditions offshore [6]. A preferable solution is to continue to operate the wind turbine until maintenance can be conducted, while sustaining power output and not eliminating the benefits of the smart rotor through increased loadings. A fault detection and correction system has been developed that does exactly that.

The state-of-the-art controller has been implemented as explained in Chapter 4 with the dq-axis smart rotor control, Section 4.4.1, with fault cases applied to the system.

10.2 Fault cases

It is judged that two main faults are likely for the trailing edge flap smart rotor: 1) a broken linkage and, 2) a jammed flap. The case where a broken linkage occurs and so the flap is 'free' is liable to induce flutter, with no mechanism to stop this happening catastrophic failure may result. The chance of this fault case occurring therefore needs to be negligible. The second scenario, of a jammed flap, is therefore considered in this chapter.

If a flap gets jammed cyclic loadings result due to an aerodynamic imbalance, caused by the one blade experiencing different aerodynamic forces than the other two. This can be exacerbated if the controller fails to recognise that a fault has occurred and continues to operate the dq-axis smart rotor control. This may be due to a disconnection between the flap and actuator, such that feedback sensor measurements are assumed correct, but the flap is jammed. This can be considered a worst case scenario.

As an example, a +5 degree flap angle is applied to one of the three flaps, while the other two are allowed to operate as normal. To see what affect this has, cumulative spectrums for the case where a) the smart rotor system is inactive (CPC), b) the smart rotor system is active and working correctly (SRC), c) the smart rotor is active but a jam has occurred (SRC fault), and d) smart rotor fault ride-through is active with a jam having occurred (SRC corrected); are shown in Figure 10.1.

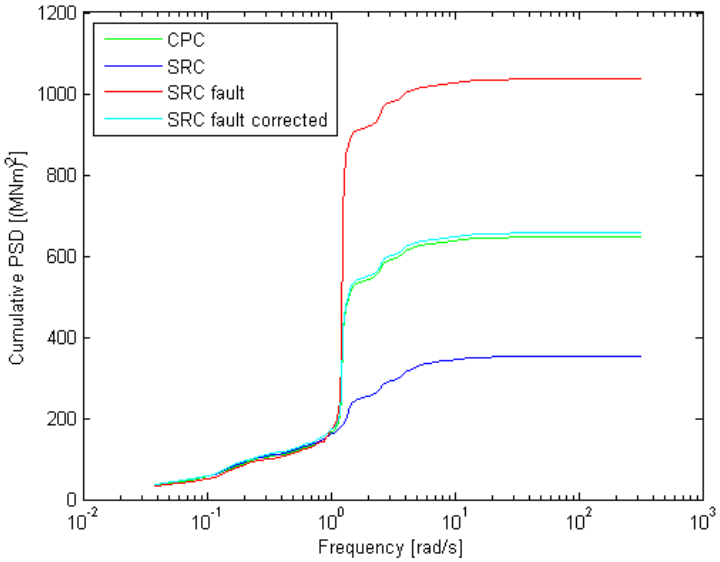

Figure 10.1: Cumulative Power Spectral Density (PSD) of the blade root out-of-plane bending moment for states a) to d). The corrected case is very similar to the collective pitch control case

The 1P peak is particularly significant when one flap is jammed while the other two still operate to the dq-axis regime. This 1P loading is due to the controller continuing to activate the other two flaps causing a significant aerodynamic imbalance. This can drastically reduce the lifetime of the turbine, as examined in Section 10.5, and highlights the importance of detection and a fault correction system.

10.3 Detection of faults

Detection of a fault is possible through a number of methods: direct feedback from sensors measuring the angle of the flap, measurement of the hinge moment of the flap, or indirect measurements of the blade root bending moment, tower motion or high speed shaft, as revealed in Figure 10.2. A rapid automatic response is required not just to reduce loads, but also to identify the fault mode and avoid automatic shutdown due to excessive vibrations.

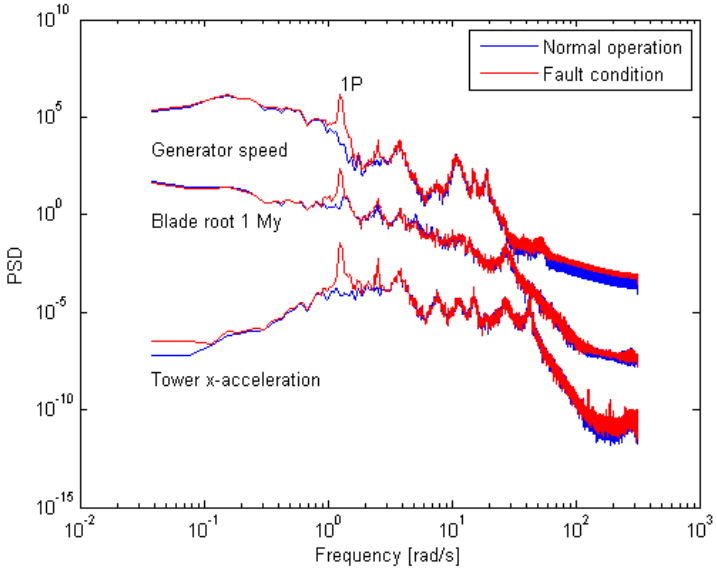

Figure 10.2: Power spectral density plots highlighting the 1P vibrations

Direct sensor measurement is a trivial case, and results in near instantaneous detection with knowledge of which and to what degree the flap is jammed. This enables rapid and accurate adjustment of the remaining flaps to mitigate the fault, with the fault correction system described in the next section.

Indirect measurements are somewhat more complex to use. The method considered here is monitoring the average power in the signal around 1P with a trigger to activate fault correction system should it exceed a given threshold. A band-pass filter is used to filter out the 1P signal and the power in this signal over a defined window is calculated. This condition monitoring system is shown in Figure 10.3, where N is the size of the window and in this case 2.6 units is the threshold limit. Z^{-k} represents a discrete signal delay of k samples.

The threshold needs to be set so as false positives do not shutdown the system and remove the benefit of the smart rotor control, while still being sensitive enough to detect faults. As the wind speed increases, the power in the spectrum naturally increases, this can be seen in Figure 10.4 when looking at tower accelerations. To combat this a normalisation procedure is adopted such that during normal operation the chance of the fault correction system being triggered is 1-in-50-years, displayed in Figure 10.5 for the normalised results.

This is handled by adjusting the output based on the wind speed. The advantage of adjusting the signal rather than the threshold is that it is easier for a human to identify when a fault occurs and simpler to determine the frequency of exceedence across a wide range of wind speeds.

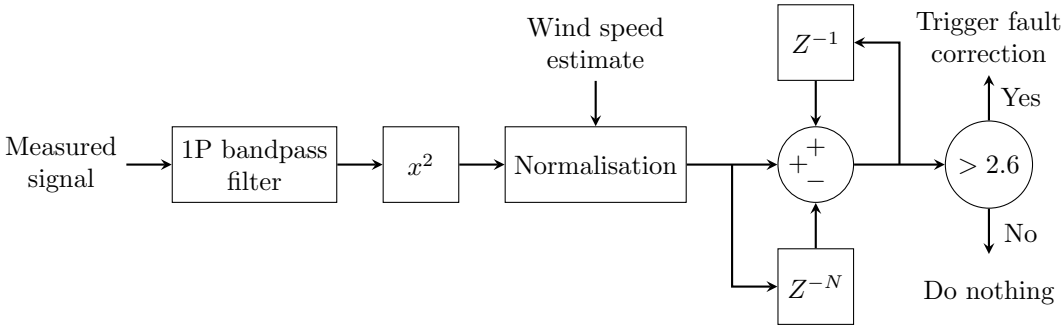

Figure 10.3: Condition monitoring system

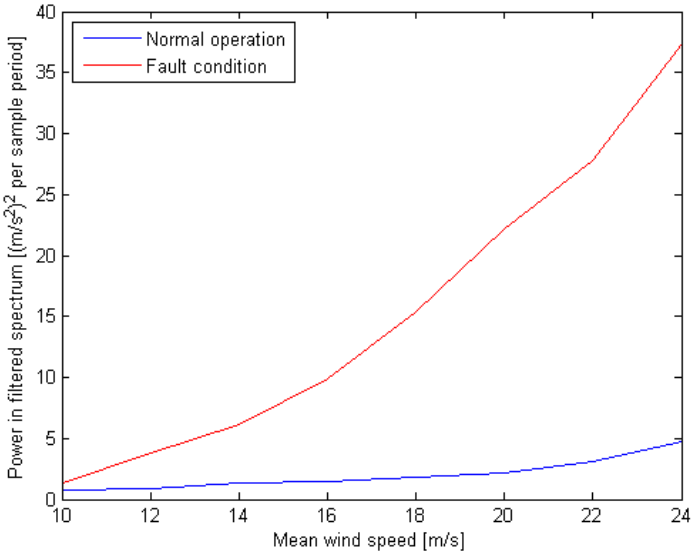

Figure 10.4: Maximum power observed in simulations across all wind speeds

The adjustment to the signal is based on the maximum observed detection signal, exhibited in Figure 10.4, for normal smart rotor control operation. A quadratic curve is fitted to this data for normalisation. The equation for this, where the signal is x, output, y, and wind speed, V, is

$$y = \frac{1.0x}{0.024V^2 - 0.57V + 4.2} \tag{10.1}$$

The result of this normalisation procedure is shown in Figure 10.6, with the maximum observed values in normal operation approximately equal to 1 across all wind speeds. The wind speed input to the normalisation procedure may be as coarse as the 10 minute mean wind speed or a more active wind speed estimation may be used. If, for example, a wind speed estimation procedure is employed (e.g. [7]), this may lead to better responsiveness as a lower threshold can be used without increasing the number of false positives.

At lower wind speeds it is observed that the fault would not always be detected with the threshold set at 2.6. This is due to the smart rotor control phasing in and out due to the operation switching between above and below rated. It is also suggestive that at higher wind speeds, detection

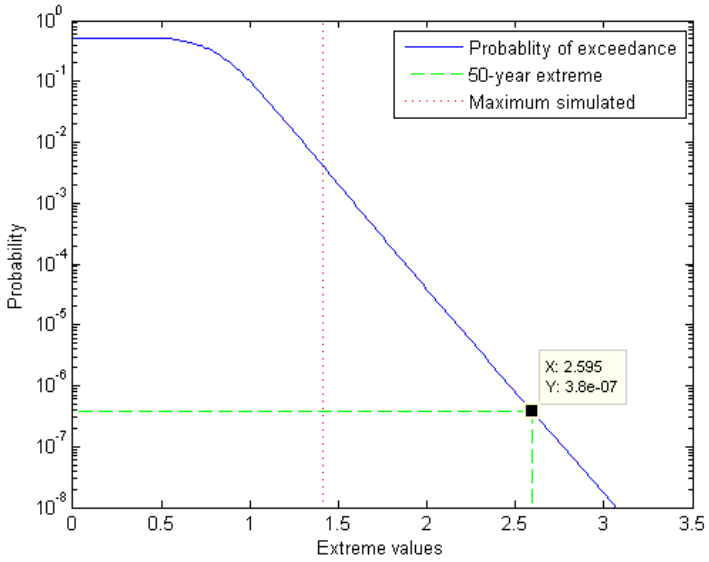

Figure 10.5: Probability of exceeding a given threshold value

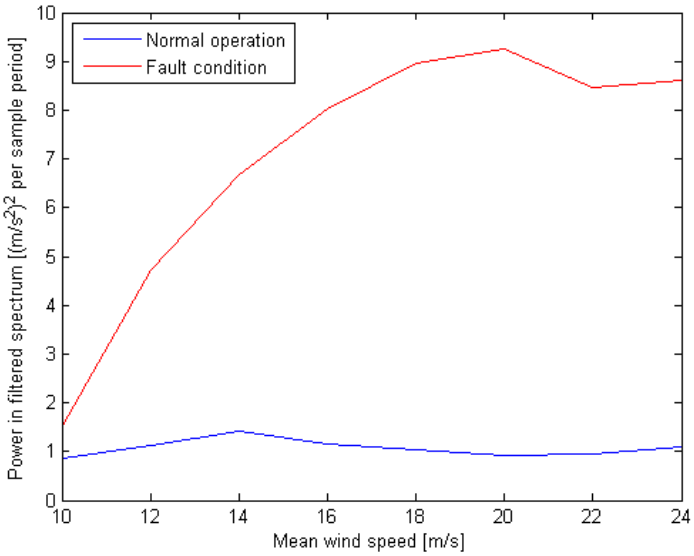

Figure 10.6: Power spectral density plots highlighting the 1P vibrations

may be quicker as the threshold is likely to be exceeded more rapidly. Table 10.1 looks at this in closer detail, with results from simulations using the detection system described, while monitoring the tower accelerations.

Table 10.1: Average time before a fault is detected at various wind speeds

Mean wind speed	Time before detection	
[m/s]	Mean [s]	Maximum [s]
10	-	-
12	255	459
14	120	305
16	79	196
18	91	196
20	87	183
22	89	181
24	90	181

As can be seen at 10 m/s mean wind speed the jammed flap is not detected at all. However, it should be noted that the the turbine only operated in the above rated region, where the smart rotor control is active, for 22% of the time, with the longest duration being 57s for an hours worth of simulation time. During this period 1P oscillations do not build up to a significant level and indeed the damage caused is therefore low. Faster detection does occur as the wind speed increases, as expected, and this is fortunate as damage accrues quicker at higher wind speeds, seen in Section 10.5.

Three examples of the detection system working are shown for wind speeds 10m/s, 16m/s and 24m/s with the fault occurring at zero seconds after an initial unrecorded minute of normal operation. As can be seen in Figure 10.7 the tower accelerations during the fault increase, but the detection system identifies the fault prior to excessive excitation thanks to the identification of 1P vibrations.

The condition monitoring system is flexible and through adjustment of the gains and threshold limits alternative sensors may be used as required for convenience. In particular measurement of the blade root bending moment, that is often for dq-axis controlled wind turbines, is an obvious choice.

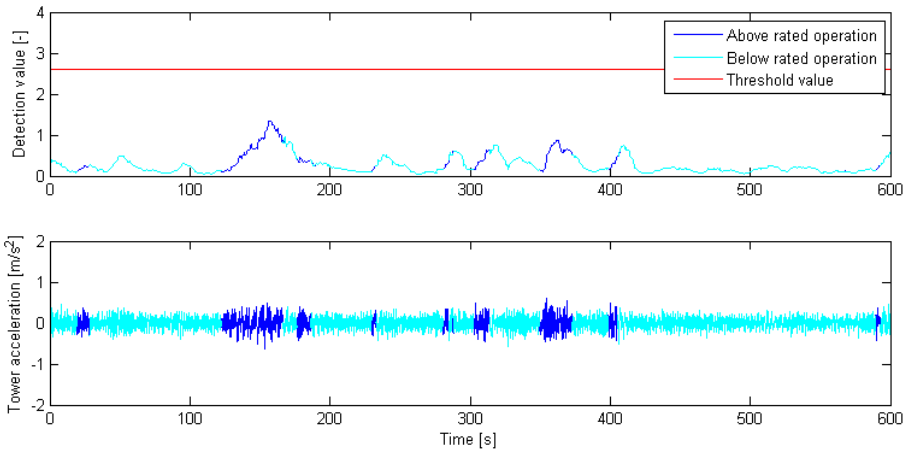

(a) 10 m/s mean wind speed

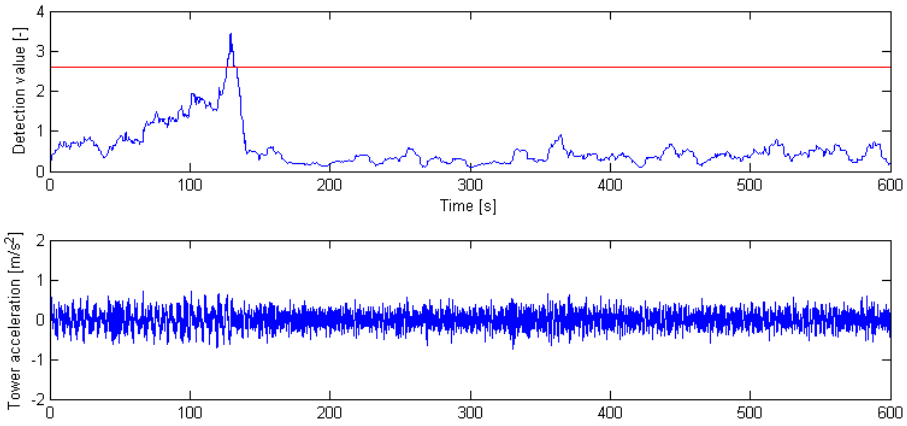

(b) 16 m/s mean wind speed

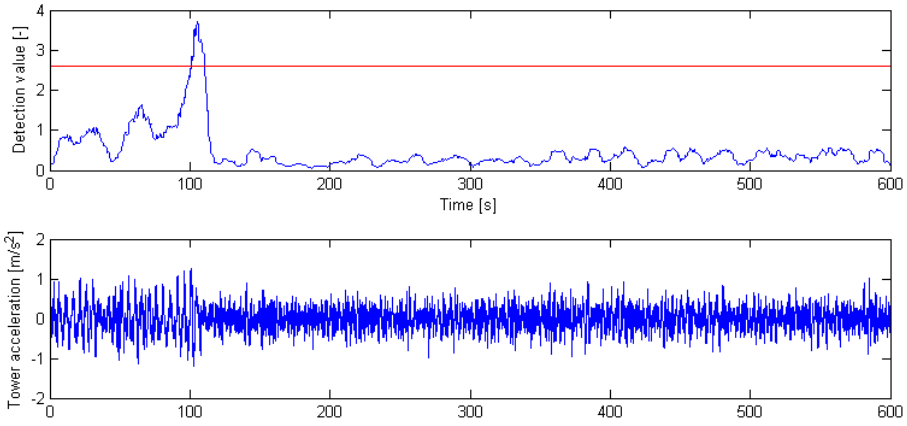

(c) 24 m/s mean wind speed

Figure 10.7: Tower accelerations and the fault detection signal. The fault occurs at zero seconds, and when the detection signal exceeds the threshold, the correction system activates

10.4 Fault correction

The fault correction system developed removes the cyclic loadings by adjusting the other two flaps to balance the third in a simple and effective way: the operational flaps are set to the angle of the jammed flap. If this is not possible to determine directly, the active flap angles are set to zero before slowly adjusting them to achieve the same mean blade root bending moment across all three blades. This effectively leads to all flaps having the same fixed flap angle.

The method for adjusting the flaps to achieve the same flap angle as the jammed flap, should the angle not be directly known, is shown in Figure 10.8. Filters are used to reject 1P and 3P signals whilst a PI controller is used to adjust the blade root bending moment of the individual blade to that of the mean collective blade root bending moment. A gain schedule is used to encourage motion while the deviation from the collective mean is large and reduce motion when it is close to the mean to reject disturbances.

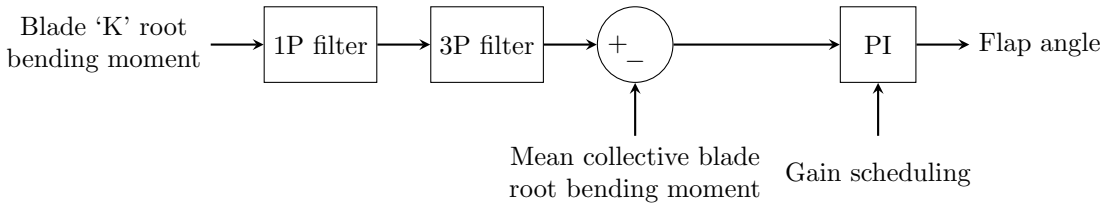

Figure 10.8: Fault ride through control system

As before the 16m/s and 24m/s wind speeds are looked at in detail to view this process, looking at the flap angles, Figure 10.9. While the flap angles for the working flaps vary about the angle of the jammed flap, these oscillations are small, and due to the control strategy adopted avoid any rotor imbalance.

This fault correction strategy described does result in a system with increased loads compared to the case where the flaps are working, however the improvement over the non-adjusted case is considerable. The loads are in effect reduced to those of the collective pitch control case, with an impact on the energy capture dependent on the severity of the jammed flap. These aspects are looked at in the following two sections.

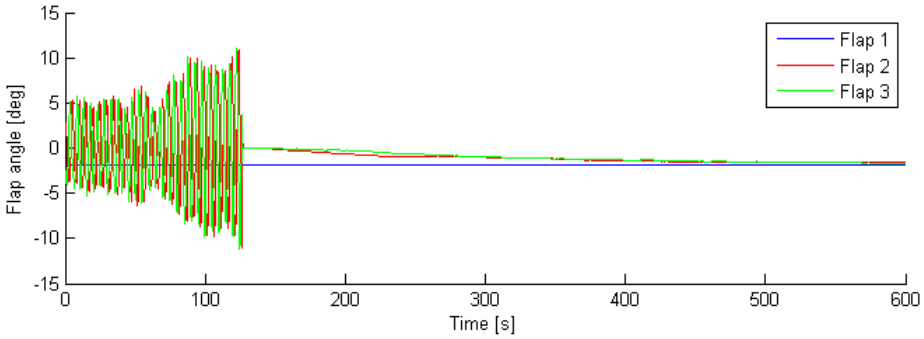

(a) 16 m/s mean wind speed

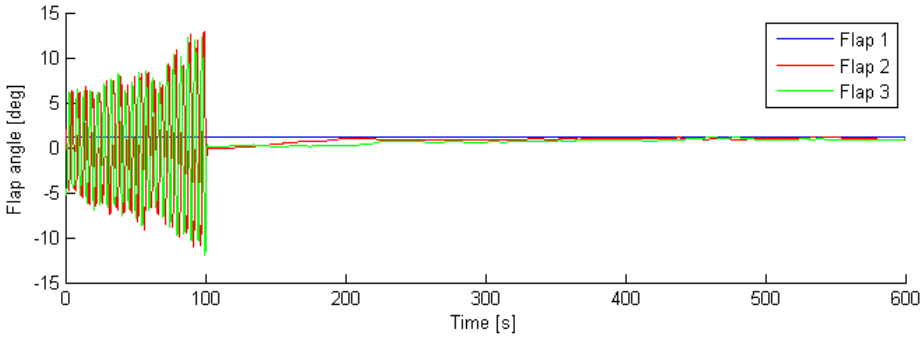

(b) 24 m/s mean wind speed

Figure 10.9: Flap angles following a fault for two different wind speeds

10.5 Loads

Calculated from IEC standard power production runs for a Class IB wind turbine, the lifetime 1 Hz blade root out-of-plane damage equivalent loads for a turbine, with an uncorrected for flap jammed at 5 degrees, are 28% greater than those had the turbine been simply operating a normal collective pitch control strategy. When these fault loads are compared to the loads when the smart rotor control is working correctly, they are 50% higher. In certain high wind speed conditions, under which a fault is perhaps more likely to occur, these figures are even worse. For example at a 22m/s mean wind speed these values are increased to 40% and 80% respectively, as shown in Figure 10.10.

This results in damage accumulating considerably faster than under normal operation and indeed if a turbine was to operate under this condition for more than 7% of the time, a collective pitch control would result in lower loads than a smart rotor control, Figure 10.11.

The loads on the tower can be even worse, as seen in Figure 10.12, with a fault condition contributing the same amount of damage in 10 days as the tower would normally experience in a year. This highlights the requirement to recognise when a fault has occurred and act quickly. Without any fault detection and correction system catastrophic failure may result requiring the turbine to be shut down, which will result in lost revenue. The detection system developed recognises faults within minutes, so the fault condition will be in operation for a very short amount of time, making damage due to a fault negligible.

Naturally though, the longer the fault duration, with the flaps held in position rather than operating as per the smart rotor control strategy, the lower the benefit the smart rotor control has

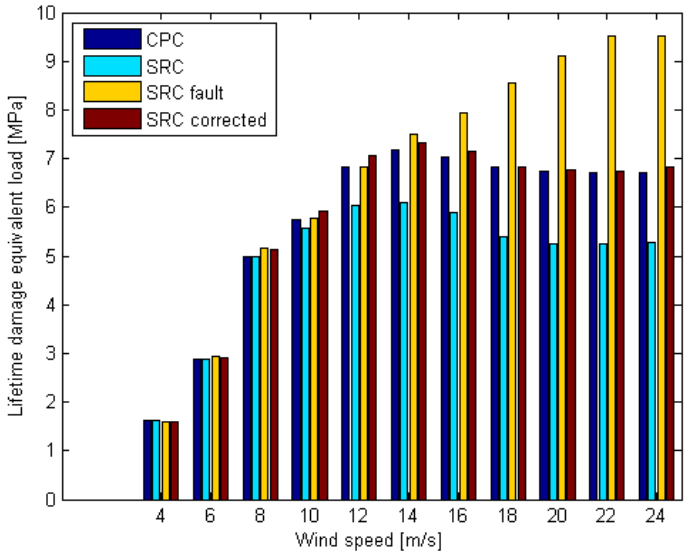

Figure 10.10: Blade root out-of-plane bending moment 1Hz lifetime damage equivalent loads for the different operational states

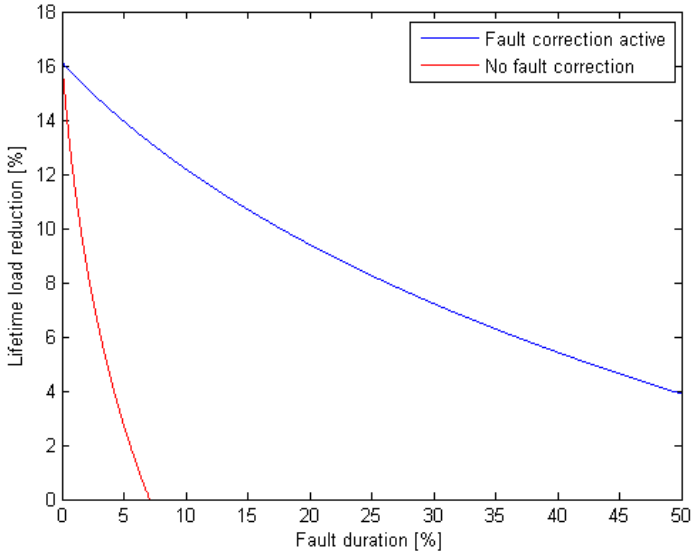

Figure 10.11: Lifetime load reduction in the out-of-plane blade root bending moment due to a fault with and without fault detection and correction

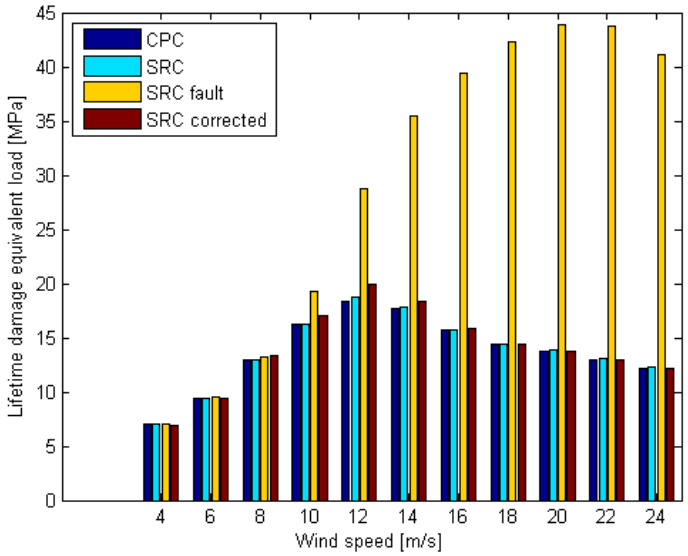

Figure 10.12: Blade root out-of-plane bending moment 1Hz lifetime damage equivalent loads for various fixed flap angles in degrees

for fatigue load reduction. However, a certain load reduction is still sustained even if corrective maintenance takes weeks before the weather conditions are practicable for offshore maintenance. A fault that is present for as much as 25% of the time still allows a load reduction of 8% over the collective pitch control case, also portrayed in Figure 10.11. This is half the potential of the smart rotor control.

This result is similar for all blades, with varying loads depending on the angle at which the flaps get jammed, see Figure 10.13. Indeed the lifetime damage equivalent loads of flaps set at negative 20 degrees can in fact result in a 10% load reductions compared to the collective pitch controlled case. Again, similar results are found for the tower, Figure 10.14. However, the non-zero flap angles have an adverse effect on the annual energy capture of the wind turbine.

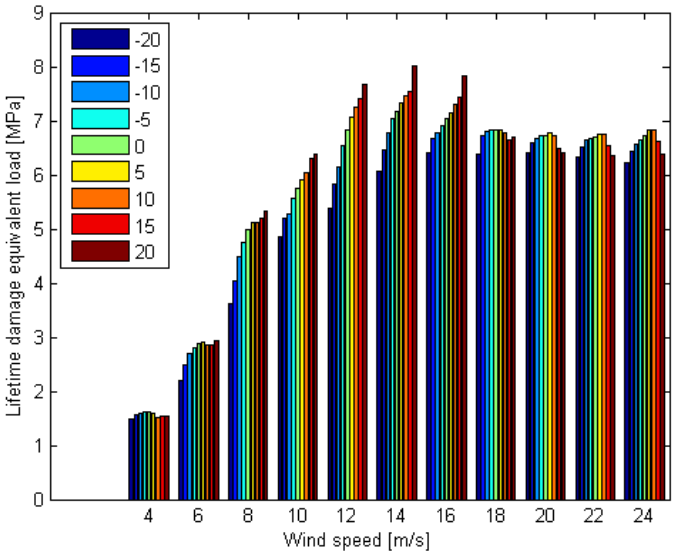

Figure 10.13: Blade root out-of-plane bending moment 1Hz lifetime damage equivalent loads for various fixed flap angles in degrees

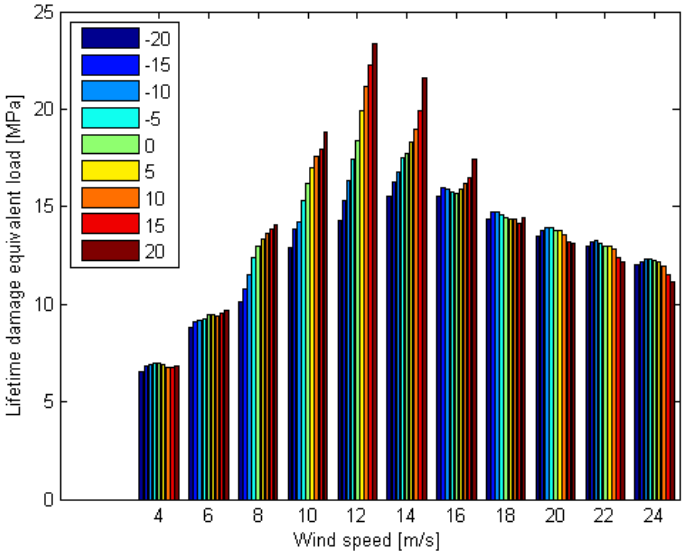

Figure 10.14: Tower fore-aft moment 1Hz lifetime damage equivalent loads for various fixed flap angles

10.6 Energy Capture

The annual capacity factors are shown in Figure 10.15 for each of the IEC wind distribution classes. The high values particularly of the Class I wind distribution case are a result of assumed 100% availability and transmission losses not being included, but are indeed comparable to some operating offshore wind farms [8].

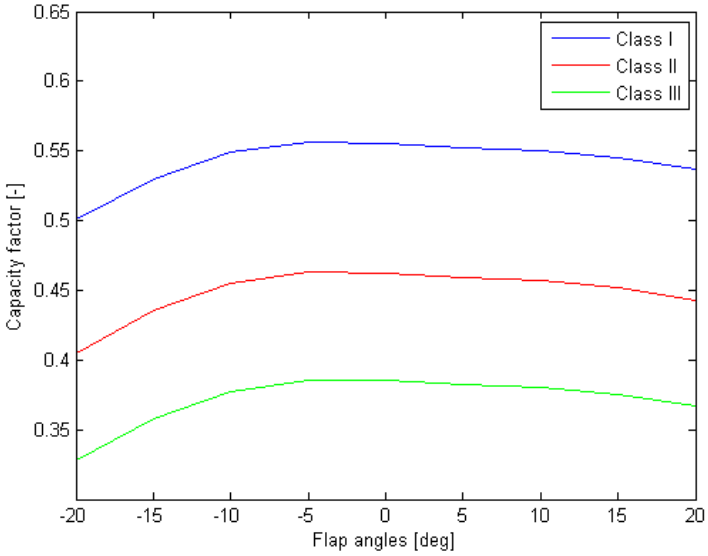

Figure 10.15: Capacity factor of the wind turbine with various fixed flap angles at sites with different mean wind speeds, IEC wind turbine classes I,II and III

The actual energy loss due to the flaps being fixed at a non-zero angle can be as high as 15% for a wind turbine with the flaps set at negative 20 degrees, as displayed in Table 10.2. The maximum losses when considering the Class I case are lower though, at close to 10%. The reason for this is that after activation of the fault correction system, above rated power capture is maintained. This is due to the pitch automatically adjusting the collective pitch angle to achieve the correct torque. Below rated though there is a loss in energy capture which is dependent on the set angle of the flaps. Looking at the 10-minute mean wind speed power curve for the negative 20 degree flap deployment the loss in energy below rated can be seen, alongside an increase in the wind speed at which rated power is reached, Figure 10.16. On the other hand, between negative 5 and zero degrees, the losses are negligible, and the operation is very similar to the zero flap angle case.

Intriguingly at low wind speeds in the region where the rotor speed is fixed, resulting in a high tip speed ratio, the loss due to the negative 20 degree fault case is even higher than on average, whilst a moderate positive flap angle can in fact improve energy capture. This goes against what might be expected when looking at the Cp-λ curves, Figure 10.17, and has at its root the dynamic change in lift coefficient due to the incoming turbulent wind field. It is possible then in this region to improve energy capture through deployment of the flaps, however exploring this issue is beyond the scope of this thesis.

The Cp-λ curve also highlights where performance is lost, with a reduction in the maximum power coefficient at the previously optimum tip speed ratio of 24%. This can be improved slightly

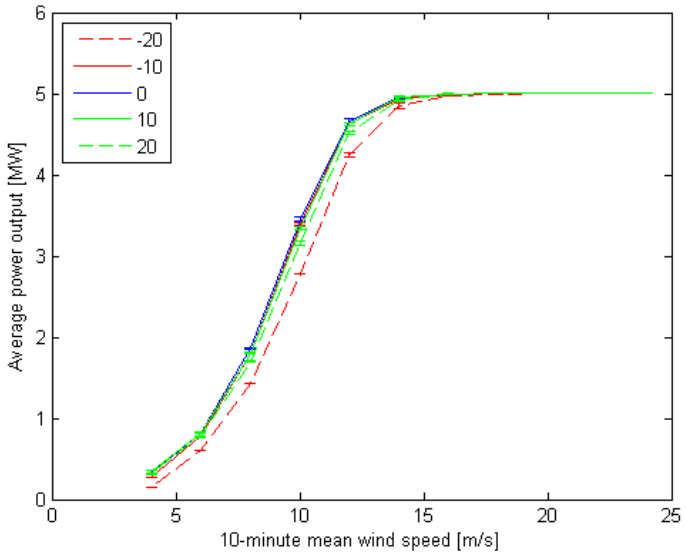

Figure 10.16: 10-minute mean wind speed power curves for various fixed flap angles

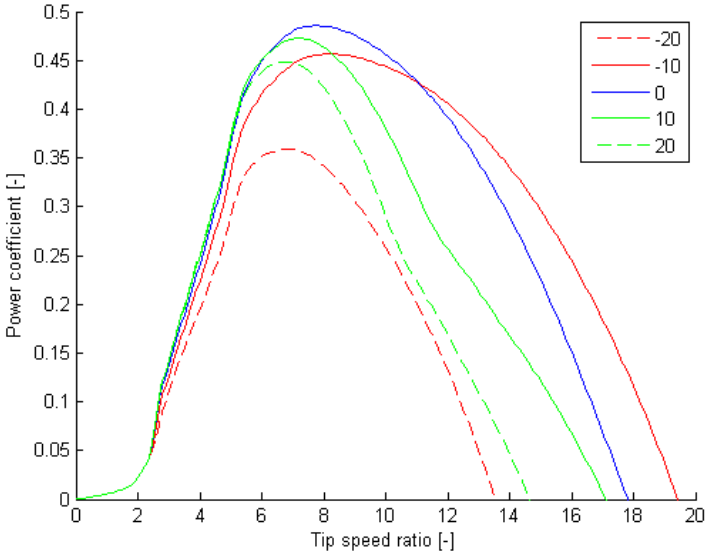

Figure 10.17: Power coefficient as a function of tip speed ratio for various fixed flap angles (Cp-λ curves)

Table 10.2: Annual energy capture compared to collective pitch controlled case (0 degree flap angle), at sites with different mean wind speeds

Fixed flap angle	Energy capture [%]		
[deg]	Class I	Class II	Class III
-20	90.1	87.4	84.9
-15	95.4	94.1	92.8
-10	98.8	98.4	98.0
-5	100.0	100.0	100.0
0	100.0	100.0	100.0
5	99.5	99.3	99.2
10	99.0	98.8	98.6
15	98.1	97.7	97.3
20	96.6	95.8	95.1

by changing the controller so that the new optimum tip speed ratio is tracked, but the improvement is small, such that during optimum tracking mode there is still a 22% reduction in power output. The longer the turbine is operating in this condition, the greater the power lost due to the jammed flap, but this is still much better than a reduction to zero output from shutting down the wind turbine that would be required had a fault correction strategy not been adopted.

10.7 Discussion

The smart rotor has the ability to reduce loads on wind turbines, which is likely to be particularly important for the next generation of multi-MW offshore machines with large swept areas. However, one of the key concerns associated with the smart rotor concept is the reliability and maintenance of the system, which could lead to increased costs or lost revenue. Indeed, it is shown in this work that if a fault occurs and the wind turbine is allowed to continue to operate without correction, the load reduction benefits are quickly eroded, ultimately requiring the wind turbine to be shut down. In an offshore environment, where corrective maintenance will take time due to distance, equipment and weather conditions, this is a serious problem, and could result in significant lost revenue. Fortunately, a solution has been found which is both simple and effective.

A fault detection and correction system has been implemented that responds rapidly to faults and allows operation of the wind turbine to continue with loads that are substantially less than that of the fault case. Operation under a fault condition has been shown to be viable even for extended periods of time, while still allowing load reductions due to the smart rotor system to be realisable. This conserves the benefits of the smart rotor, while the reliability and maintenance requirements are made not to be too arduous, as load reductions and close to optimum power output may still be achieved even in cases where a flap jams. This helps facilitate the deployment of the smart rotor on commercial wind turbines by recognising and eliminating one of the barriers.

Reliability and maintenance requirements for the smart rotor are much more lenient than one might expect, and the fears that faults could hinder deployment of the smart rotor are not wholly substantiated.

References

[1] T. K. Barlas and G. A. M. van Kuik, "Review of state of the art in smart rotor control research for wind turbines," *Progress in Aerospace Sciences*, vol. 46, pp. 1–27, Jan. 2010.

[2] J. Berg, B. R. Resor, J. Paquette, and J. White, "SMART Wind Turbine Rotor: Design and Field Test," tech. rep., Sandia National Laboratories, Albuquerque, New Mexico and Livermore, California, 2014.

[3] D. Castaignet, T. K. Barlas, T. Buhl, N. K. Poulsen, J. J. Wedel-Heinen, N. A. Olesen, C. Bak, and T. Kim, "Full-scale test of trailing edge flaps on a Vestas V27 wind turbine: active load reduction and system identification," *Wind Energy*, vol. 17, pp. 549–564, Apr. 2014.

[4] G. J. W. V. Bussel, "Offshore wind energy, the reliability dilemma," in *1st World Wind Energy Conference*, no. 31, (Berlin, Germany), 2002.

[5] P. Jamieson, *Innovation in Wind Turbine Design*. Wiley, 2011.

[6] J. Dowell, A. Zitrou, L. Walls, T. Bedford, and D. Infield, "Analysis of Wind and Wave Data to Assess Maintenance Access to Offshore Wind Farms," in *European Safety and Reliability Association Conference*, (Amsterdam, Netherlands), 2013.

[7] K. Z. Ostergaard, P. Brath, and J. Stoustrup, "Estimation of effective wind speed," *Journal of Physics: Conference Series*, vol. 75, July 2007.

[8] Energistyrelsen, "Register of wind turbines," tech. rep., ENS, Copenhagen, 2014.

Chapter 11

Conclusion

This chapter brings together the conclusions from this thesis and proposes some future areas that may be explored building upon this foundation. A brief summary of the thesis is given in Section 11.1 and this is followed by Section 11.2 describing the deductions, implications and limitations of the various aspects of this thesis. Finally, a number of future directions are proposed in Section 11.3.

11.1 Summary

The increase in the use of wind energy and the desire to bring down the cost of energy from it have led to some innovative concepts being considered. The smart rotor is one such concept that has been shown to reduce loads on the wind turbine, which ultimately could lead to a reduction in the cost of energy. This thesis contributes to a number of areas involving smart rotor research:

- The understanding of the influence wind fields can have on load reduction results, Chapter 6
- The selection of trailing edge flaps based on actuator requirements in consideration with the chord width of the flaps, Chapter 7
- The potential of smart rotor control in direct comparison with individual pitch control, Chapter 8
- Demonstration of the potential to reduce pitch actuator requirements by supplementing the collective pitch control with smart rotor control, Chapter 9.
- Detection and mitigation of faults on the smart rotor, Chapter 10

These areas are analysed in a rigorous methodical manner to provide the ability for others to repeat this work, build upon it and make accurate comparisons with it: the baseline wind turbine is described in detail in Chapter 4, with the methods to make quantitative comparisons discussed in Chapter 5. The deductions and implications from these studies are described in the following section.

11.2 Deductions, implications and limitations

11.2.1 Wind field synthesis and performance

It is found that the nature of the conditions under which smart rotor control, and indeed individual pitch control, are operated can have a significant effect on the load reductions observed. For a turbine operating in high wind shear environments, or equivalently in yawed flow, the cyclic loadings are high, as too are the rotor imbalances. As the smart rotor and individual pitch control are effective at removing these imbalances, significant load reductions with these wind field conditions may be achieved.

Conversely, in high turbulence wind fields, increased loading is a result of stochastic disturbances with only large scale structures resulting in cyclic loadings that the advanced load reduction controllers examined are able to target effectively. This has two fundamental implications.

The first is in the realm of academia. When conducting research into control strategies, results should be shown for a common wind field, preferably taken from the IEC standard, to conduct fair comparisons of different controllers. The reason for this is that the results can easily be biased to suggest superiority. For example a smart rotor turbine simulated with high wind shear and low turbulence will achieve significantly larger load reductions than one simulated with a low wind shear and high turbulence. This is also why a standard baseline wind turbine and state-of-the-art controller are required, as alternatives will also alter the significance of conclusions that may be made.

The second implication regards the implementation of these advanced load reduction controllers in reality. It would appear that for greatest benefit these advanced controllers should be implemented in locations where high wind shear is expected. In these cases the maximum load reductions and so potential cost reductions can be achieved. An example of this is to mitigate the effect of low level jets using individual pitch control [1].

The study in this thesis however is limited in scope. In particular the number of different shear exponents and turbulence intensities mean a trend can not be accurately determined. It should also be pointed out only normal turbulence wind field models are used. This means extreme loads are not fully taken account of as certain loads are dependent on transient events or even fault conditions. The nature of these results however still rings true, especially as regards to future studies which, should they wish to take account of these transients, should also use examples defined in the IEC standard to facilitate comparisons.

The other criteria of the wind field that has been considered is the grid resolution. It is found that time resolution sampling of the wind field converges linearly to a point, with periods of even a few seconds diverging from the highest resolution results by less than the standard deviation due to the stochastic nature of the wind fields being simulated. The spatial resolution of the wind field grid is also considered with grid spacings of under 5m, as suggested by the GL standard, being more than suitable for this wind turbine. This is tested using the Kaimal wind field model, with parameters of the Mann wind field model also being checked. The potential differences between the two wind field models is of some concern, but mainly in the actual certification of wind turbines. The reason being that the true nature of the wind may not be accurately defined by either of these models and so could promote loads that are not predicted by the simulations conducted.

11.2.2 Trailing edge flaps

The torque and power requirements of trailing edge flap actuators are shown to be low and this is highly desirable, as if the actuator is to be integrated into the blade the space available will be constrained and lower torque and power requirements will allow a smaller actuator to be used. The actuator demands of trailing edge flaps are also shown to be dependent on the chord width of the flaps. The longer the chord width, the lower the deflection, rates and accelerations required, but the higher the torques needed.

Proportionally the torque increases more rapidly with increased chord than the reduction in actuator motion, meaning larger flaps consume more power. This means flaps with shorter chord widths would be preferable, but there is also a downside to them. With smaller chord width flaps the deflections required for the same change in lift are increased. This can lead to flow separation, which reduces aerodynamic efficiency and can lead to increased noise. This study aids in the selection of trailing edge flaps, complementing work previously done on their location [2] and design [3].

A major drawback with this study though is that friction has not been taken into account. An accurate friction model may find this alters the results significantly. Naively perhaps, the addition of friction is expected to bias towards larger flaps, assuming a constant friction coefficient, as the smaller flaps undergo more travel, however, uneven loads on the bearings may result in something quite different due to deformation of the blades and flaps.

This work also informs the selection of flaps used in the thesis, which have the same percentage chord and span as the Sandia smart rotor demonstration plant. This is a trade-off between the actuator motion and torques, with the additional benefit that comparisons can then be made directly with the demonstration plant and knowledge that this design is feasible.

11.2.3 Individual pitch and smart rotor control

The smart rotor is shown to be capable of similar load reductions as individual pitch control. By running simulations where this is the case, a direct comparison between the two regarding other aspects of the wind turbine is possible. For individual pitch control, the load reductions come at the cost of increased actuator duty and power requirements. This will also affect the pitch bearing requirements. These costs need to be less than the savings achieved due to the reduced loads offered by the individual pitch control, and for the trailing edge flap smart rotor the cost of implementing the system needs to be less than the savings achieved by the reduced loads. Trailing edge flaps also have the ability to reduce pitch actuator requirements too, so this may also count towards cost savings. No actual cost analysis is conducted, but the results may be used to inform a cost analysis.

An additional drawback with this work is that while two different controllers have been tested, a more through investigation into the trade-off between load reductions and actuator requirements is not conducted. This could see limits reached beyond which either of the controllers is able to respond and so divergence suggesting one or other system is preferable.

11.2.4 Supplementary control

Following on from the comparison between individual pitch and smart rotor control, the question of using smart rotor control to conduct other control functions is considered. Previous work has demonstrated the ability of the smart rotor to supplement pitch control as an addition to individual

pitch control [4] [5]. In this work it is demonstrated that trailing edge flaps may supplement the main pitch controller and in so doing reduce the pitch actuator requirements. A similar conclusion to [6].

The sensitivity analyses based on the cut-off frequency of the filter splitting pitch and flap demands suggests a balance between pitch actuator reductions and the risk of saturating the flap deflections. The smart rotor is also shown capable of more than one function, as demonstrated by aiding in rotor speed control, while also reducing loads on the wind turbine. Again though there is a trade to be had between load reduction, supplementary control for the pitch actuator and flap actuator requirements.

The ability of the smart rotor to reduce pitch actuator requirements implies that when designing smart rotor wind turbines supplementary control is an aspect that should be considered.

11.2.5 Faults

It is shown that if a fault occurs in the smart rotor system and the wind turbine is allowed to continue to operate without correction, the load reduction benefits are quickly eroded, ultimately requiring the wind turbine to be shut down. A fault detection and correction system is demonstrated in this thesis that responds rapidly to faults and allows operation of the wind turbine to continue with loads that are substantially less than that of the fault case.

When the fault correction system is used, operation can be extended for long periods of time, while still allowing load reductions due to the smart rotor system to be realisable. This conserves some of the benefits of the smart rotor, while the reliability and maintenance requirements are eased.

This has significant implications for the deployment of the smart rotor on wind turbines. Without recognising or considering faults, catastrophic damage could occur. Equally, without a fault correction system, shutting down the turbine will result in significant lost revenue. This is true particularly offshore, where maintenance is more difficult and takes longer. The system implemented effectively solves these two problems and as such this is an important contribution to the acceptance of the smart rotor for adoption by industry.

11.3 Future work

Finally, from this work a number of future directions are proposed:

- Conduct a comprehensive analysis of loads, particularly extreme loads, using the IEC standard cases to further research the ability of both individual pitch and smart rotor control. This could also include tests of fault conditions including of the trailing edge flap
- Re-run simulations with other aerodynamic flow control devices to validate the claim that the results will stand for any change in lift coefficient device
- Extend supplementary control such that rather than targeting certain aspects it comprehensively covers all pitch actions, so that the pitch actuator benefits fully and there is no requirement to extensively retune and redesign controllers, e.g. simply splitting the pitch demand between the smart rotor and pitch actuators based on frequency
- Create a flap actuator model that includes friction
- Conduct a cost analysis to quantify the benefits of individual pitch and smart rotor control systems
- Adapt the work to use open source software to ease in comparisons and to facilitate continuation of this work by any individual without the need for licensed software. This would also allow adaptation of the modelling code to cope with the specific aerodynamics of the aerodynamic flow control devices implemented
- Test different control strategies including control of smart rotor wind turbines with multiple flaps per blade, e.g. as per the Sandia demonstration plant
- Validate the model and results against field data

References

[1] D. Robb, C. Gonzalez, P. Clive, W. E. Leithead, and A. Giles, "Offshore Low Level Jets - Mitigating the Damage with Lidar and Individual Blade Control," in *EWEA Offshore*, (Messe Frankfurt, Germany), 2013.

[2] P. B. Andersen, L. C. Henriksen, M. Gaunaa, C. Bak, and T. Buhl, "Deformable trailing edge flaps for modern megawatt wind turbine controllers using strain gauge sensors," *Wind Energy*, vol. 13, pp. 193–206, Mar. 2010.

[3] N. Troldborg, "Computational study of the Risø-B1-18 airfoil with a hinged flap providing variable trailing edge geometry," *Wind Engineering*, vol. 29, no. 2, pp. 89–114, 2005.

[4] D. G. Wilson, D. Berg, B. R. Resor, M. F. Barone, and J. Berg, "Combined individual pitch control and active aerodynamic load controller investigation for the 5MW upwind turbine," in *AWEA Wind Power Conference*, (Chicago, Illinois), 2009.

[5] M. A. Lackner and G. A. M. van Kuik, "A comparison of smart rotor control approaches using trailing edge flaps and individual pitch control," *Wind Energy*, vol. 13, pp. 117–134, Mar. 2010.

[6] L. C. Henriksen, L. Bergami, and P. B. Andersen, "A model based control methodology combining blade pitch and adaptive trailing edge flaps in a common framework," in *EWEA*, (Vienna, Austria), 2013.

Appendices description

In the following appendices the computer files created for this thesis are made available. Where propriety software is used (i.e. Bladed), an attempt is made to supply the raw data and reports as well as the project file. This is done in the interest of openness, to facilitate future work, and for the merely curious. A brief description of the files is also supplied. Visual Studio for the C++ code compilation is available to download for free online, as too is Octave, an open source alternative to MATLAB.

The files are embedded in the pdf version of this thesis, which is available from the University of Strathclyde, for easy and complete access. To download the files, where a pin is seen in the following pages, right click on it and select, 'Save Embedded File to Disk...' A number of the files have been zipped together using 7-Zip, so that upon extraction they work together.

Appendix A

Wind turbine model parameters

In this appendix files relating to the wind turbine model are supplied.

The Bladed version 4.5 project file contains all the information regarding the wind turbine model, including the structure of the turbine, aerodynamics of the blade sections and actuator information. Using this model a Bladed simulation of the smart rotor wind turbine presented in this report can be run. Additionally, a controller dll should be selected as the external controller file, as the path will be otherwise incorrect, and a 3D turbulent wind field file should also be selected for use.

The wind turbine model parameters are also attached in this appendix, because Bladed is proprietary software and so access to it is by no means guaranteed. This is done as an export report from Bladed, and includes all the characteristics of the wind turbine. It has been split in two, one pertaining to the general parameters, and the second to the aerodynamic characteristics of the blade sections, excluding those with flaps. This exclusion is done due to the large number of coefficients required for the flaps at various angles, and instead the method for attaining them is provided in Appendix B.

Wind turbine Bladed model 

Wind turbine model parameters 

Aerodynamic coefficients 

Appendix B

Flap aerodynamic characteristics from XFOIL

This appendix contains the process of obtaining the aerodynamic data for the blade sections with flaps.

Where the flaps are present on the blades the NACA 64618 aerofoil profile is used, the coordinates of which are included here. This profile is input into XFOIL using MATLAB through running a script that interfaces between XFOIL and MATLAB and then writes the output polars to Excel files. This aerodynamic data is then extracted from the produced Excel spreadsheets and replaces the aerodynamic characteristics of the NACA 64618 aerofoil for the blade sections with the flaps present in Bladed.

The MATLAB script, XFOIL_FlapAerodynamicCoefs.m, is set up to output the aerodynamic data for the NACA 64618 blade profile with flaps of 10, 20 and 30% chord width, flap angles of -22 to + 22 degrees deployment in 2 degree steps, and for angles of attack ranging from -20 to +20 degrees. See the README file in the zipped folder for how to use it. This is done utilising the 'XFOIL - MATLAB interface,' copyright Rafael Fernandes de Oliveira, which is included, with an adjustment made to allow flap adjustments. A copy of Mark Drela's XFOIL is also included in the package.

Appendix C

External Bladed controller

The NREL external Bladed controller is a C++ interpretation of the FORTRAN controller code supplied in the definition of the 5MW NREL conceptual wind turbine. Whilst the source code is supplied below, it was only used in this work to validate the model and not for smart rotor control. To compile it replace the UpWind source code with this one in the Visual Studio project and build the project. The name of the external controller dll remains the same.

The UpWind external Bladed controller is created in C++ and includes all control options experimented with in this thesis. These include the use of various filters, constant torque or constant power ability above rated, options for dq-axis or independent control and individual pitch or smart rotor control, the testing of supplementary and consolidated smart rotor control, and options for various faults. These options are activated in Bladed through adjustment of the flags in the 'External Controller data' box, which means no changes to the C++ code are needed for experimentation with it. The source code and Visual Studio project are nonetheless supplied alongside a compiled controller dll that works with the Bladed project, so that those interested can see exactly what is going and adjust things for new projects as desired.

In the controller code SI units are used (e.g. rad/s) and floating points precision is used (4-byte, 32-bit precision).

NREL C++ controller 

UpWind controller Visual Studios project plus compiled dll 

Appendix D

MATLAB scripts for load calculations

There are a number of MATLAB scripts required to process the loads. These include a rain-flow counter, 1Hz damage equivalent load calculator, an extreme load extrapolation script, and a method for quickly importing the binary data files from the runs in Bladed into MATLAB. These are as an alternative to using using Bladed's data post-processing methods.

Load calculation scripts 

Appendix E

Reading 3D turbulent wind files

For importing the 3D turbulent wind (.wnd) files into MATLAB a function has been created. This facilitates manipulation of the velocity field data in MATLAB. A reverse script is then used to write the new turbulent wind, with the adjusted data, back into the wind file format. This might be done, for example, to add wake deficits or veer to the wind field.

Files for reading and writing wind files